Understanding the mechanisms of landslide path dependency (LPD): The role of topography, post-landslide soil properties, and earthquakes

by

Harsimran Singh Sodhi

B.Sc., Punjab Agricultural University, 2019
M.Sc., Forest Research Institute (Deemed to be University), 2021

AN ABSTRACT OF A DISSERTATION

submitted in partial fulfillment of the requirements for the degree

DOCTOR OF PHILOSOPHY

Department of Geography and Geospatial Sciences
College of Arts and Sciences

KANSAS STATE UNIVERSITY
Manhattan, Kansas

2026

Abstract

Landslides are one of the most important geohazards, causing widespread damage to human life, infrastructure, and ecosystems. They commonly occur in mountains and are controlled by a combination of conditioning factors, such as slope morphology, soil, and geology, as well as triggering factors, including rainfall, earthquakes, and volcanic eruptions. In addition to these controlling factors, a recent study demonstrates that landsliding is also dependent on its history. One such process in landslide-prone areas is landslide path dependency (LPD), which was detected in Collazzone (Italy) and later confirmed in central Nepal. LPD refers to the tendency of earlier landslides to cause subsequent landslides through one or more legacy effects. Although LPD was detected, the mechanism controlling it remains unclear. This dissertation investigates the mechanisms behind LPD by examining the impacts of topography, post-landslide alterations in soil physical properties, and earthquakes. The study areas for this dissertation are Collazzone in the Umbria region (Italy) and the Nepal Himalayas.

In Chapter 2, results show that LPD is stronger in downslope directions than in lateral directions. This pattern is likely due to a landslide soil-feedback mechanism controlling subsequent landslide processes. In Collazzone, many landslides occurred on slopes with concave downslope and lateral profiles, so landslide deposits remain on the hillslope rather than being fully removed. During heavy rainfall, water accumulates and pore pressure increases in these deposits, enhancing downward susceptibility and therefore greater LPD in the downslope direction.

In Chapter 3, the impacts of landslides on soil physical properties were investigated. Results show that soil organic carbon (SOC) stocks and surface soil resistance are significantly lower in landslide-affected soils than in adjacent stable soils immediately after failure. However, these differences gradually decrease with landslide age, and some soil properties within the landslide show a convergent trend with those of the adjacent soil within approximately 7-10 years. Chapter 3 results show that landslides transiently impact soil properties, creating conditions favorable for LPD.

In Chapter 4, the impacts of extreme events, i.e., earthquakes, on LPD were investigated. To study the relationship between earthquakes and LPD, the Collazzone inventory (1937- 2014) was divided into pre- and post-earthquake periods associated with the 1997 and 2009 earthquakes. The results show that earthquakes in Collazzone did not affect rainfall-triggered landslide occurrences; however, they strengthened the overall LPD by increasing overlap between

successive landslides, i.e., landslides tend to overlap more with earlier landslides after an earthquake. One possible explanation is that shaking intensity, as measured by the Modified Mercalli Intensity (MMI), was 4-5 (light to moderate shaking), indicating that these earthquakes, rather than producing widespread hillslope damage, preconditioned areas near earlier landslides, resulting in more overlaps and thus a greater LPD effect.

To test whether this impact is consistent across different geomorphic settings, a similar analysis was conducted in Nepal following the 2015 earthquakes. In contrast to Collazone, the Nepal earthquakes were stronger and had a greater impact on the MMI scale (7-8.6, very strong to severe shaking). Correspondingly, rainfall-triggered landslide numbers were higher in Nepal in the few years after the 2015 earthquakes than in the pre-earthquake period, decreasing to pre-earthquake levels in 4 years, but the impact on LPD was low. One possible reason is that the 2015 earthquakes caused more direct hillslope damage wherever they were felt, triggering additional landslides, even in previously unaffected areas, resulting in a low apparent LPD. The conceptual model that emerges from this is that earthquakes under light to moderate shaking conditions can either precondition slopes near existing landslides and thereby strengthen LPD or, under strong shaking, may cause greater hillslope damage and trigger landslides even in previously landslide-unaffected areas, leaving LPD unaffected. Overall, this dissertation demonstrates that LPD is controlled by a combination of topographic, soil, and seismic processes. Topography and post-landslide-altered soil properties create a landslide-soil feedback loop that favors LPD, while earthquakes modify overall LPD.

Understanding the mechanisms of landslide path dependency (LPD): The role of topography, post-landslide soil properties, and earthquakes

by

Harsimran Singh Sodhi

B.Sc., Punjab Agricultural University, 2019
M.Sc., Forest Research Institute (Deemed to be University), 2021

A DISSERTATION

submitted in partial fulfillment of the requirements for the degree

DOCTOR OF PHILOSOPHY

Department of Geography and Geospatial Sciences
College of Arts and Sciences

KANSAS STATE UNIVERSITY
Manhattan, Kansas

2026

Approved by:	Approved by:
Co-Major Professor Dr. Douglas G. Goodin	Co-Major Professor Dr. Arnaud Temme

Copyright

Abstract

Landslides are one of the most important geohazards, causing widespread damage to human life, infrastructure, and ecosystems. They commonly occur in mountains and are controlled by a combination of conditioning factors, such as slope morphology, soil, and geology, as well as triggering factors, including rainfall, earthquakes, and volcanic eruptions. In addition to these controlling factors, a recent study demonstrates that landsliding is also dependent on its history. One such process in landslide-prone areas is landslide path dependency (LPD), which was detected in Collazzone (Italy) and later confirmed in central Nepal. LPD refers to the tendency of earlier landslides to cause subsequent landslides through one or more legacy effects. Although LPD was detected, the mechanism controlling it remains unclear. This dissertation investigates the mechanisms behind LPD by examining the impacts of topography, post-landslide alterations in soil physical properties, and earthquakes. The study areas for this dissertation are Collazzone in the Umbria region (Italy) and the Nepal Himalayas.

In Chapter 2, results show that LPD is stronger in downslope directions than in lateral directions. This pattern is likely due to a landslide soil-feedback mechanism controlling subsequent landslide processes. In Collazzone, many landslides occurred on slopes with concave downslope and lateral profiles, so landslide deposits remain on the hillslope rather than being fully removed. During heavy rainfall, water accumulates and pore pressure increases in these deposits, enhancing downward susceptibility and therefore greater LPD in the downslope direction.

In Chapter 3, the impacts of landslides on soil physical properties were investigated. Results show that soil organic carbon (SOC) stocks and surface soil resistance are significantly lower in landslide-affected soils than in adjacent stable soils immediately after failure. However, these differences gradually decrease with landslide age, and some soil properties within the landslide show a convergent trend with those of the adjacent soil within approximately 7-10 years. Chapter 3 results show that landslides transiently impact soil properties, creating conditions favorable for LPD.

In Chapter 4, the impacts of extreme events, i.e., earthquakes, on LPD were investigated. To study the relationship between earthquakes and LPD, the Collazzone inventory (1937- 2014) was divided into pre- and post-earthquake periods associated with the 1997 and 2009 earthquakes. The results show that earthquakes in Collazzone did not affect rainfall-triggered landslide occurrences; however, they strengthened the overall LPD by increasing overlap between

successive landslides, i.e., landslides tend to overlap more with earlier landslides after an earthquake. One possible explanation is that shaking intensity, as measured by the Modified Mercalli Intensity (MMI), was 4-5 (light to moderate shaking), indicating that these earthquakes, rather than producing widespread hillslope damage, preconditioned areas near earlier landslides, resulting in more overlaps and thus a greater LPD effect.

To test whether this impact is consistent across different geomorphic settings, a similar analysis was conducted in Nepal following the 2015 earthquakes. In contrast to Collazone, the Nepal earthquakes were stronger and had a greater impact on the MMI scale (7-8.6, very strong to severe shaking). Correspondingly, rainfall-triggered landslide numbers were higher in Nepal in the few years after the 2015 earthquakes than in the pre-earthquake period, decreasing to pre-earthquake levels in 4 years, but the impact on LPD was low. One possible reason is that the 2015 earthquakes caused more direct hillslope damage wherever they were felt, triggering additional landslides, even in previously unaffected areas, resulting in a low apparent LPD. The conceptual model that emerges from this is that earthquakes under light to moderate shaking conditions can either precondition slopes near existing landslides and thereby strengthen LPD or, under strong shaking, may cause greater hillslope damage and trigger landslides even in previously landslide-unaffected areas, leaving LPD unaffected. Overall, this dissertation demonstrates that LPD is controlled by a combination of topographic, soil, and seismic processes. Topography and post-landslide-altered soil properties create a landslide-soil feedback loop that favors LPD, while earthquakes modify overall LPD.

Table of Contents

List of Figures

List of Tables

Acknowledgement

First and foremost, I want to thank **God** for giving me strength, patience, and the opportunity to pursue a Ph.D. in Geography at Kansas State University (USA). I want to thank him for always guiding me and helping me follow the true path in my entire life.

I am deeply grateful to my co-major advisor, **Dr. Arnaud Temme**, who brought me to the United States to pursue a Ph.D. Geography. His guidance, vision, and support played an important role in completing my Ph.D. research. Through his mentorship, I learned important skills in applying geospatial technology to solve real-world geomorphological problems and in thinking critically about the mechanisms behind landslides. Moreover, I want to thank him for encouraging me to take a field study in Italy and participate in the European Geosciences Union 2025.

I would also like to thank my other co-major advisor, **Dr. Douglas Goodin**, for his continuous support and guidance through my Ph.D. He was always willing to help whenever I needed assistance, and I greatly appreciate his encouragement and advice. Moreover, I want to thank him for teaching remote sensing and machine learning, which enhanced my technical skills. Apart from research, he always manages time to help me both in science and with future steps.

I am thankful to my committee members, **Dr. Sarah Boulton, Dr. Abigail Langston,** and **Dr. Helene Avocat**, for their valuable feedback, insights, and time dedicated to improving this work. With their scientific guidance and suggestions, I was able to incorporate meaningful discussions in my dissertation. Also, I want to thank **Dr. Shawn Hutchinson** for teaching GIS classes and for helping me improve my GIS skills.

Also, I am thankful to my collaborators at CNR-IRPI, **Dr. Mauro Rossi** and **Dr. Francesca Ardizzone**, for their guidance, support, and collaboration throughout my research, specifically during my field study in Italy. Moreover, I would like to thank the **Working Group** from the University of Innsbruck (Austria), which has continued to support me, and with their help, I was able to improve my dissertation.

I am grateful to **Dr. Charles Martin**, who supported me while I was in India by providing a letter for my visa processing to the embassy. I also sincerely thank **Dr. Marcellus Caldas** for supporting me during my Ph.D. and for helping provide the necessary letter when I traveled to Austria to attend the EGU conference. Special thanks to **Dr. Raj Khosla** for supporting me with funding during the last summer, which greatly helped me continue my research. Moreover, I am grateful to **Dr. Bikram Singh Gill** for his motivation and support during my Ph.D.

I am also grateful to my former advisors who introduced me to research and guided me in the early stages of my academic journey: **Dr. Sompal Singh** (Prof. in Punjab Agricultural University, India)**, Dr. Manoj Kumar** (Scientist at Forest Research Institute, India)**, Dr. Amit Kumar Verma** (Senior Technical Officer at Forest Research Institute, India)**, and Dr. Raj Setia** (Scientist at Punjab Remote Sensing Centre, India)**.** Their mentorship laid the foundation for the work I pursue today.

I would like to thank **Penny Crawford** for her kind words and warm smile, which made my scientific life more cheerful. I am also grateful for her support during my time as a Graduate Teaching Assistant; whenever I needed help with teaching materials, she was always there to assist and guide me.

I would like to express my deepest gratitude to my parents, **Mr. Pritpal Singh Sodhi** and **Mrs. Rosepreet Kaur Sodhi**, whose love, encouragement, and sacrifices have made everything possible. I also wish to honor the memory of my grandparents, (Late) **Mr. Gurdev Singh Sodhi** and (Late) **Mrs. Harbimal Kaur Sodhi**, whose blessings and values continue to inspire me. I am also thankful to my brother, **Prabhjeet Singh Sodhi**, for his constant support and to my friend **Gurjot Singh Sidhu,** who motivated me to pursue a Ph.D. in the United States.

Finally, I want to thank the whole Geography department of Kansas State University and my friends in Manhattan for making the United States feel like home.

Chapter 1 : Landslides and its path dependency

1.1. Landslides and their impact

A landslide is the movement of rock mass, soil, debris, or artificial fill downslope (Cruden, 1991; Simonett, 1997). Landslides are present on every continent and play a significant role in the landscape evolution (Gariano & Guzzetti, 2016). They are one of the important geomorphic processes that shape topography by transferring sediments and soil mass from elevated land by denudation and depositing them in valley floors and sedimentary basins (Jemec Auflič et al., 2023). Landslides are frequent in mountainous regions; however, they are not limited to these areas. They can also occur in incised valleys in locations of otherwise low slope, lake margins, fjords, and on the seafloor along the edges of the continental shelves (Clague & Stead, 2012). Landslides significantly impact human life and infrastructure. From 2004 to 2016, landslides killed approximately 4000 people per year worldwide, and in the United States, they killed 25-50 people per year (Pollock & Wartman, 2020). In addition to causing loss of life, they cause extensive damage to buildings, roads, railways, and other infrastructure. Landslides occur in 50 states of the United States and cause \$1-2 billion in losses per year (USGS, 2012). Globally, since 2000, landslides have claimed tens of thousands of lives and are predicted to cost \$20 billion per year (Sim et al., 2022). Landslides disrupt transportation networks, significantly impairing regional and economic activity, increasing network vulnerability, and restricting accessibility (Q. Zhang et al., 2020). Other impacts of landslides on the environment include damage to vegetation, destruction of agricultural crops, changes in surface and subsurface water hydrology, and impacts on flora and fauna (Nikolic, 2014).

Landslides are classified according to the system proposed by Varnes (1978) (Table 1.1; Figure 1.1) and updated by Cruden and Varnes (1996) and the International Geotechnical Society's UNESCO Working Party on World Landslide Inventory (WP/WLI; Table 1.2). Later, Hungr et al. (2014) classified landslides based on forming material types (Table 1.3) and geomorphological analysis. Moreover, landslides can be classified according to the geometry of the failure surface: translational or rotational. A translational slide is the downslope movement of soil or rock along a planar surface under gravity, whereas motion on a curved surface is known as a rotational slide (Jackson, 2013).

Table 1.1: Classification of slope movements (Cruden & Varnes, 1996; Varnes, 1978)

Movement	Rock (Bedrock)	Coarse Grained Material	Fine Grained Material
Fall	Rock fall	Debris fall	Earth fall
Topple	Rock topple	Debris topple	Earth topple
Slide	Rock slide	Debris slide	Earth slide
Spread	Rock spread	Debris spread	Earth spread
Flow	Rock flow	Debris flow	Earth flow

Table 1.2: Classification of landslides based on velocity

Velocity Class	Description	Velocity (mm/s)
7	Extremely Rapid	5000
6	Very rapid	50
5	Rapid	0.5
4	Moderate	0.005
3	Slow	0.00005
2	Very slow	0.0000005
1	Extremely slow	-

Table 1.3: Classification of landslides based on material types

Material	Description	Field description	Unified Soil classes
Rock	Strong Weak	Strong – broken with hammer Weak – peeled with knife	
Clay	Stiff Soft Sensitive	Plastic, can be molded when wet, has dry strength	GC, SC, CL, MH, CH, OL, and OH
Mud	Liquid	Plastic, unsorted remolded, and close to Liquid Limit	CL, CH, and CM
Silt, sand, gravel, and boulders	Dry Saturated Partly saturated	Nonplastic or low plasticity, granular, sorted. Silt particles cannot be seen with naked eye	ML SW, SP, and SM GW, GP, and GM
Debris	Dry Saturated Partly saturated	Low plasticity, unsorted and mixed	SW-GW SM-GM CL, CH, and CM
Peat		Organic	
Ice		Glacier	

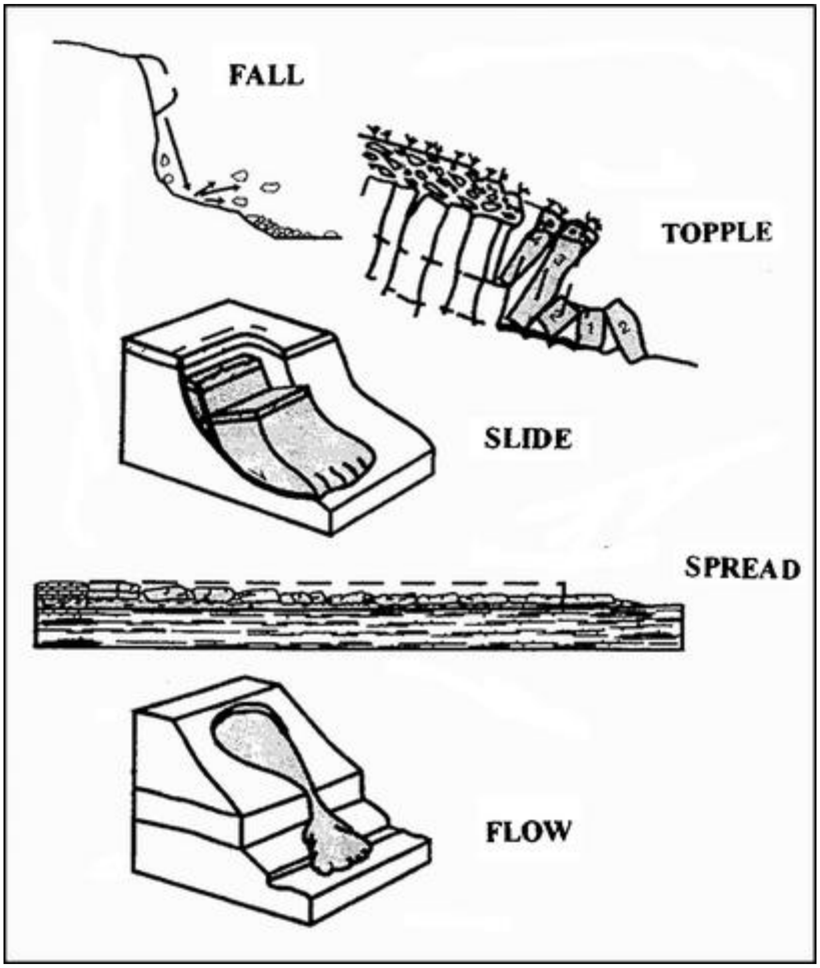

Figure 1.1: Landslide types according to Cruden and Varnes (1996) (Hungr et al., 2014)

1.2. Triggering and Conditioning factors causing landslides

Landslides are influenced by multiple factors, including triggering and conditioning factors (Figure 1.2). Triggering factors are external processes that disrupt slope stability and initiate a landslide, including intensive rainfall, snowmelt, earthquakes, and human activities (Jaafari, 2024). Earthquakes and other factors can also trigger underwater landslides, also known as submarine landslides (Hampton et al., 1996). Submarine landslides can trigger tsunamis that damage coastal areas. Whereas landslide conditioning factors are long-term environmental and geological conditions that control the probability of landslides, they do not directly trigger them. The landslide prediction system analyzes the relationship between landslide occurrences and selected conditioning factors (B. Kalantar et al., 2019). Therefore, identification of appropriate conditioning factors is important for predicting potential landslide areas. These include topographical, geological structural, and other environmental factors, such as land use and land cover, distance from rivers, etc. (Liao et al., 2022). Actual conditioning factors are difficult to measure at large scales and to incorporate into susceptibility models; therefore, parameters such as indices or distance variables are used to represent them, which are known as proxy variables. These proxy variables are generally derived from digital elevation models (DEM) to represent hillslope topographic conditions, land cover, lithology, and soil data. For example, distance from rivers is used as a proxy for fluvial erosion and slope undercutting, which can lead to landslides (J. G. Liu et al., 2004). Therefore, steep slopes near rivers are more susceptible to landslides than those farther away. Similarly, topography, represented by slope, aspect, and curvature, conveys hillslope stability. Steeper slopes, such as those in the Himalayas, are more susceptible to landslides due to stronger gravitational pull. Lithology is another important conditioning variable that influences landslide susceptibility. For instance, eroding landscapes developed on marly lithology, which are common in many circum-Mediterranean regions, are susceptible to landsliding. This situation has been observed in Collazzone, where hillslopes are largely developed on marly deposits and clay-rich soils, which favor shallow landslides (Guzzetti, Galli, et al., 2006).

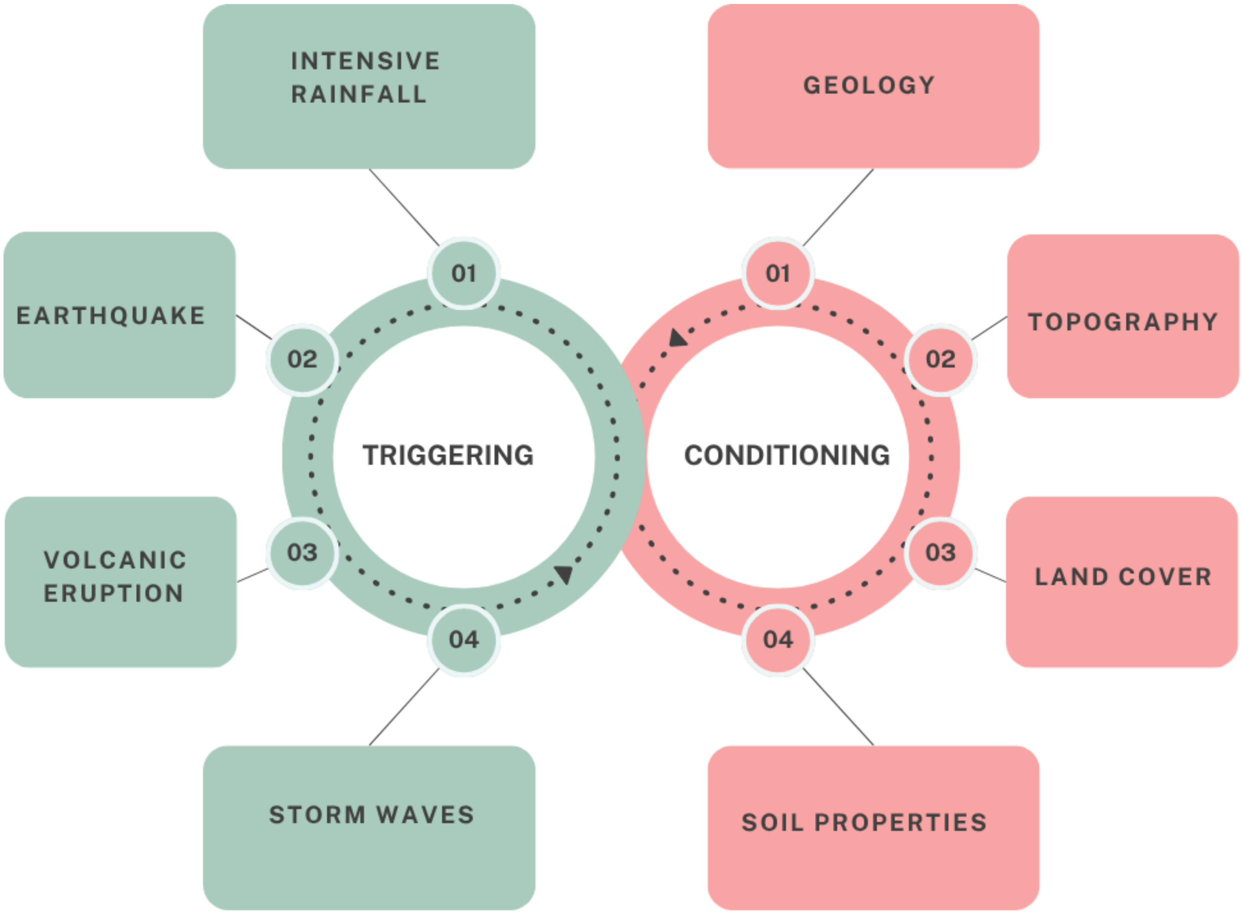

Figure 1.2: Triggering and Conditioning Factors of landslides

1.3. Landslide inventory

A landslide inventory is a database that provides basic information about landslides. They consists of records of the location of landslides, the date of their occurrence, the direction of landslide movement, information about the material involved and its estimated thickness, and the types of landslides that have produced identifiable geomorphic evidence (Wieczorek 1984; Pašek 1975).

Landslide inventories are classified by event, scale, mapping type, and approach. Event-based inventory records landslides to have occurred due to individual triggering events, such as earthquakes and precipitation (Karakas et al., 2024). Based on the type of mapping, the landslide inventory is classified as an archive or a geomorphological inventory. Archive inventory refers to the landslide database prepared from existing written or recorded sources, whereas the geomorphological inventory consists of landslides prepared from expert interpretations of aerial imagery and can be recognized by geomorphologists (Ardizzone et al., 2023).

Landslide inventories are produced using conventional methods and advanced methods. Conventional methods of mapping landslide inventory include geomorphological field mapping (Brunsden, 1985) and stereo aerial photo interpretation (Ardizzone et al., 2007). Advanced methods include mapping using advanced satellite remote sensing and artificial intelligence (B. Fang et al., 2021; Bernat Gazibara et al., 2019; Chandra & Vaidya, 2024; X. Liu et al., 2018).

1.4. Landslide susceptibility and its modelling

Landslide susceptibility means the probability of a landslide occurring in an area based on topography and environmental conditions (Brabb, 1984). It refers to the potential for terrain to be impacted by future landslides. Susceptibility does not account for landslide size, although separate assessments can be conducted for landslides of different sizes (Reichenbach et al., 2018). Moreover, it does not account for the temporal probability of the landslide occurrence (Samia, 2018). Therefore, landslide susceptibility is considered static and independent of time.

Landslide susceptibility can be estimated using qualitative, quantitative, and semi-quantitative methods. Qualitative methods of susceptibility assessment are subjective, as the weights assigned to parameters that contribute to vulnerability are determined by experts' knowledge and experience (Biswakarma et al., 2023). Whereas, quantitative methods use deterministic, statistical, mathematical modelling, and artificial intelligence techniques, which are more realistic and objective (Wang et al., 2021; Shen et al., 2024). Qualitative-semi-quantitative methods combine the other two methods (Biçer & Ercanoglu, 2020; Y. Wang et al., 2021). Methods to assess landslide susceptibility are based on some assumptions: 1) landslides leave identifiable evidence, 2) landslides are controlled by physical laws that can be analyzed statistically, empirically, and deterministically, 3) past and present landslides inform future events, and 4) their occurrence can be predicted using heuristic, statistical, and physical models (Reichenbach et al., 2018).

An important and commonly overlooked decision in landslide susceptibility modeling (LSM) is the selection of the mapping unit; the most commonly used are pixels and slope units, while others include terrain, geo-hydrological, political, and topographic units (Reichenbach et al., 2018). Pixel-based mapping unit is the most commonly used in LSM. Pixel-based models account for spatial variation of explanatory factors across each pixel; however, they rely on information based on a single pixel, thus neglecting correlations between the pixels (Liao et al., 2022). In contrast, slope units capture spatial neighborhood by averaging values of explanatory variables across a defined range of pixels; however, they may mask the local variability of these factors within the unit (Chang et al., 2023). As a result, areas with contrasting conditions may be represented by the mean, thereby reducing the ability to capture localized conditions that influence landslide occurrence.

Landslide hazard (Figure 1.3) is a distinct term often confused with landslide susceptibility. Landslide hazard refers to the likelihood, frequency, and size of a landslide and is more difficult to determine than susceptibility, as susceptibility is the spatial component of hazard (Guzzetti, 2006; Guzzetti et al., 2005). The combination of landslide susceptibility, landslide inventory, and landslide hazard mapping defines landslide risk, which reflects potential loss of life and social, economic, and environmental damage (Samia, 2018).

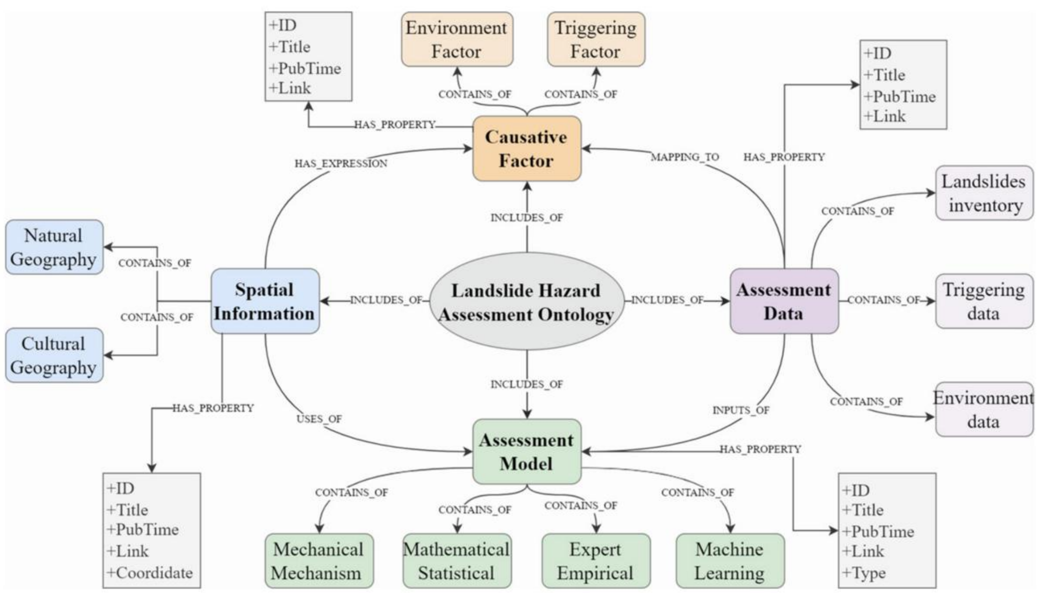

Figure 1.3: Conceptual model of landslide hazard assessment (Sun et al., 2025)

1.5. Concept of landslide path dependency

The concept of landslide path dependency (LPD) was detected by Samia et al. (2017a), which emerged from a concept of complexity theory and non-linear dynamics (Phillips, 2006; A. J. A. M. Temme et al., 2015). According to the complexity theory, geomorphic systems are non-linear, that is, output cannot be linked to input through a simple direct linear relationship due to the presence of thresholds, feedbacks, self-organization, storage, and saturation (Murray et al., 2014; Phillips, 2014). According to Phillips (2006), landscape evolution is path-dependent, i.e., the current landscape depends on past events. Applied to landslides, when a slope fails, it changes the surface morphology, soil properties, vegetation, and slope geometry (Chen, 2009; Schuster & Highland, 2003; K. Singh et al., 2014; van Westen et al., 2006) all of which change landslide susceptibility. Therefore, landslide history can be considered a form of path dependency in shaping changes in landslide susceptibility.

The theory, i.e., geomorphic systems carry forward the memory of past events through non-linear dynamics, provided the scientific basis for Samia et al. (2017a) to test whether LPD existed in Collazzone, Italy, leading to its detection. Samia et al. (2017a) defined LPD as the mechanism by which previous landslides influence the probability, location, and size of subsequent landslides through a legacy effect. Slopes that have already failed do not simply recover and return to their background state; instead, they retain their past history in the form of physical and hydrological signatures, such as altered soil, slope steepness, and vegetation. In some cases, landslides may reduce susceptibility through a negative feedback mechanism, for example, by lowering slopes, leading to less susceptibility to future landslides (A. J. A. M. Temme, 2021a). However, landslides can also increase susceptibility through positive feedback loops, such as the formation of a weakly permeable soil layer along a sliding surface, which increases the pore pressure and thus landslides within that layer (Duzgoren-Aydin & Aydin, 2006; Parry et al., 2000). This latter behavior forms the basis of LPD as it increases the probability that new landslides will overlap or occur adjacent to pre-existing landslides (Roberts et al., 2021; Samia et al., 2017b). If LPD holds, then landslide susceptibility cannot be static, as previously stated, but rather dynamic over time, as the history of the landslide is important in determining it. LPD is not only found in Collazzone but also in Nepal, indicating that it is not site-specific; it occurs across different geomorphic settings (Roberts et al., 2021). Therefore, in susceptibility assessments, it is important to incorporate past events alongside other conditioning factors.

Moving beyond the detection of LPD, Samia et al. (2020) proposed a framework to quantify LPD to capture the strength, spatial extent, and temporal decay of path dependency using space-time clustering (STC) derived from Ripley's K function using a multi-temporal landslide inventory. By fitting an exponential decay function between STC and the time difference between landslides, they found that LPD is higher within 60m of a landslide, and decays over a timescale of 17 years. Building on this methodological approach, Samia et al. (2020) tested its practical application by incorporating path dependency variables (maximum smoothed STC value and sum of all smoothed STC values) in a pixel-based LSM. It was found that incorporating path-dependency variables alongside conventional topographic variables significantly improved LSM performance. Therefore, LSM is not only a function of present geomorphic and climatic conditions but also depends upon past landslide events.

Apart from quantifying LPD, Samia et al. (2017a) also investigated the roles of the geometry (size and roundness) and spatial location of previous landslides in predicting the occurrence of follow-up landslides. They found that larger landslides are associated with a higher risk of a follow-up landslide. Moreover, they stated that landslide shape and topographic properties, including DEM derivatives such as the topographic wetness index, topographic position index, LS factor, slope, and aspect, are important for predicting whether a follow-up landslide will occur.

Samia et al. (2017a) also quantified LPD by fitting an exponential function to the number of follow-up landslides (measured as fractional overlaps) and the time difference between the initial and follow-up landslides. Based on this approach, they found that susceptibility is 15 times higher and returns to pre-background values after 15 years. This means that earlier landslides transiently affect the slope, temporarily increasing its susceptibility to subsequent landslides. However, this susceptibility decreases with time as hillslopes progressively recover. This analysis was conducted for the entire inventory, excluding extreme events such as earthquakes and snowmelt, thereby highlighting an important research gap regarding how these external events may modify LPD. Moreover, earthquakes can act as a preconditioning factor for future landslides by weakening hillslopes without immediately triggering them. Parker et al. (2015) showed that earthquakes can weaken hillslopes and influence the spatial distribution of landslides triggered by later earthquake events beyond what is explained by time-independent factors. Similarly, Marc et al. (2015) studied the relationship between climate-normalized landslide rates and earthquakes and found that, immediately after an earthquake, climate-normalized landslide rates were higher and tended to return to background levels within 1-4 years. As earthquakes precondition future landslide occurrence by reducing slope strength and altering soil physical conditions, it is important to investigate whether these extreme events modify LPD.

1.6. Research gaps

Previous research proved the existence of LPD in Collazzone and Nepal (Roberts et al., 2021; Samia et al., 2017b), however understanding the underlying mechanism behind LPD remains lacking. In hillslopes, gravitational processes direct the movement of sediments and water along the direction of the maximum slope gradient; therefore, it is unclear whether the LPD effect varies in the downslope (along the direction of maximum gradient) and lateral directions (perpendicular to downslope). Samia et al. (2020, 2017a) conducted a quantitative analysis of LPD in Collazzone using Ripley's K function and showed that landslide susceptibility is dynamic, remaining higher near recent landslides; however, they did not explain the mechanisms underlying this pattern. Also, when calculating Ripley's K, they measured spatial distance using the Pythagorean theorem and therefore treated distance as isotropic, without separating it into downslope and lateral components. Yet hillslope processes might be anisotropic, as gravitational transport occurs along the steepest descent. Therefore, it remains unclear whether LPD or spatial association between earlier landslides and subsequent landslides is stronger in the downslope direction or in the lateral direction.

Moreover, landslides modify soil properties through the landslide-soil feedback loop mechanism (Samia et al., 2017b; A. J. A. M. Temme, 2021a). During a landslide, soil is smeared along the slide surface, and it may displace in the downslope direction, leading to clay-rich deposits near the landslide's toe. These deposits have more water holding capacity due to more clayey content, which increases the pore pressure due to rainfall and thereby increases the likelihood of landslides in the downslope direction, contributing to anisotropic patterns of follow-up landsliding. Moreover, previous work (Roberts et al., 2021; Samia et al., 2017b, 2017a) emphasized landslides' geometric and topographic properties derived from DEM influence subsequent landslides; however, the role of soil properties as a mechanism remains unexplored. For example, Van Eynde et al. (2017) studied the impact of landslides on soil properties and reported that landslides lower soil organic carbon (SOC), and SOC increases progressively with landslide age, becoming similar to undisturbed soils after approximately 60 years. They also found that soils within a landslide contain higher levels of rock fragments and sodium ions than adjacent undisturbed soils. Moreover, Mirus et al. (2017) demonstrated that landslides reduce hydraulic conductivity, porosity, and drainage efficiency, resulting in prolonged water saturation and subsequent landslides. If landslides transiently alter soil hydrological and other physical properties, then they may increase slope susceptibility during the recovery phase. Therefore, it is important to investigate whether landslide-induced changes in soil properties constitute a key process causing LPD.

It has also been observed that earthquakes precondition future landslides by inducing mechanical damage and reducing ground strength, even when an immediate landslide does not occur. This can result from cracking, dilation, and brittle failure induced by earthquakes, leading to weakening of the hillslope (Parker et al., 2015). Moreover, Marc et al. (2015) reported that rainfall-triggered landslides were higher immediately after major earthquakes than in the pre-earthquake period, and their rate decreased progressively over the following few years. Similarly, in Nepal, following the 2015-Gorkha earthquake ($M_w = 7.8$), landslide rates were higher than coseismic levels even 3.5 years after the earthquake (Kincey et al., 2021). Together, these studies demonstrate that earthquakes do impact hillslopes by weakening their strength and stability and increasing susceptibility to future landslides. Both LPD and earthquake preconditioning show that past events influence future landslide occurrences, yet an important question remains unresolved: whether earthquakes amplify or suppress LPD, nor is it known whether the strength and duration of path dependency change after major seismic events.

1.7. Objectives

Based on existing research gaps in LPD, the overall goal of my dissertation is to understand the underlying mechanisms of LPD by investigating the roles of geomorphic factors, soil properties, and earthquakes that may drive it. To achieve this goal, my dissertation pursues three primary objectives:

Objective 1: To investigate whether the LPD is anisotropic by separating spatial distance into downslope (along the direction of maximum descent) and lateral directions (direction perpendicular to downslope).

In this objective, I will evaluate whether the LPD in Collazzone occurs more in the downslope direction or whether the lateral direction is equally or more important. This objective will enhance a scientific process-based understanding of the LPD mechanism on hillslopes, which controls the development of subsequent landslides. Separating the spatial distance into downslope and lateral components will help determine whether LPD is stronger in the downslope, where gravitational forces and sediment transport are dominant, or in the lateral direction.

Objective 2: To examine whether landslide produces transient changes in soil physical and hydrological properties in Collazzone, and to analyze how long the soils within landslides differ from adjacent stable soils. Can this timescale and transient alteration in physical properties be a mechanistic driver of LPD?

This objective will explore the LPD mechanism in Collazzone by investigating whether landslides produce transient changes in soil physical properties. I will examine how long soil properties within landslides remain altered relative to stable soils, and whether these alterations create conditions for LPD.

Objective 3: Analyze whether earthquake preconditioning affects LPD in Collazzone and other geomorphic settings.

In this objective, I will investigate how extreme events, such as high magnitude earthquakes, alter LPD in Collazzone and examine whether their impact is visible in other geomorphic settings, such as central Nepal. In contrast, non-extreme events include lower-magnitude earthquakes and more frequent processes such as seasonal rainfall, which induce gradual changes in slope stability.

Specifically, I will examine whether LPD becomes stronger or is suppressed after a large earthquake. By comparing LPD responses in Collazzone and Nepal, this objective will determine the impact of earthquake preconditioning on LPD, and test whether it differs across geomorphic conditions.

Chapter 2 : The role of relative topographic position in determining landslide path dependency

Harsimran Singh Sodhi[1] (harsimran94@ksu.edu, harsimransodhi94@gmail.com, ORCID: 0000-0001-9851-0399), Alessia Giarola[2], Jalal Samia[3], Mauro Rossi[4], Francesca Ardizzone[4], Arnaud Temme[2]

[1]Department of Geography and Geospatial Sciences, Kansas State University, Manhattan, Kansas, United States of America

[2]Institute for Geography, University of Innsbruck, Innrain 52f, 6020 Innsbruck, Austria

[3]Department of Geography, University of Mazandaran, Pardis Campus, 47416-13534 PB, Babolsar, Iran

[4]Consiglio Nazionale delle Ricerche, Istituto di Ricerca per la Protezione Idrogeologica, via della Madonna Alta 126, 06128 Perugia, Italy

Abstract

Landslide susceptibility is controlled not only by predisposing factors but also by landslide path dependency (LPD): the tendency of past landslides to increase the probability of subsequent nearby landslides. LPD remains poorly investigated despite its importance in determining spatiotemporal landslide patterns. Existing methods use only geographic coordinates, obscuring to the role of relative topographic position on hillslopes, which may hold clues to the LPD mechanisms.

We focused on shallow landslides at a site in Italy, using a 3104-landslide multi-temporal landslide inventory (1939 - 2014). We aimed to examine whether LPD can be quantified using topographic coordinates by measuring the distance between consecutive slides in downslope and slope-lateral directions. This would allow a more process-based interpretation than the use of relative geographic coordinates. For confidence-testing, we used simulated annealing to create 20 artificial multi-temporal landslide inventories that replicated the real inventory's characteristics but lacked LPD. We then calculated Ripley's K to measure the space-time clustering of landslides and analysed its relationship with the slope-lateral distance (dL), downslope distance (dD), and time difference (dT) between landslides. If the Ripley's K of the observed inventory is greater than that of the artificial inventory, it is interpreted as evidence of LPD. Our results reveal that Ripley's K of the observed inventory, compared to the artificial inventories, is initially 47 times larger, and decreases nonlinearly with increasing dL, dD, and dT. It is thus possible to capture the impact of earlier landslides on susceptibility along downslope and lateral directions, with the downslope direction having a greater and longer impact. This provides clear evidence that the unresolved process behind path-dependency is slope-anisotropic, with downslope emerging as a dominant control on LPD.

Keywords: Landslide path dependency, simulated annealing, Ripley's K, spatial temporal clustering, landslide susceptibility.

2.1. Introduction

Landslides are among the most severe geohazards in mountainous regions worldwide, affecting these regions' societal and economic stability (Pyakurel et al., 2024; A. Singh et al., 2024). They are primarily triggered by rainfall, earthquakes, snowmelt, and anthropogenic activities (Guzzetti et al., 2009; Malamud et al., 2004; Meusburger & Alewell, 2008). Understanding and predicting landslide patterns is a challenging task that is of both scientific and societal interest and that may help save lives and protect infrastructure from damage.

The probability of a slope failure occurring at a specific site based on the local characteristics is known as landslide susceptibility (Guzzetti et al., 2005; Kovács et al., 2019; Reichenbach et al., 2018). Susceptibility assessments rely on records of historical landslide occurrences and aim to relate these records with topographic and remote sensing datasets. Many such datasets have been used in assessments to predict locations most prone to future landslides (Yeon et al. 2010; Kayastha et al. 2013; Liu et al. 2019; Nhu et al. 2020). Although logistic regression approaches have been the most popular, machine learning (ML) methods have recently been adopted to more flexibly estimate the relations between landslides and environmental factors (Tehrani et al., 2022).

However, susceptibility assessment commonly ignores the transient or permanent impacts of landslides on soil properties, vegetation, and slope morphology (Noviyanto et al., 2020; Samia et al., 2017b; K. Singh et al., 2014; van Westen et al., 2006). This is either because the maps and satellite imagery used as explanatory factors are not updated between landslide events, or because these datasets do not capture changes caused by previous landslides at all. Not accounting for these impacts creates apparent path dependency in the landslide systems: new landslides seem to be impacted by the legacy of previous landslides rather than present-day environmental conditions (Samia et al., 2017b). The empirical characterization and quantification of this effect have started only recently, and its mechanistic underpinning remains unknown (A. Temme et al., 2020).

Recent studies show that measuring the spatio-temporal strength of path dependency in geographic space (i.e., in the latitude-longitude plane) is at least possible (Samia et al., 2020). Path-dependent landslides were found to be larger, rounder, and more likely to experience a new, overlapping landslide over the next decade (Samia et al., 2017b). Additionally, Samia et al. (2018) concluded that including landslide path dependency (LPD) in landslide susceptibility assessment drastically improved the performance of conventional models in the landslide-prone Collazzone area (Samia et al., 2020). Adopting Samia et al.'s (2017) methodology, Roberts et al. (2021) confirmed the existence of LPD in the Himalayas and found that the length of the landslide inventory, the size of the research region, and the size and type of the mapped landslides all have an impact on the rate and magnitude of the quantified LPD dynamics. This confirms the existence of LPD across differing geomorphic settings and suggests that it should be more widely considered in landslide susceptibility assessments.

Samia et al. (2020) adopted Ripley's (1976) K function in one spatial and one temporal dimension to measure the extent of landslide clustering. In this work, the space dimension was the Pythagorean distance between landslide centroids in the geographic coordinate plane, and the time dimension was the time between consecutive landslides. Samia et al. (2020) found that the observed Ripley’s K values were well captured by an exponential decay function of the space and time dimensions, using a characteristic decay time of about 17 years, and a characteristic decay distance of about 60 m. Thus, keeping all other factors constant, the probability of landslide occurrence near a previous landslide was initially about 45% higher and decreased by a factor of e (Euler’s number) every 17 years and every 60 meters from a previous landslide to a background susceptibility value that is no longer determined by the time-space proximity of previous landslides. The characteristic decay parameters, which separately capture the importance of the space and time distance to previous landslides, have been found helpful in studying the spatial-temporal relationships between multi-temporal landslides (Samia et al. 2018, 2020). However, reducing the spatial relation between consecutive landslides to the Pythagorean distance between them is unsatisfactory because it assumes that the pattern of landslide-on-landslide impact is independent of landscape morphology, and it does not help us understand the mechanism behind path dependency. Thus, a method is needed to quantify path-dependency that uses metrics derived from the relative landscape position between subsequent landslides on the same hillslopes.

Here, we introduce and test such a method that quantifies landslide path dependency in a geomorphologically relevant manner. We hypothesized that the impact of previous landslides on landslide susceptibility is optimally captured along two perpendicular spatial directions, the downslope and the slope-lateral direction, as opposed to the single, slope-blind metric used so far. We expect path dependency effects to differ between the downslope and lateral directions, potentially suggesting the mechanisms underlying path dependency and improving susceptibility assessment.

2.2. Study Area and data

The 80 km^2 large Collazzone area (Figure 2.1) lies in the central Italian province of Perugia, in the Umbria region. The area's geology comprises alternating layers of recent river deposits along the valley floors, continental deposits of gravel, sand, and clay, as well as sandstone, marl, travertine, and thinly layered limestone (Lombardo et al., 2020; Volpe et al., 2022). The terrain is primarily hilly, with elevations ranging from 145 m near the Tiber River flood plain (North-Northwest of Todi) to 634 m at Monte di Grutti, and the lithology and bedding plane attitude affect the shape of the slopes, as well as the quantity and frequency of the landslides (Lombardo et al., 2020; Santangelo et al., 2015). The region's soils have a fine or medium texture, a thickness that ranges from a few decimeters to more than one meter and is characterized by a xeric moisture regime which is typical of the Mediterranean climate. The mean annual temperature and precipitation in Collazzone are 13.8 °C and 859 mm, respectively (Climate-Data.org, 2025). Many landslides have occurred in the area over the last decades, ranging in size and volume from deep seated to shallow slides and flows (Guzzetti, Galli, et al., 2006).

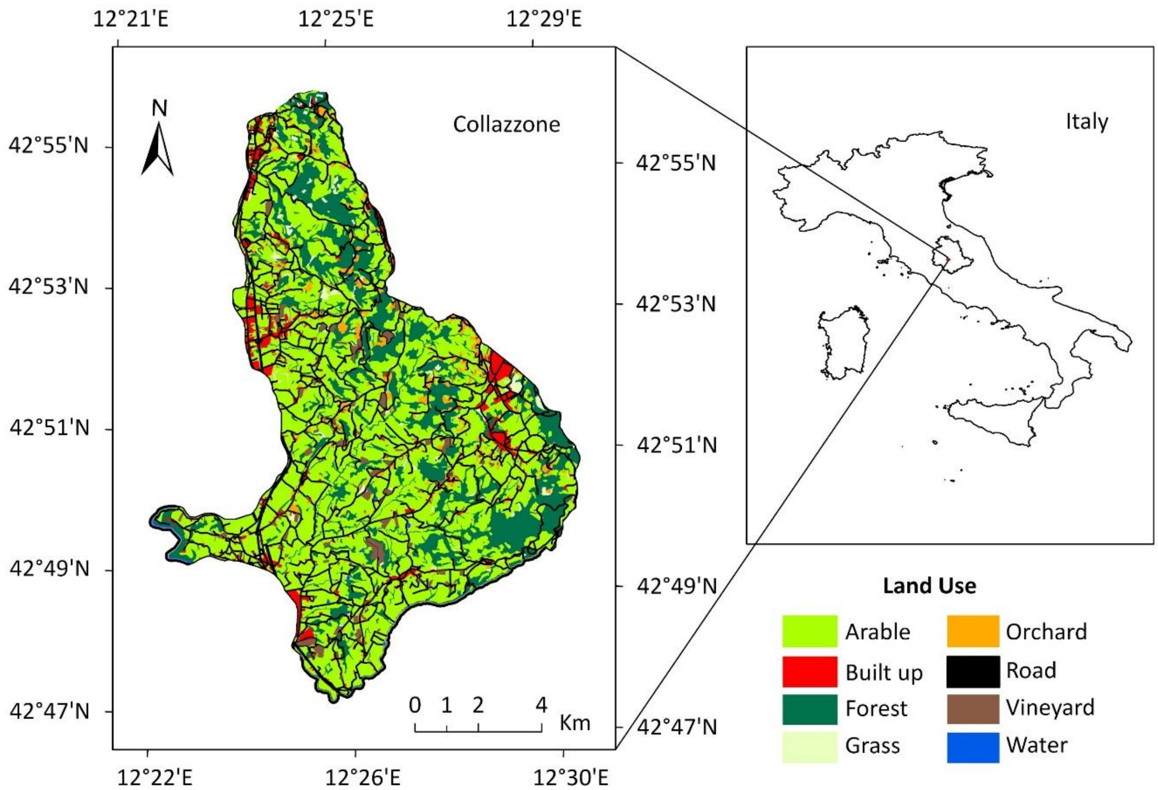

Figure 2.1: Collazzone study area (left map) and Umbria region in Italy (right upper map)

2.2.1. Multi-Temporal landslide inventory description

For the Collazzone region, a comprehensive multi-temporal landslide inventory (Figure 2.2), which exclusively includes shallow landslides, is available from 1939 to 2014 (Guzzetti, Reichenbach, et al., 2006; Samia et al., 2018). The initial inventory was created at a 1:10,000 scale by visual interpretation of aerial images acquired unsystematically between 1941 and 1997 at scales varying from 1:13,000 to 1:33,000, while the landslides that occurred from 1999 to December 2005 were mapped through field surveying of the area following extended rainy periods (Samia, 2018). Stereo satellite images taken in March and May 2010 were used after similar events, while 2013 and 2014 slope failures were mapped using stereo pairs from GEOEYE and WorldView sensors, respectively (Ardizzone et al., 2013; Samia et al., 2017b). The landslide age was determined from aerial photograph dates and the morphological features of landslides: landslides appearing fresh on the aerial photographs were assigned the date of that imagery, while older-looking landslides were attributed to the time between the imagery in which they were first identified and the date of earlier imagery (Samia et al., 2017b).

The study area was divided into geomorphological areas by a series of previously defined "slope units", confined by drainage and division lines (Alvioli et al., 2016; Samia et al., 2018). In total, 894 slope units are identified for Collazzone (Guzzetti, Galli, et al., 2006). We used these slope units and the time of landslide occurrence to select landslide pairs that share slope units but are not from the same time – assuming that only landslides in these pairs possibly share a path-dependent relationship.

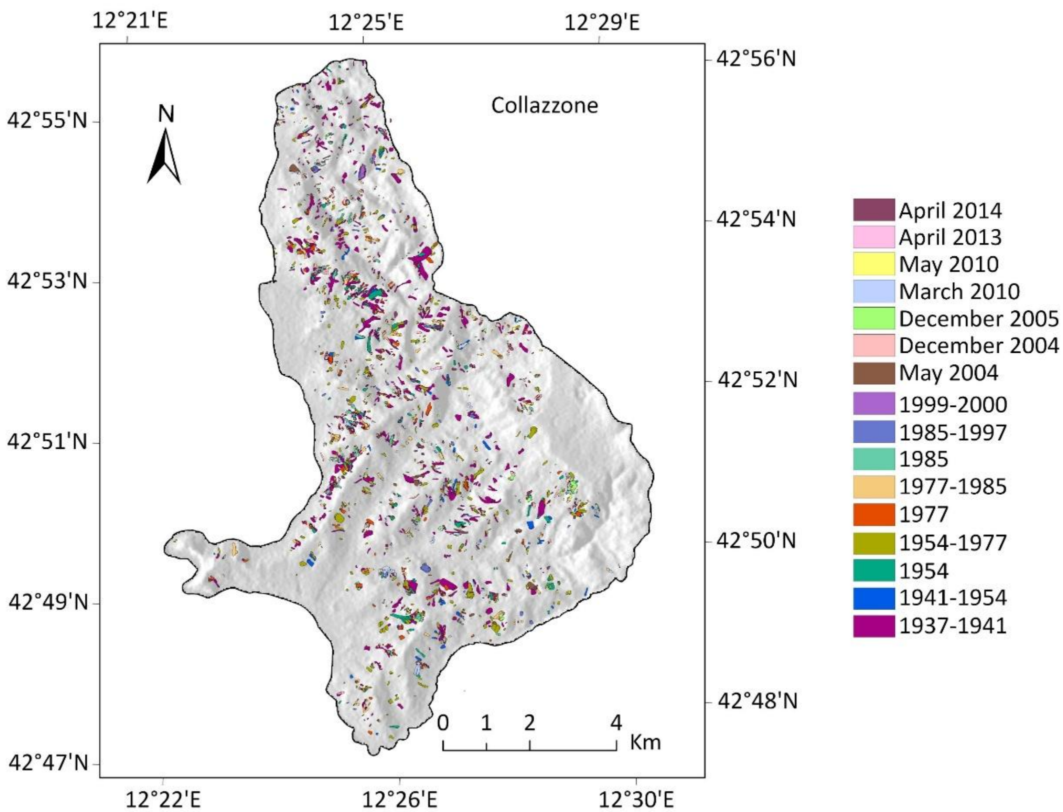

Figure 2.2: Multi-temporal landslide inventory of Collazzone study area overlying on hillshade image

2.3. Methods

The first step in the LPD analysis was to structure the landslide inventory by retaining important parameters: landslide ID, time of occurrence, and the latitude and longitude of landslide centroids. This was followed by integrating topographic attributes, including elevation, slope steepness and aspect, derived from a Digital Elevation Model (DEM). The DEM source was the ASTER version 3, with a spatial resolution of approximately 30 meters, created in 2019 and downloaded from NASA's Earthdata Search website.

Based on this dataset, we used simulated annealing (Figure 2.3) to create 20 artificial multi-temporal landslide inventories that share topographic properties with the observed multi-temporal landslide inventory, but that do not have spatial clustering or dispersion, such that there is no landslide path dependency. It means that each landslide occurs independently, without being influenced by the location of previous landslides.

Landslides in the artificial inventories also share the relative temporal frequency observed in the original landslide inventory. After that, we calculated Ripley's K from the real and 20 artificial landslide inventories. The Ripley's K values from the artificial inventories were then compared with the Ripley's K values from the real inventory. The 20 sets of ratios between artificial and real Ripley's K values were used to calculate confidence bounds on the impact of downslope and lateral distance.

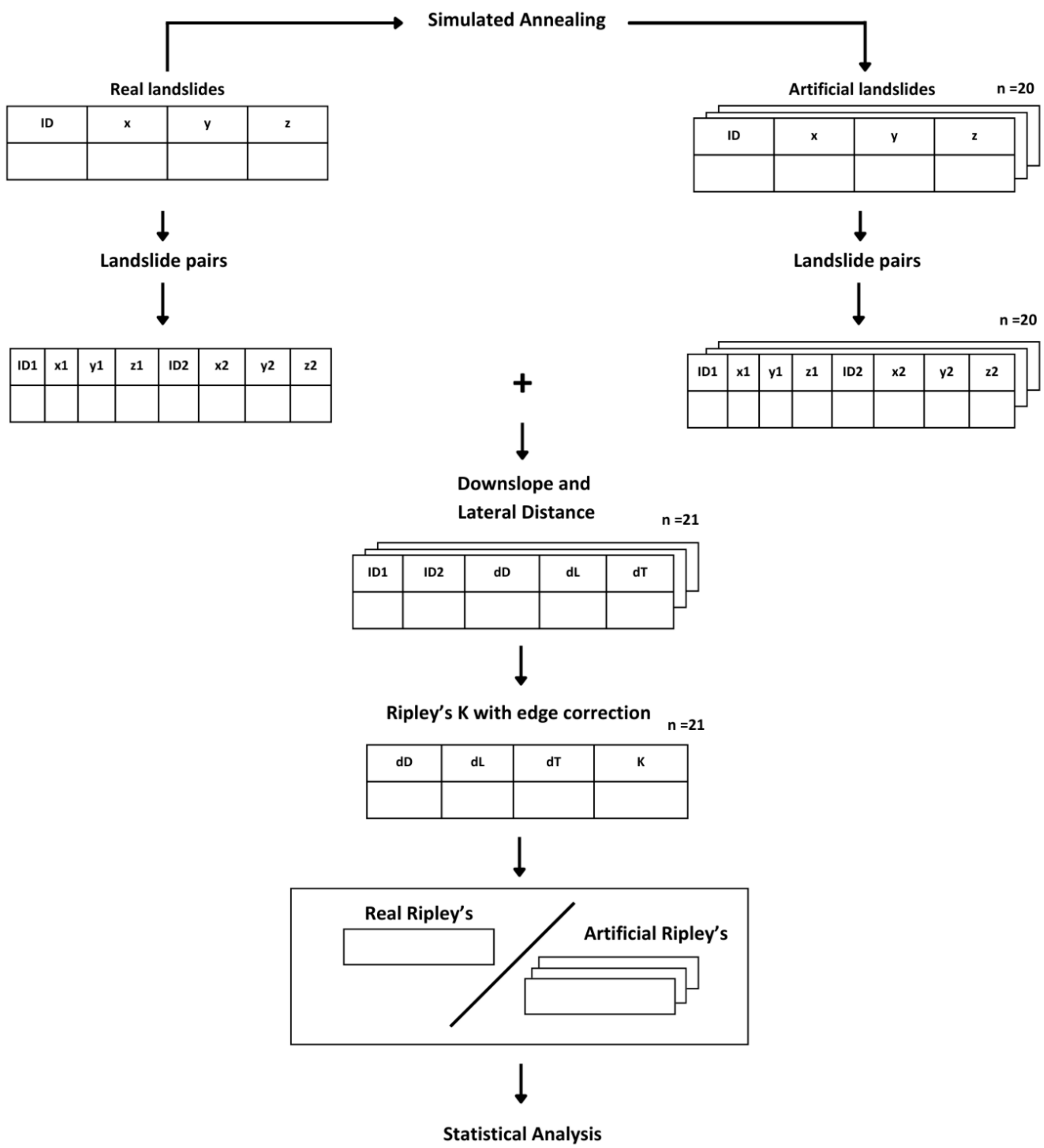

Figure 2.3: Flowchart of Methodology – Simulated annealing generating artificial landslide inventory from the real multi-temporal landslide inventory, followed by spatial distance calculations. Ripley's K is used to quantify LPD.

2.3.1. Simulated annealing

Simulated annealing (SA), an optimization process (Metropolis et al., 1953) was used to randomly place the same number of landslide centroids in the landscape as observed in the real multi-temporal landslide inventory while as closely as possibly matching the mean and standard deviation of the slope steepness and aspect of the landslides in the real inventory. We leveraged the “spsann” package (Samuel-Rosa, 2019), version 2.2.0, in R and used that package’s user-specified optimization function (optimUSER) to calculate the mean and the standard deviations (sd) of the slope steepness and aspect values of the simulated landslide centroids. The average difference between these values and the corresponding values from the observed inventory was calculated as:

$$\text{Error} = \frac{\left|\overline{\tan(\Theta)_{real}} - \overline{\tan(\Theta)_{sim}}\right|}{\left|\overline{\tan(\Theta)_{real}}\right|} + \frac{\left|\overline{a_{real}} - \overline{a_{sim}}\right|}{\left|\overline{a_{real}}\right|} + \frac{\left|\sigma_{\tan(\Theta)\_real} - \sigma_{\tan(\Theta)\_sim}\right|}{\left|\sigma_{\tan(\Theta)\_real}\right|} + \frac{\left|\sigma_{a\_real} - \sigma_{a\_sim}\right|}{\left|\sigma_{a\_real}\right|}, \tag{2.1}$$

where $\overline{\tan(\Theta)_{real}}$, $\overline{\tan(\Theta)_{sim}}$, $\overline{a_{real}}$, $\overline{a_{sim}}$, $\sigma_{\tan(\Theta)\_real}$, $\sigma_{\tan(\Theta)\_sim}$, σ_{a_real}, σ_{a_sim} are, respectively, the mean slope of the real landslide points, mean slope of the current simulated points, mean aspect of the real landslide points, mean aspect of the current simulated points, standard deviation of the slopes of the real landslide points, standard deviation of the slopes of the current simulated points, standard deviation of the aspect of the real landslide points, and standard deviation of the aspect of the current simulated points respectively.

The error value from equation (2.1) was used in simulated annealing as the objective function, i.e., the quantity that is minimized.

2.3.2. Calculation of spatial distances

The distance between the centroids of both landslides in a pair, along the slope-plane, is defined as the Pythagorean product (d) of the slope-lateral distance (dL), and the downslope distance (dD) (Figure 2.4):

$$d = \sqrt{dL^2 + dD^2} \tag{2.2}$$

The downslope distance (dD) is the distance between landslides along the steepest downslope direction:

$$dD = \frac{\Delta h}{\mathrm{Sin}(\Theta)}, \tag{2.3}$$

where Δh is the difference in the elevation of the two landslides and Θ is the steepness of the hillslope.

Then, dL, the lateral distance between any two landslides on the same hill slope unit, can be calculated from equations (*2.2*), and (*2.3*):

$$dL = \sqrt{d^2 - \left(\frac{\Delta h}{\mathrm{Sin}(\Theta)}\right)^2} \tag{2.2}$$

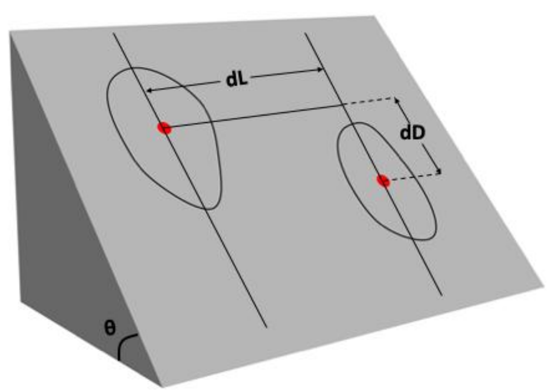

Figure 2.4: Downslope distance (dD) and lateral distance (dL) between two landslides on the same hillslope

2.3.3. Ripley’s space time K function for quantification of landslide path dependency

To quantify the LPD in spatial and temporal dimensions we used Ripley's (1976) K function. A particular point distribution is often compared to a random distribution using Ripley's K-function; in other words, the null hypothesis that the points are randomly and independently distributed is tested against the point distribution under examination (Kiskowski et al., 2009; Pu & Bell, 2017). While Ripley’s K is mainly used to assess spatial point clustering, Diggle et al. (1995) extended into spatial-temporal setting, and further extensions of Ripley’s K into multiple dimensions can be made (Dixon, 2014). Practically, in our case, a cuboid (Figure 2.5) defined by a lateral distance, a downslope distance, and a temporal distance from the centroid of a first landslide is used to define Ripley’s identity function as:

$$I_{(dD,dL,dT)}\left(d_{ij}, l_{ij}, t_{ij}\right) = \begin{cases} 1, & (d_{ij} < dD, \quad l_{ij} < dL, \quad \text{and } t_{ij} < dT \\ & 0, \ \text{otherwise} \end{cases}, \qquad (2.4)$$

where dD, dL, and dT are the current maximum distances in the downslope, lateral, and time directions, respectively, determining the spatial and temporal extent of the analysis.

Here, i and j are two landslide centroids, and d, l, and t are the downslope distance, lateral distance, and time respectively between two landslide centroids. This function results in a value of 1 when a landslide is inside the cuboid produced by the centre of the previous landslide and a value of zero when a landslide is outside that cuboid.

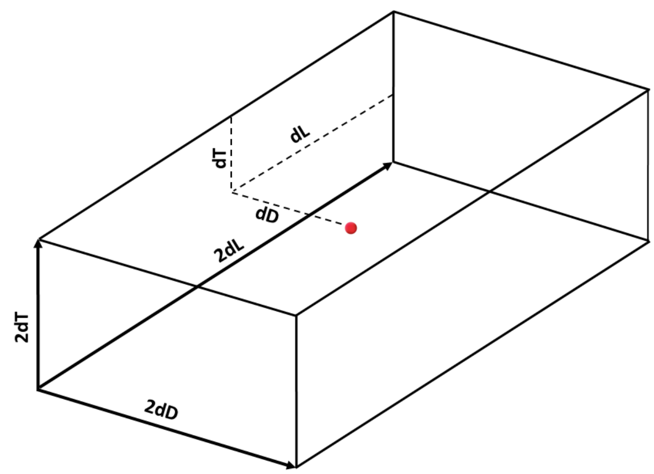

Figure 2.5: Space-time cuboid. The red point represents the centroid of a given landslide around which a space-time cuboid is formed. The cuboid's dimension is a function of dL, dD, and dT, with its sides extending 2dL, 2dD, and 2dT, respectively. This cuboid represents the spatial and temporal dimension so that if any younger landslide that falls into the cuboid will receive $I_{(dD,dL,dT)}$ equal to '1' in Eq. (2.4).

Using this identity function, summing over all observed landslides and dividing by the number of landslides and landslide intensity gives the observed Ripley space-time K function ($\widehat{\mathrm{K}}$):

$$\widehat{\mathrm{K}}\,(\mathrm{dD}, \mathrm{dL}, \mathrm{dT}) = \frac{1}{\widehat{\lambda}_{\mathrm{st}} \cdot \mathrm{n}} \sum_{i=1}^{n} \sum_{j \neq 1} \mathrm{I}_{(\mathrm{dD},\mathrm{dL},\mathrm{dT})}\,(\mathrm{d}_{ij}, \mathrm{l}_{ij}, \mathrm{t}_{ij})], \tag{2.5}$$

where λ_{st}, the average space-time landslides intensity, is given by

$$\lambda_{\mathrm{st}} = \frac{\mathrm{n}}{\mathrm{a(R)} \times (\mathrm{t}_{\max} - \mathrm{t}_{\min})} \tag{2.6}$$

Here, n is the number of landslides in the landslide inventory, a(R) is the total study area size, and t_{max} and t_{min} are the start and end times of the landslide inventory. In our case, these values are 3104 for n, 79632683 m^2 for a(R), 2014 and 1939 for $t_{max}$and t_{min} respectively. Thus λ_{st} equals 5.19 e-07 landslides per square meter per year.

Equation (*2.5*) results in one value of Ripley's K for every combination of dL, dD, and dT. We calculated Ripley's K for dT ranging from 2.5 years to 27.5 years with an increment of 2.5 years, and dL and dD ranging from 10m to 250m with an increment of 10m. Thus, 3750 Ripley K values were generated per landslide inventory.

In simpler cases where it can be assumed that landslides are randomly distributed in space-time, the corresponding expected value for Ripley's K function, for comparison with the observed value, is merely a function of λ_{st} and the size of the cuboid:

$$K\,(dD, dL, dT) = \frac{1}{\lambda_{st}\,.\,n}\sum_{i=1}^{n}\sum_{j\neq 1} E\,[I_{(dD,dL,dT)}\,(d_{ij}, l_{ij}, t_{ij})] \qquad (2.7)$$

However, in our case the expected distribution of landslides in space-time is not random – for instance, landslides are more likely to happen in steeper terrain. We have therefore repeated the calculation of the observed Ripley's K values for all 20 artificial inventories and compared these values to the Ripley's K values from the real inventory.

2.3.4. Edge correction

When examining spatial point patterns near the boundary or edge of a study region, Ripley's K exhibits bias because the likelihood of observing an event decreases when part of the cuboid extends beyond the study area. To address this issue, Ripley proposed a two-dimensional edge correction technique (Ripley, 1979), which we adapted and applied here.

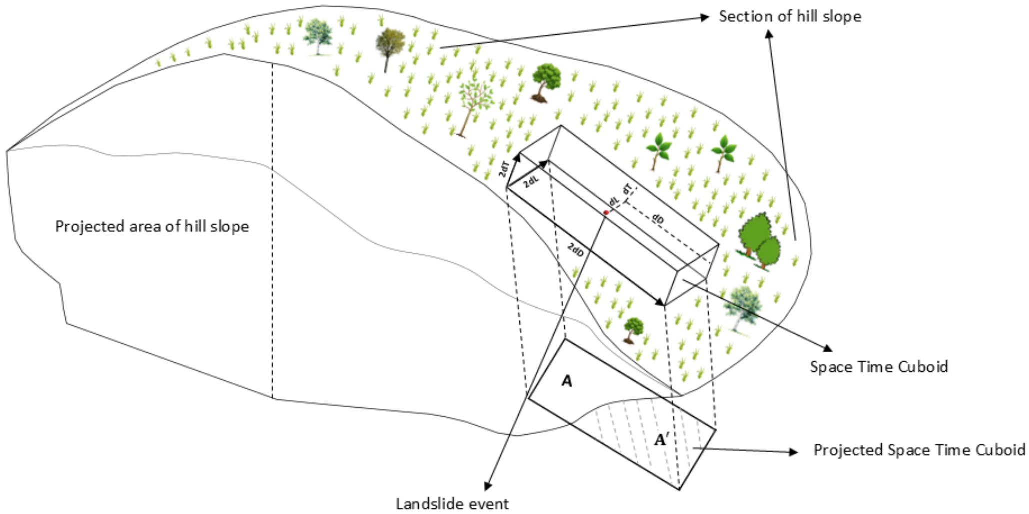

Figure 2.6: Projected space-time cuboid for performing edge corrections. A section of a hill slope is the single slope unit. The projected area of the hill slope is the 2D projected area of the slope unit. A and A' represent the area inside and outside the projected cuboid area, respectively.

Starting from our three-dimensional setting, the space-time cuboid is projected with basic trigonometry to ground level as a 2D rectangle (ignoring the time dimension, Figure 2.6). A spatial weighting factor (w_s) is then calculated, representing the fraction of the rectangle that is in the study area:

$$w_s = \frac{A}{A + A'}, \tag{2.8}$$

where A represents the part of the 2D rectangle that is inside a slope unit, while A' is the area that lies outside a slope unit.

The time weight (w_t) is calculated based on the position of space-time cuboid. If the space time cuboid lies within the time range ($t_{max} - t_{min}$), then w_t is given the value of 1; however, if the space-time cuboid extends beyond this range, the time weight is calculated based on the fractional overlap. The final space time weight w is calculated by multiplying w_s and w_t. We then corrected our Ripley K values for the edge effect by dividing w.

2.3.5. Meta modelling STC values

When the observed Ripley's K ($\hat{K}$) for the real multi-temporal landslide inventory is larger than Ripley's K for the artificial multi-temporal landslide inventories (K), landslides are clustered at separations of dD, dL, dT, and in the opposite case, landslides are dispersed. Using this as a starting point, we define space time clustering (STC), which signifies the tendency of landslides to occur together in space and time (Samia et al., 2020) as:

$$\mathrm{STC}\,(\mathrm{dD},\mathrm{dL},\mathrm{dT}) = \frac{\hat{\mathrm{K}}\,(\mathrm{dD},\mathrm{dL},\mathrm{dT})}{\mathrm{K}\,(\mathrm{dD},\mathrm{dL},\mathrm{dT})} - 1 \qquad (2.9)$$

STC > 0 indicates clustering, while STC < 0 indicates the dispersion of landslides. Since we have 20 artificial multi-temporal landslide inventories, we have 20 values of STC for every combination of dD, dL, and dT. This allows us to perform confidence testing on whether STC is larger or smaller than zero and to calculate an average of the 20 STC values for every combination of dD, dL, and dT.

Samia et al. (2020) fitted an exponential decay function to his similarly calculated STC values to summarize the impact of time and Pythagorean distance on STC. For more flexibility, we used the Generalized Additive Model (GAM) to predict STC values using dD, dL, and dT as independent variables. GAM can handle complex and non-linear relationships between response and independent variables (Hastie & Tibshirani, 2014). Concretely, we fitted the following equation to our STC values:

$$\mathrm{STC} = \beta_0 + f(\mathrm{dD}) + f(\mathrm{dL}) + f(\mathrm{dT}) + e, \qquad (2.10)$$

where β_0 is the value of the intercept, e is the model error, and f(dT), f(dL), f(dD) represent smooth nonlinear functions of dT, dL and dD, respectively.

2.4. Results

2.4.1. Validity of Simulated annealing approach

Simulated annealing results (Table 2.1) revealed a low overall error (4.79%), confirming that the simulated inventories closely match the real landslide inventory. From the four similarities that we sought (mean slope, standard deviation of slope, mean aspect, and standard deviation of aspect), the median error of the mean of slope is 18.24% - much higher than the other errors. This is because of a few landslides that occurred on rare very steep terrain in the real multi-temporal landslide inventory. The simulated annealing process did not often randomly place artificial landslides in these rare locations before the process timed out.

Table 2.1: Simulated annealing errors for the four aspects of the real inventory that were requested to be replicated in each artificial inventory

Parameter	**Median error in the 20 artificial inventories**
Error in the mean of slope	18.24%
Error in the mean of aspect	0.07%
Error in the standard deviation of slope	0.80%
Error in the standard deviation of aspect	0.06%
Overall error	4.79%

2.4.2. Empirical STC values

STC (i.e., the measure of clustering) decreases with increasing dT, dL and dD (Figure 2.7). The predicted STC value from the GAM model when dT, dL, and dD are all equal to zero is 47.26. In other words, landslide susceptibility is 47 times higher immediately after earlier and nearby landslides occur. STC decreases faster with increasing dL than with increasing dD (Figure 2.8). To assess model performance, we analysed the statistical significance of GAM, which showed significant relationships between STC and the predictors dT, dL, and dD with a p-value less than 2e-16. The model achieved a high adjusted R^2 value of 0.98. For comparison, a linear model also showed a general decrease in STC with an increase in spatial and temporal distances, albeit without capturing the nonlinear trend in the data.

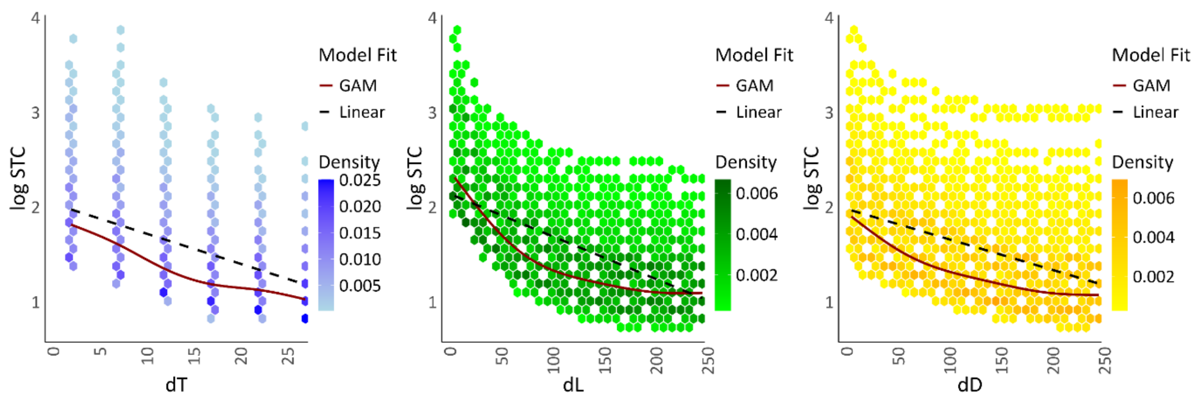

Figure 2.7: Hexbin density, GAM and Linear model trend for log STC and other predictors (dT, dL, dD).

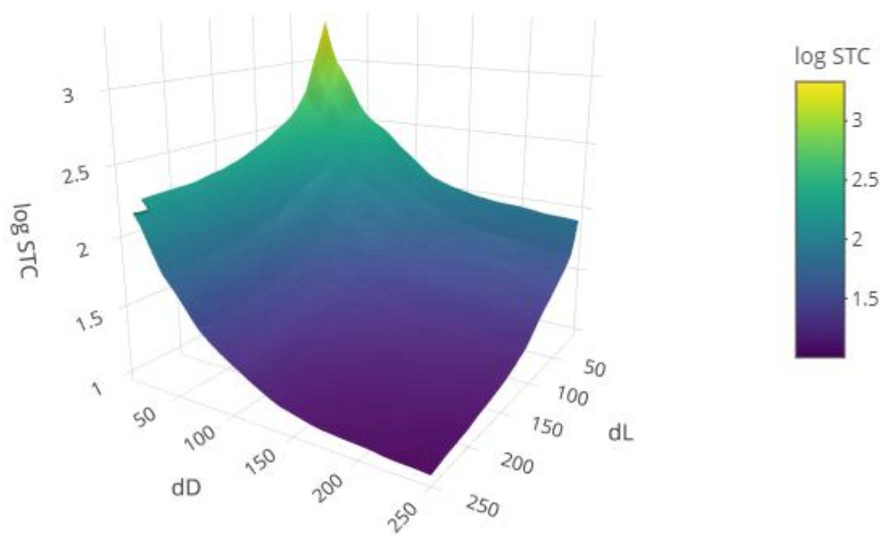

Figure 2.8: Surface plot showing variation of log STC as a function of downslope and lateral distance.

2.5. Discussion

2.5.1. Path dependency quantification

The quantification of LPD using Ripley's space-time K function indicates that path dependency (represented by the STC measure) decreases non-linearly as time, lateral, and downslope distance between landslides increase, indicating a positive but diminishing influence of nearby landslides on subsequent landslide susceptibility (Samia et al., 2020). This confirms the findings by Samia et al. (2020), who reported that STC is influenced by proximity to earlier landslides, and it decays exponentially in space and time. Our analysis reveals that the effect of LPD is stronger in the downslope direction than in the lateral direction. Therefore, we accept our hypothesis that the impact of earlier landslides is more optimally captured in along two perpendicular spatial directions, with the downslope direction showing stronger influence than the lateral direction. A possible reason for the stronger LPD effect in the downslope direction is a positive feedback loop of the soil-landslide system (A. J. A. M. Temme, 2021b) in the downslope direction. As landslides move downslope, they smear the soil, thus creating weakly permeable soil layers that decrease the water permeability in the soil. This results in water saturation, which increases the soil's pore pressure, making the hillslope susceptible to future landslides in a downslope direction (Parry et al. 2000; Duzgoren-Aydin and Aydin 2006). Our findings are consistent with this theory, but do not prove it.

The nonlinear decreasing relationship between STC and the time difference between landslides indicates that landslides that are closer in time are more strongly clustered, whereas landslides separated by a higher temporal distance show reduced clustering. The possible reasons for the decreasing temporal trend are: 1) slope stabilization from vegetation regrowth and repair of soil structure and cohesion, 2) removal of topographic instabilities due to subsequent landslides, and 3) gradual break up of a possible weakly permeable layer by root growth and other forms of bioturbation (Samia et al., 2017b).

2.5.2. Implications for landslides mapping

Most existing landslide inventories are limited to a single period and do not consider the spatial effects in lateral and downslope directions. From such inventories, it is difficult to capture the propagation impact of past landslides on subsequent landslide susceptibility. In the geomorphic environments where the likelihood of landslides happening in the downslope direction is stronger than in the lateral direction, this may lead to spatially biased landslide susceptibility assessment when the LPD effect is not considered. In other words, if the downslope effect on landslides is strong, landslide susceptibility assessment might be biased in the lateral direction, making downslope areas appear safe. On the contrary, if the downslope effect on landslides is overestimated, landslide susceptibility maps might show safe areas to be landslide-prone in the downslope direction. Therefore, there is a need for more multi-temporal, comprehensive, and multidirectional landslide inventories to map landslide susceptibility accurately. The ways for preparing the multi-temporal landslide inventory include conventional and new techniques, including visual interpretation of aerial photographs and remote sensing methods such as Synthetic Aperture Radar (SAR) and other radar technologies (Guzzetti et al., 2012).

2.5.3. Redefining Landslides from purely spatial term to a multi-dimensional process

Traditionally, landslides were considered purely spatial events defined as the gravitational movement of rock, debris, or earth (Gariano & Guzzetti, 2016). The landslide susceptibility assessment was based on static factors such as topography, geology, distance from roads, curvature, and elevation. Apparently, susceptibility is considered time-invariant; in other words, landslides occur independently. However, Samia et al. (2017) claimed that landslides are time-variant; landslide susceptibility may change over time, and the effect decreases with time. Therefore, they gave different meanings to landslides by adding a temporal dimension, as spatial conditions and the temporal impacts of earlier landslides determine the landslide susceptibility. We extended Samia et al.'s (2017) approach by showing that landslide susceptibility is dependent on spatial and temporal conditions and the directional relationship to earlier landslides. In other words, the lateral and downslope directions distinctly affect landslide occurrence. In the dynamic landslide susceptibility framework, spatial, temporal, and directional information of past landslides must be integrated with the predisposing factors for assessing landslide hazards accurately. When landslide happens during rainfall event, susceptibility in and around such landslides is increased at exponential rate. As a result, even a moderate amount of rainfall can trigger subsequent landslides, specifically in the downslope direction where landslide susceptibility is higher. Thus, a landslide is a complex, dynamic, and multi-dimensional process caused by spatial, temporal, and directional force interactions.

2.6. Conclusion

In our study area near Collazzone, Italy, quantification of landslide path dependency shows that the path dependency effect differs in lateral and downslope directions. Therefore, the impact of earlier landslides on landslide susceptibility is best captured when considering these two spatial dimensions in addition to the temporal dimension. Importantly, the downslope direction exerts a stronger influence on landslide path dependency than the lateral direction. Therefore, spatial dimension–specific downslope distance and the temporal dimension should be incorporated in landslide susceptibility models to enhance the prediction accuracy and make the model more dynamic.

Statements and Declarations: The authors declare no competing interests.

Funding: This research is part of H.S. Sodhi's Ph.D. dissertation at Kansas State University and was supported by internal funding from the Department of Geography and Geospatial Sciences, Kansas State University.

Author Contributions: All authors contributed to the study conception and design. Data analysis were performed by Harsimran Singh Sodhi and Arnaud Temme. The first draft of the paper was written by Harsimran Singh Sodhi. All authors contributed by providing feedback, revising, and approving the final version of the paper.

Chapter 3 : Investigating the transient/short-term impact of shallow landslides on soil physical properties

Harsimran Singh Sodhi[1] (corresponding author; harsimransodhi94@gmail.com; harsimran94@ksu.edu), Fabian Ellermann[2] (Fabian.Ellermann@uibk.ac.at), Mauro Rossi[3] (mauro.rossi@irpi.cnr.it), Francesca Ardizzone[3] (francesca.ardizzone@cnr.it), Arnaud Temme[2] (Arnaud.Temme@uibk.ac.at)

[1]Department of Geography and Geospatial Sciences, Kansas State University, Manhattan, Kansas, United States of America

[2]Institute for Geography, University of Innsbruck, Innrain 52f, 6020 Innsbruck, Austria

[3]Consiglio Nazionale delle Ricerche, Istituto di Ricerca per la Protezione Idrogeologica, via della Madonna Alta 126, 06128 Perugia, Italy

Abstract

Landslides cause various forms of damage and environmental changes, including significant alterations to soil properties. Understanding these changes in soil physical properties following a landslide can provide insight into potential mechanisms influencing hillslope instability in areas affected by earlier landslides. In this study, we investigated the effects of landslides on soil physical properties by analyzing samples from 5 landslide sites in Collazzone area near Perugia in Italy, where landslides occurred less than 11 years ago. We compared soil properties between landslide-affected locations and adjacent stable locations to assess temporal and spatial variations. Our results indicated that shortly after a landslide, slide soils exhibit lower bulk density, reduced surface soil resistance, and lower soil organic carbon stocks than in stable locations. In contrast to findings in the literature, hydraulic conductivity differences were not statistically significant. We also found that landslides transiently affect soil physical properties, with differences between slide and stable locations being more immediate after failure, gradually decreasing with landslide age, showing a trend toward convergence within approximately 7-10 years.

Keywords: landslides, soil properties, soil organic carbon, soil hydraulic conductivity, landslide path dependency, soil resistance

Highlights

- Landslide soils remain altered with respect to stable soils for at least 7-10 years
- Landslide soils show reduced soil organic carbon stock in youngest landslide
- In young slides, slide soils has less surface soil resistance than stable soils.
- No significant differences in median grain size between slide and adjacent stable soils.

3.1. Introduction

Landslides are among the most widespread and destructive natural hazards globally (Rossi et al., 2017). They pose a serious threat to human life and infrastructure, causing socio-economic disruption, casualties, and long-term environmental damage (Van Eynde et al., 2017). In forested areas, landslides destroy vegetation and change soil physical, chemical, and biological properties (Błońska et al., 2018; Cheng et al., 2012). Landslides also reshape topography by altering slope height, shape, and steepness (Tao et al., 2020), thereby causing significant soil loss, sediment deposition, and mixing of soil material (Van Eynde et al., 2017).

Beyond the immediate physical impact on the environment, landslides are long-term geomorphic processes that reshape the landscape. Landslides lower slope steepness by transferring soil from the head scarp to the toe, thereby reducing the gradient and soil thickness, and generally increasing slope stability, and decreasing future landslide susceptibility (Prancevic et al., 2020; R. G. Singh et al., 2008; A. J. A. M. Temme, 2021a). However, landslides can also temporarily create conditions that enhance future landslide susceptibility - a phenomenon known as landslide path dependency (Samia et al., 2017b). For instance, landslides may create a thin, weakly permeable soil layer beneath the landslide body that increases water saturation, elevates pore pressure, and increases the likelihood of triggering additional landslides (Duzgoren-Aydin & Aydin, 2006; Parry et al., 2000). This generally occurs in areas with frequent shallow landslides. Landslides can also change soil properties by exposing the underlying parent material (C horizon) by removing the upper soil layers (O, A, and B horizons) and transporting them downslope (Goyal et al., 2022). Such redistribution can result in a mix of pedogenic stages across a landscape - for example, a landslide may remove a Podzol, exposing a Regosol, thus resetting the soil formation process (Geertsema et al., 2009). These changes in soil properties can be long-lasting even after removing the visible damage.

Because of their geomorphic and pedological impacts, landslides also change hydrological conditions, which, in turn, control slope stability. Hydrologically, landslides are caused by one of three conditions: 1) a loss of frictional strength due to the advancement of the wetting front after rainfall or snowmelt (Matsushi et al., 2006), 2) groundwater rise leading to exfiltration through fractured bedrock (Montgomery et al., 2009), and 3) development of positive pore pressure when infiltration raises the piezometric head above a low-conductivity layer (Alessio, 2019). Landslides have been known to change the conditions under which such hydrological mechanisms may occur. For instance, translational landslides can disrupt soil structure, reduce micro- and overall porosity, and decrease hydraulic conductivity, thereby limiting hillslope drainage. This case has been demonstrated by Mirus et al. (2017), who compared the soil properties of a recently landslide-affected hillslope in Washington, United States, with those on an undisturbed hillslope next to the landslide. They found that the slope affected by the landslide had less vegetation, weaker soil structure, lower matrix porosity, and lower hydraulic conductivity than the undisturbed hillslope. This resulted in altered hillslope hydrology, causing earlier seasonal wetting, elevated antecedent pore pressure, and prolonged saturation compared to undisturbed hillslopes. These conditions can lead to repeated landslides on the landslide-disturbed hillslope.

In other words, landslide-caused changes in soil physical and hydraulic properties may contribute to apparent path dependency, the situation in which previous landslides affect future landslide susceptibility. Landslide path dependency was first identified in Collazzone, Italy (Samia et al., 2017b). Samia et al. (2017) found that path dependency in Collazzone is strongest within 10 years following a first landslide and gradually decreases thereafter. These authors suggested that the decrease in path dependency occurs as hillslopes stabilize due to either vegetation regrowth, the recovery of soil structure and soil cohesion, or the removal of topographic instabilities that remained after earlier landslides, or a combination of these factors. Later, Samia et al. (2020) quantified landslide path dependency spatio-temporally, showing that the probability of a subsequent landslide decays to the background level with a characteristic timescale of 17 years and a spatial scale of 60 meters from the previous landslide. Similarly, path dependency has been observed in the Nepal Himalayas, where Roberts et al. (2021) found that the degree of path dependency additionally depends upon the size and type of landslides. However, so far, the underlying mechanism behind landslide path dependency remains enigmatic.

Here, we test the hypothesis that landslides cause transient changes in the properties of soils, which make subsequent landslides more likely in a natural laboratory in Collazzone (Umbria, Italy), where shallow translational landslides without strong vegetation and slope morphological impacts are frequent.

3.2. Study Area

The Collazzone study area (Figure 3.1) covers 80 km^2 in the Perugia Province, located in Umbria, Italy (Galli et al., 2008; Guzzetti, Reichenbach, et al., 2006) in the river Tiber catchment. The area's elevation is between 145m to 634m above sea level, and the slope steepness has an average value of about 10° (Guzzetti et al., 2009). The terrain is hilly, with asymmetrical valleys, and slope morphology is controlled by lithology and attitude of bedding, and exhibits gravel, sand, clay, travertine, sandstone, marl, and limestone from the Lias to Holocene (Guzzetti, Reichenbach, et al., 2006). Soil thickness ranges from a few decimeters to 1 meter, having a fine to medium texture and a xeric moisture regime.

Most precipitation is in October and November, with an average rainfall of 884mm from 1921 to 2001. Many landslides have been recorded in Collazzone, ranging from large, deep-seated landslides to small, shallow ones (Guzzetti et al., 2009). Most landslides are triggered by events such as intense, prolonged rainfall and rapid snowmelt (Ardizzone et al., 2007; Cardinali et al., 2000).

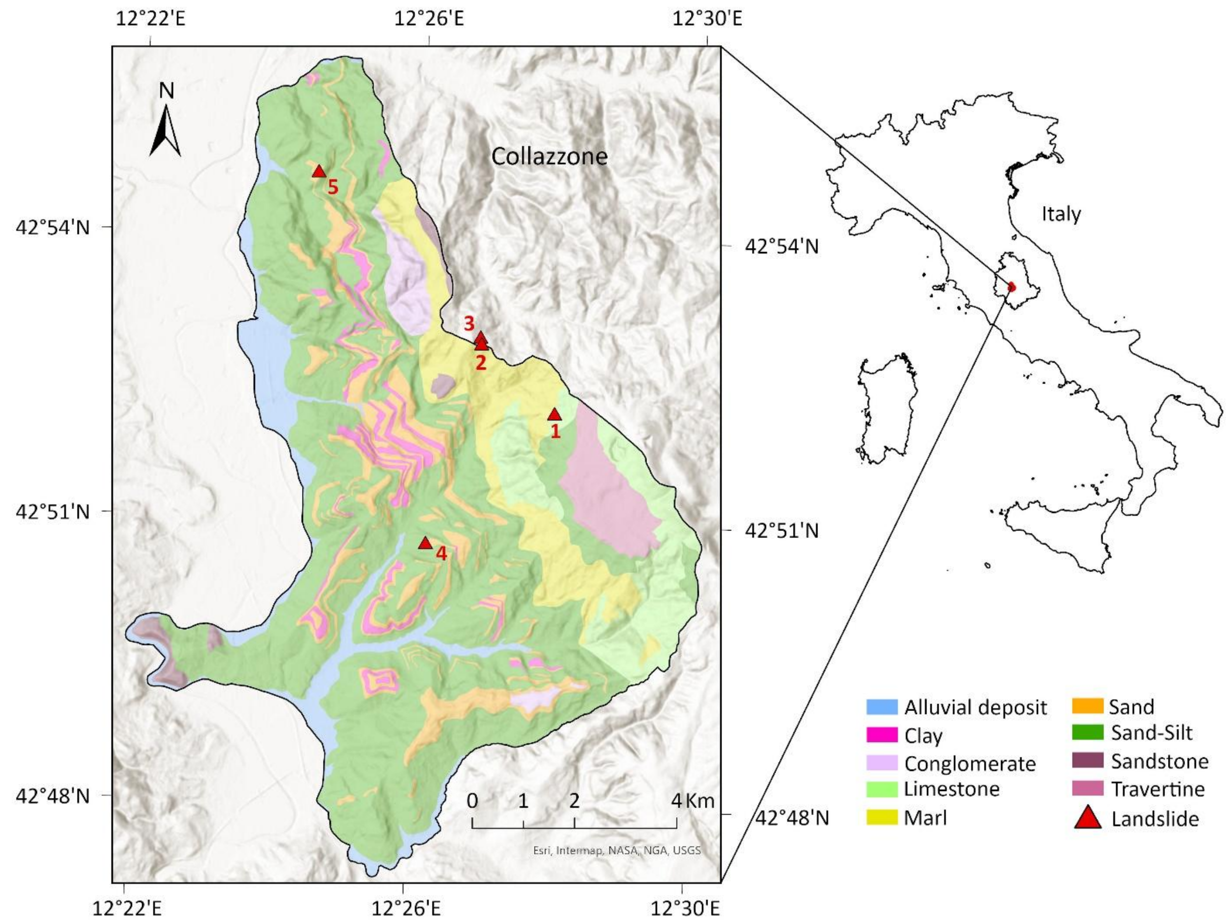

Figure 3.1: Geological map of the Collazzone (Umbria, Italy) overlaid on hillshade. The numbered red triangles (1-5) indicate the shallow landslides where soil samples were collected.

3.3. Methods

3.3.1. Data Collection and Sample Preparation

Five recent landslides of different ages were selected across different landslide-prone slope units in Collazzone. The selection criteria were accessibility, relatively good control over landslide age, and the arable use of the land to ensure that vegetation differences due to landsliding were minor. To estimate the dates of landslide occurrence, we first used Google Earth Pro's time-slider tool to inspect the imagery of pre- and post-landslide events. These estimated time intervals were then refined by analyzing the rainfall records from the nearby Collepepe weather station. In all five cases, there was a single intensive rainfall event in the interval indicated by the aerial photos. We assigned the date of this event to the landslide. Landslide polygons were digitized from the post-landslide Google Earth Pro image. Penetrometer readings were recorded, and soil samples were collected from 2 to 9 July 2024. During fieldwork, most days were cloudy, with rainfall recorded only on 3 July.

Slope steepness of the landslides varied from 8° to 13° and was therefore only moderately steep, and landslide length ranged from 58 to 159 meters. In all five cases, the landslides did not reach the channel network and halted still inside their slope unit. The size of the landslides varied significantly, from 585 m^2 to 3066 m^2. The time between landslide occurrence and soil sampling ranged from about 3 years to up to 10 years (Table 3.1). These five landslides also differ in topographic properties, underlying soil and geological settings. Landslide 1 is developed on limestone-derived soils, landslide 2 and landslide 3 on marl, landslide 4 on sand-silt, and landslide 5 on sandy material.

Table 3.1: Details of landslides with climate based predicted landslide dates, time lag to soil sampling, landslide size, topographic properties, lithology and soil texture

Slide	Location	Date of occurrence	Age of landslide (y)	Age of precursor landslide (y)	Size (m^2)	Slope	Landslide Length (m)	Lithology	Texture
L1	42.8687° N, 12.4652° E	07-2024	10	>77	1178	8°	58	Limestone	Silt
L2	42.8809° N, 12.4471° E	12-2017	6.6	None known	1163	12°	65	Marl	Silt
L3	42.8816° N, 12.4473° E	08-2020	3.9	6.6	585	13°	68	Marl	Silt
L4	42.8455° N, 12.4357° E	07-2014	10	>47	3066	9°	124	Sandstone - siltstone	Silt
L5	42.9103° N, 12.4073° E	09-2021	2.8	3.9	1994	12°	159	Sandstone	Silt-loam

For each landslide, four locations were selected: two inside the landslide (which we called 'slide') and two outside (which we called 'stable'). A pair of slide and stable locations were selected both at the top and at the bottom of each landslide (Figure 3.2). At each location, soil samples were collected from the surface and at 30 cm depth using a cutting ring sampler to quantify soil physical properties (Figure 3.3). We hypothesize that there is a significant difference in soil properties between the slide and stable locations in each slide-stable pair. Specifically, we expect higher bulk density, lower soil organic carbon, and lower soil hydraulic conductivity at slide locations than at stable locations. In contrast, we hypothesize that soil texture does not differ significantly between slide and stable locations.

Similarly, soil penetrometer readings were taken between the slide and stable locations at both top and bottom positions, with measurements taken at a mean spacing of approximately 2 meters to capture the possible impact of sliding on soil resistance. We hypothesize that slide locations have lower soil resistance than stable locations.

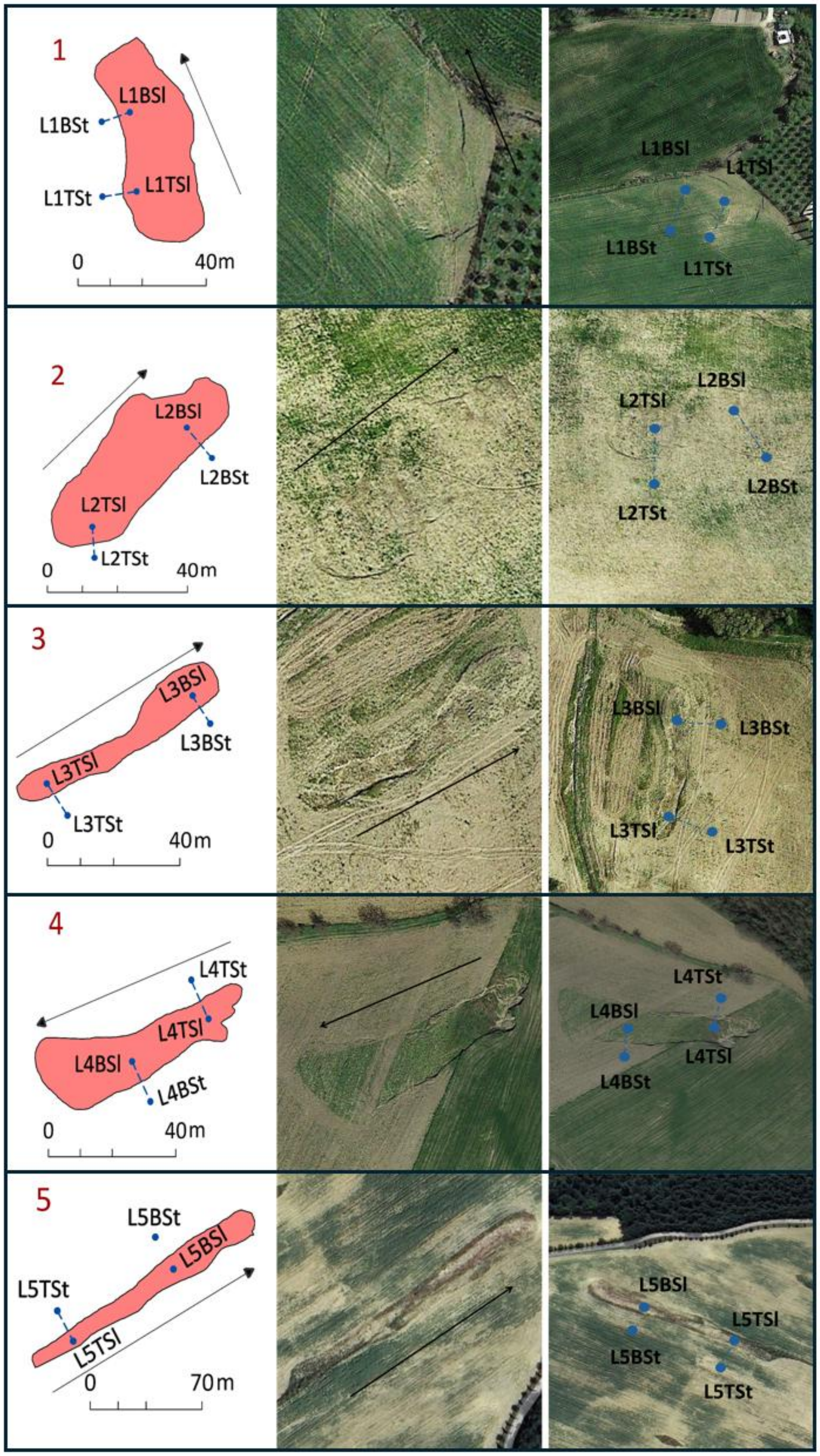

Figure 3.2: Soil sampling locations and penetrometer transects across five landslides (1-5) in Collazzone (Italy). For each landslide, the left panel shows the geometry, and the central and right panels show the aerial imagery of the corresponding landslide. Blue dots in the right panel are the soil sampling locations, and blue dashed lines indicate the penetrometer transects

extending from stable to slide (landslide-affected) areas. Codes indicate landslide ID, position, and location: L1TSl = landslide 1 Top-Slide, L1TSt = Top-Stable, L1BSl = Bottom-Slide, L1BSt = Bottom-Stable (similarly up to L5). Black arrows indicate the direction of a landslide.

Figure 3.3: Procedure to take soil samples at the landslide site. A) Collection of surface soil samples, B-C) Excavation of a 30cm deep pit to access subsurface soil, D) Sampling of soil from 30cm depth below the ground surface.

Laboratory analysis followed the procedures outlined by Blume et al. (2011) to measure sample mass, volume, bulk density, and soil organic carbon (SOC) stock. Before analysis, soil samples were contained in steel cylinders or plastic tubes and stored until measurements in waterproof plastic wrapping in the refrigerator at 2 to 4°C. Outer surfaces were then cleaned, and excess material was removed to create an even surface without disrupting the soil structure. Following cleaning, the ring diameter, ring height, and unfilled height were measured to calculate the soil sample volume and surface area. Weight was measured in the field-fresh state. Samples were then dried at 40°C for three days inside the steel cylinders or plastic tubes, followed by weighing. This preparatory step is recommended by Blume et al. (2011) as it prevents biological and chemical alterations to soil samples.

3.3.2. Saturated hydraulic conductivity and bulk density measurement

The hydraulic conductivity of the soil samples was determined using the Ksat system based on Darcy's law (Meter Group, 2025) with water temperature maintained at 10°C. The samples were saturated in their rings for three days using a base plate with a coffee filter inside the water container to prevent material loss. Measurements were repeated three times. Ultimately, the best-fitting curve measurement was selected, followed by weighing the samples in their saturated state. Following Ksat measurements, samples were transferred into crucibles and dried at 105 °C for three days to ensure complete water evaporation and uniform drying (Blume et al., 2011). Following drying, samples were cooled in a desiccator and weighed. Samples were then sorted and sieved into fine earth (<2mm), coarse fragments (stones), and coarse organic material fractions using the procedure given by Blume et al. (2011). Each fraction was weighed, and the bulk density was calculated using the Blume et al. (2011) procedure.

3.3.3. Loss on ignition and soil organic carbon stock

To determine loss on ignition, a random sub-sample (approximately 8 g) of the dried fine earth fraction was weighed and carefully grinded. Samples were placed in a muffle furnace at 450 °C for 5 hours. Then the samples were weighed. This procedure is a modification of the Blume et al. (2011) method and avoids 550 °C heating to prevent thermal alteration of the samples, which contained marls and limestones from which carbonates could potentially oxidize. Water content, loss on ignition, and residue on ignition (expressed as mass percentage) were calculated, and soil organic carbon stocks were determined following the approach of Poeplau et al. (2017).

3.3.4. Grain size analysis

The grain size analysis was conducted using a Malvern Mastersizer 3000. Sub-samples from ignited samples were sieved (<2mm) and hydrated using demineralized water to allow clay particles to soak and expand. A small portion of the saturated sample was then transferred into the suspension chamber until an obscuration of about 5-6% was achieved. The remaining aggregates were broken apart through stirrer motion and 60 seconds of ultrasonic treatment at 80% intensity. Three measurements were averaged per sample. The goal was to maintain the standard error between the three measurements below 3% for the d10 and median grain size of the sample, and below 5% for the d90 grain size. To avoid long measurement sessions, d90 standard errors above 5% were tolerated when repeated measurements failed to improve the results, and the overall shape of the grain size distribution (GSD) curves remained similar.

3.3.5. Statistical analysis

A three-way analysis of variance (ANOVA) was applied to evaluate the impacts of landsliding on soil properties. Position (Top vs Bottom), location (Slide vs Stable), and depth (Surface and Subsurface) were used as factors. The response variables included saturated hydraulic conductivity, bulk density, total water content, soil organic carbon stock, grain size distribution, and soil resistance.

3.4. Results

The saturated hydraulic conductivity of the soil samples (Ksat, Figure 3.4**)** varies between slide and stable locations across individual landslides (L1-L5), slope positions (top vs. bottom), and soil depths (surface vs. subsurface). Ksat was higher at slide locations compared to adjacent stable locations, except in landslide 3. Mean Ksat values were more than twice as high at slide locations (147 cm day^{-1}) than at stable locations (63 cm day^{-1}), though this difference was not statistically significant ($p = 0.12$). Similarly, no significant slide-stable differences were observed when interaction terms were included. At the top and bottom slope positions, Ksat was higher at slide locations than at stable locations.

The largest slide-stable contrast was observed at the bottom subsurface, where slide locations showed substantially higher Ksat (253 cm day^{-1}) than stable locations (47 cm day^{-1}; $p = 0.06$).

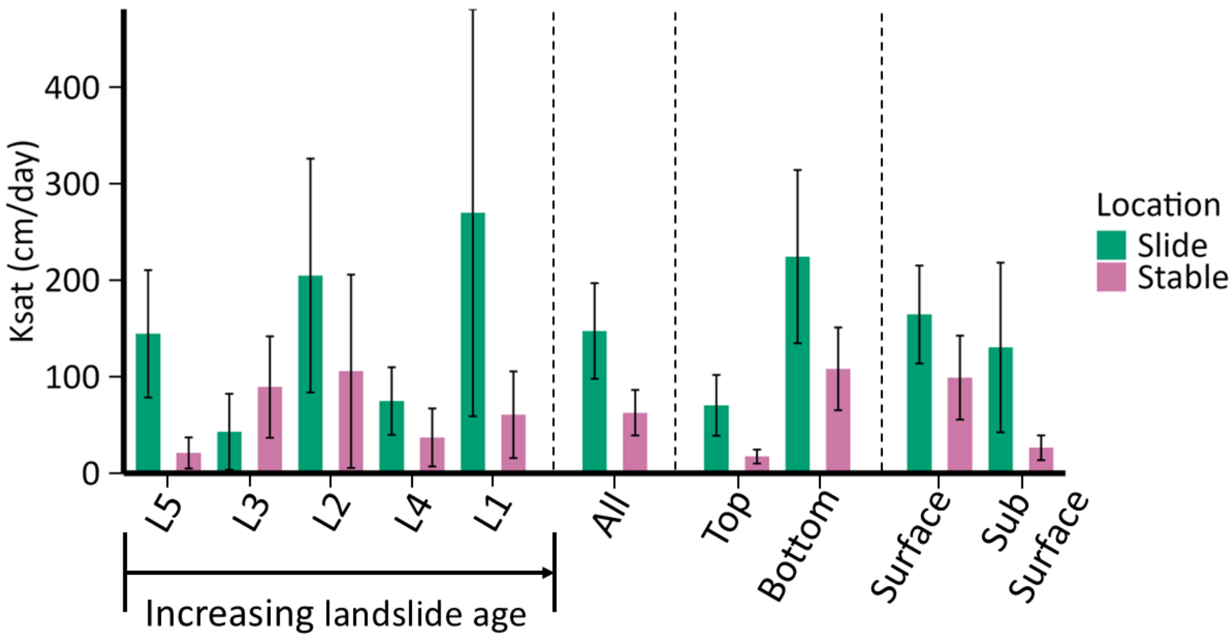

Figure 3.4: Comparison of saturated hydraulic conductivity (Ksat) between slide and stable locations across different landslide sites, slope position, and soil depth. Bars show the mean Ksat values and the error bars represent standard error.

The total water content (TWC, Figure 3.5) does not display a clear trend with increasing landslide age, although the youngest landslide (L5) has the lowest average TWC of all slide and stable locations in the 5 landslides. Slide locations overall show slightly higher TWC (17.4%) than stable locations (15.9%), but the difference is not statistically significant ($p = 0.41$). Also, at the top (i.e., close to scarp) and bottom (i.e., close to toe) locations separately, slide soils have marginally higher TWC than stable soils, but this difference is also non-significant.

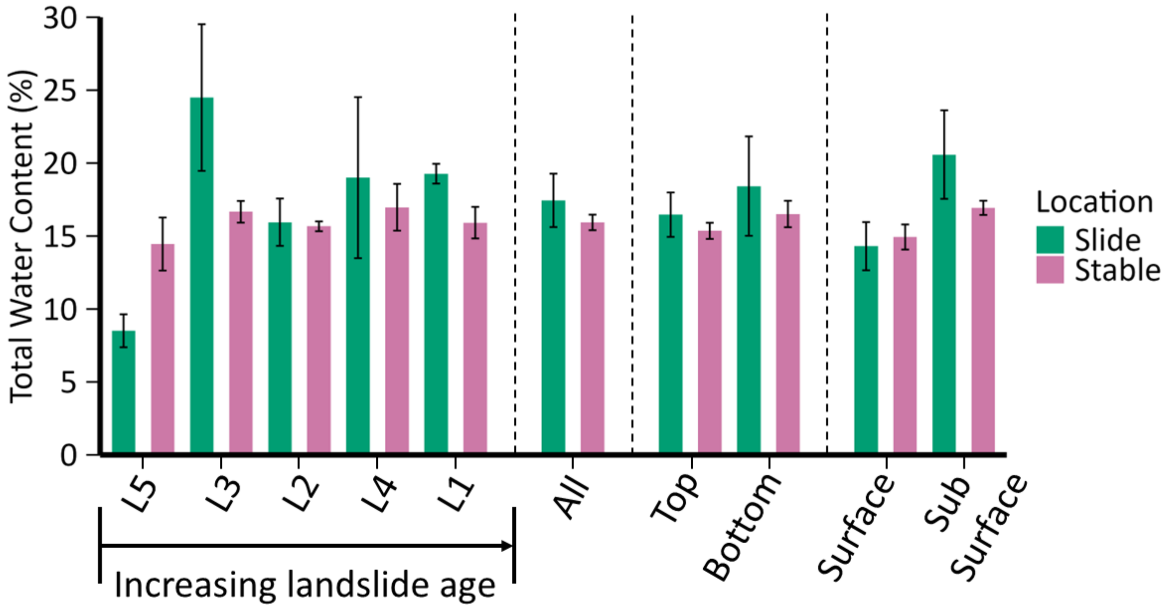

Figure 3.5: Comparison of Total Water content (TWC) between slide and stable locations across different landslide sites, slope position, and soil depth. Bars show the mean TWC, and the error bars represent standard error.

Bulk density (Figure 3.6) was significantly higher at the stable locations (1.48 g cm^{-3}) than at slide locations (1.40 g cm^{-3}; p=0.02). The interaction between position and location was non-significant. At the top and bottom slope positions, bulk density was lower at the slide location than at the stable location. The interaction between depth and location revealed distinct patterns. At the surface, bulk density differences between slide (1.38 g cm^{-3}) and stable (1.37 g cm^{-3}) locations were negligible ($p = 0.88$). However, in the subsurface, stable soils (1.59 g cm^{-3}) have significantly higher bulk density than slide soils (1.43 g cm^{-3}; $p < 0.05$).

At the top position, surface soils exhibit no significant bulk density differences, while subsurface soils at stable locations (1.61 g cm^{-3}) have higher bulk density than slide locations (1.50 g cm^{-3}; $p = 0.09$). A similar pattern is found at bottom positions, where subsurface soils again showed significantly lower ($p < 0.01$) bulk density at slide locations (1.35 g cm^{-3}) than stable locations (1.57 g cm^{-3}).

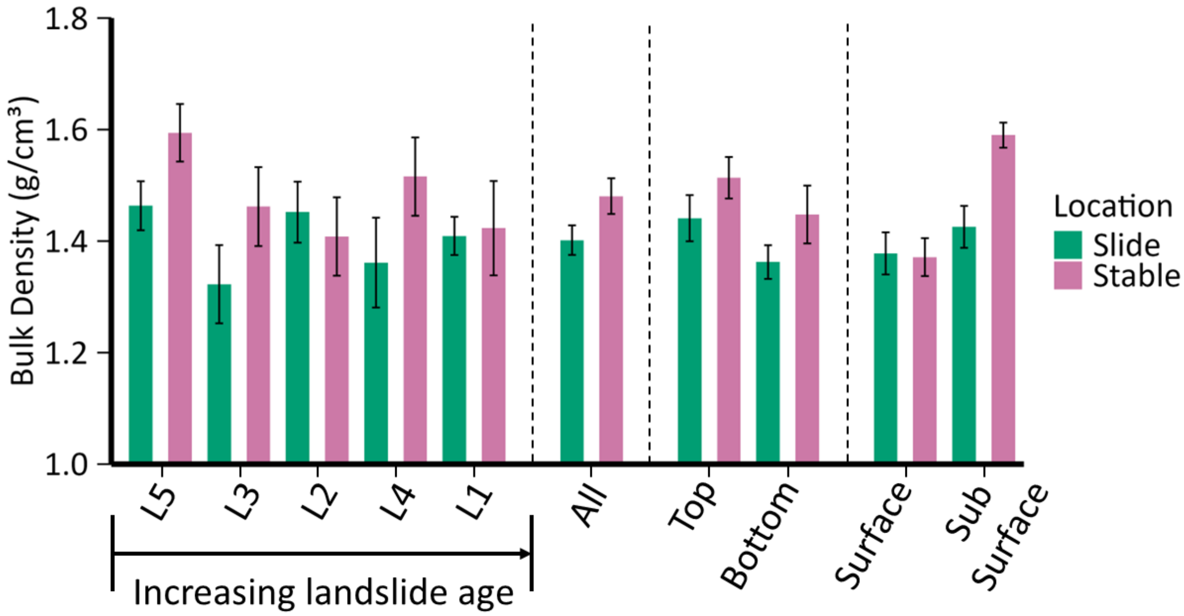

Figure 3.6: Comparison of bulk density between slide and stable locations across different landslide sites, slope position, and soil depth. Bars show the mean bulk density and the error bars represent standard error.

The difference in soil organic carbon (SOC) stock (Figure 3.7) between slide and stable locations was greatest at the youngest slide (L5), where slide location exhibited lowest SOC stock. The difference in SOC stock was minimum at the oldest slide (L1). At both top and bottom positions, stable locations had higher SOC stocks than slide locations; however, the differences were not statistically significant. A similar pattern was observed for the interaction between soil depth and location.

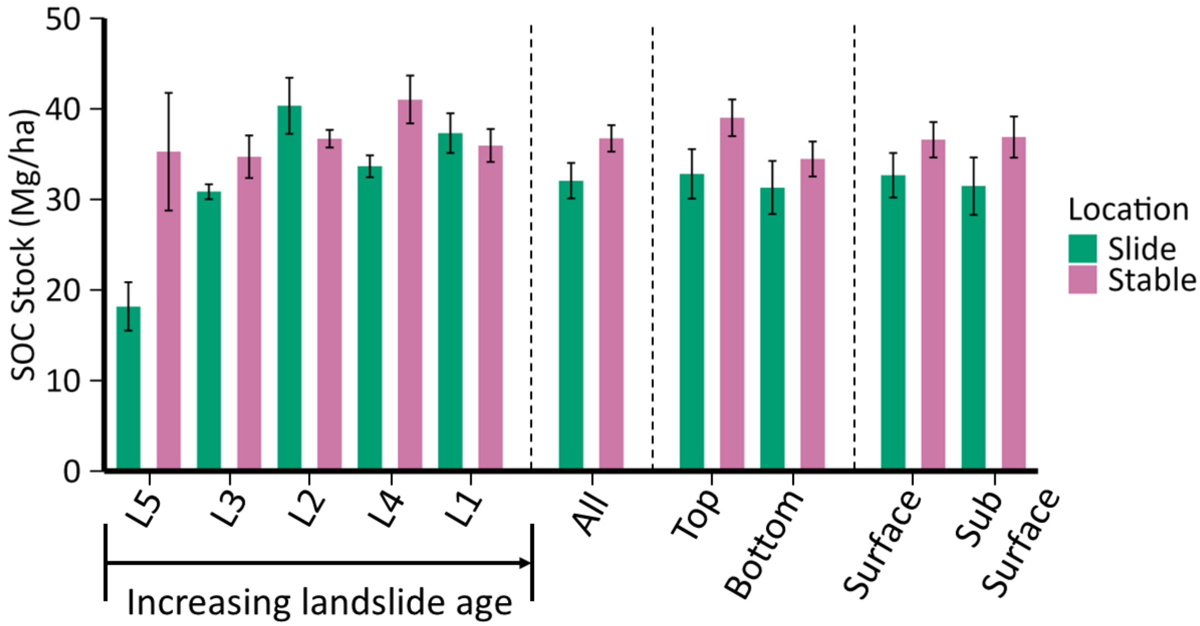

Figure 3.7: Comparison of SOC stock between slide and stable locations across different landslide sites, slope positions, and soil depths. Bars represent the mean SOC stock, and error bars indicate the standard error.

As expected, median grain size (Figure 3.8) did not differ significantly ($p = 0.18$) between the slide (18.4 µm) and stable landslide (12.6 µm) locations. Similarly, no significant differences were observed between the top and bottom positions or between surface and subsurface, and all interaction terms were non-significant.

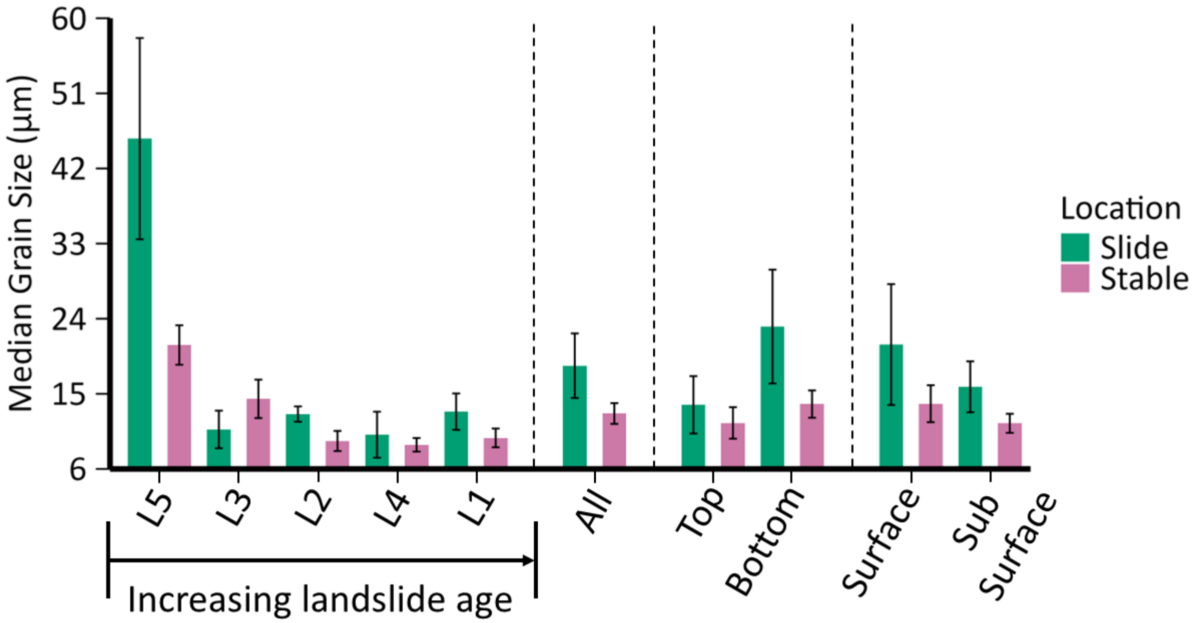

Figure 3.8: Comparison of median grain size between slide and stable locations across different landslide sites, slope positions, and soil depths. Bars represent the mean median grain size, and error bars indicate the standard error.

The penetrometer readings (Figure 3.9) reveal distinct and consistent patterns and differences in soil resistance across different positions between stable and slide locations for all landslides. In general, soil resistance is higher at the stable landslide locations compared to slide locations, a pattern observed at both top and bottom landslide positions. Landslide 5, the youngest landslide, exhibits the highest mean surface soil resistance at the top position, while the lowest mean surface soil resistance values occur at the top position of Landslide 1, the oldest landslide. The relationship between soil resistance and landslide age varies by position and depth. At the surface of top landslide positions, mean soil resistance values consistently decrease with increasing landslide age. However, subsurface resistance at the top position fluctuates and does not follow this trend. At bottom positions, the trend reverses: surface resistance fluctuates with age, while subsurface soil resistance shows a non-linear increase with landslide age: it rises from the L3 to L2, decreases slightly at L4, and then increases again at the oldest landslide (L1).

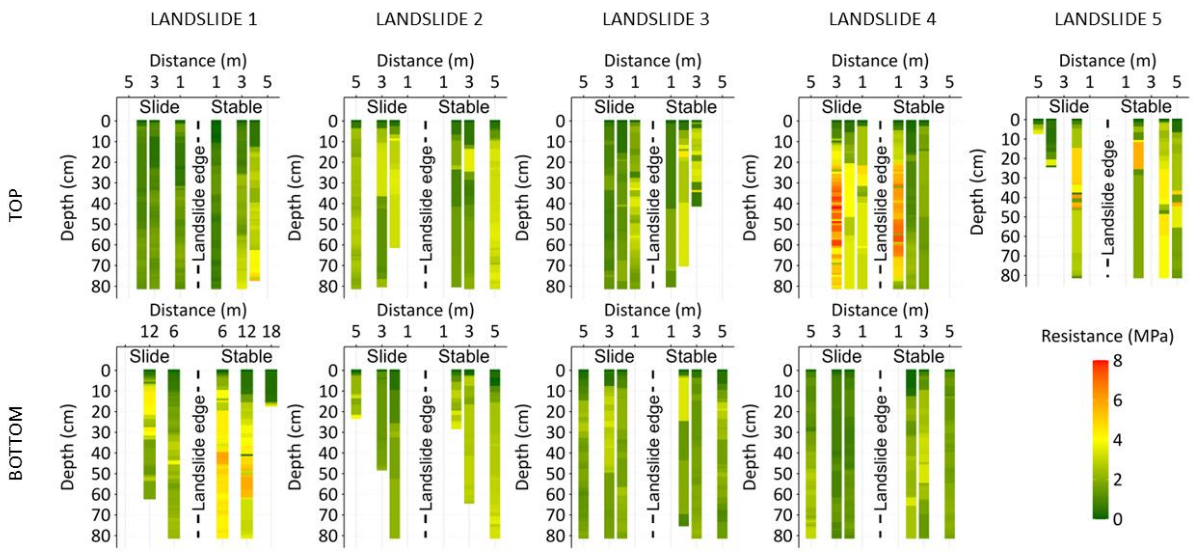

Figure 3.9: Penetrometer-measured soil resistance (MPa) with depth across five landslides. Each plot shows top and bottom positions, except for landslide 5, where only top was measured. The bottom position of landslide 5 was excluded because narrow base and steep scarp prevented accurate penetrometer insertion and stable measurements.

The Pearson correlation matrix (Figure 3.10) highlights a strong negative relationship between bulk density and hydraulic conductivity (r = -0.40). Bulk density also showed weak negative correlations with total water content (r = -0.23) and the median grain size (r = -0.01), and a weak positive correlation with soil organic carbon stock (r = 0.10). Median grain size showed a negative relationship with SOC stock (r = -0.55) and total water content (r = -0.41), and a weak positive correlation with hydraulic conductivity (r = 0.20). Similarly, soil hydraulic conductivity showed a weak relationship with the SOC stock (r = 0.06) and the total water content (r = -0.15). Finally, SOC stock and total water content exhibited a weakly positive correlation (r = 0.23).

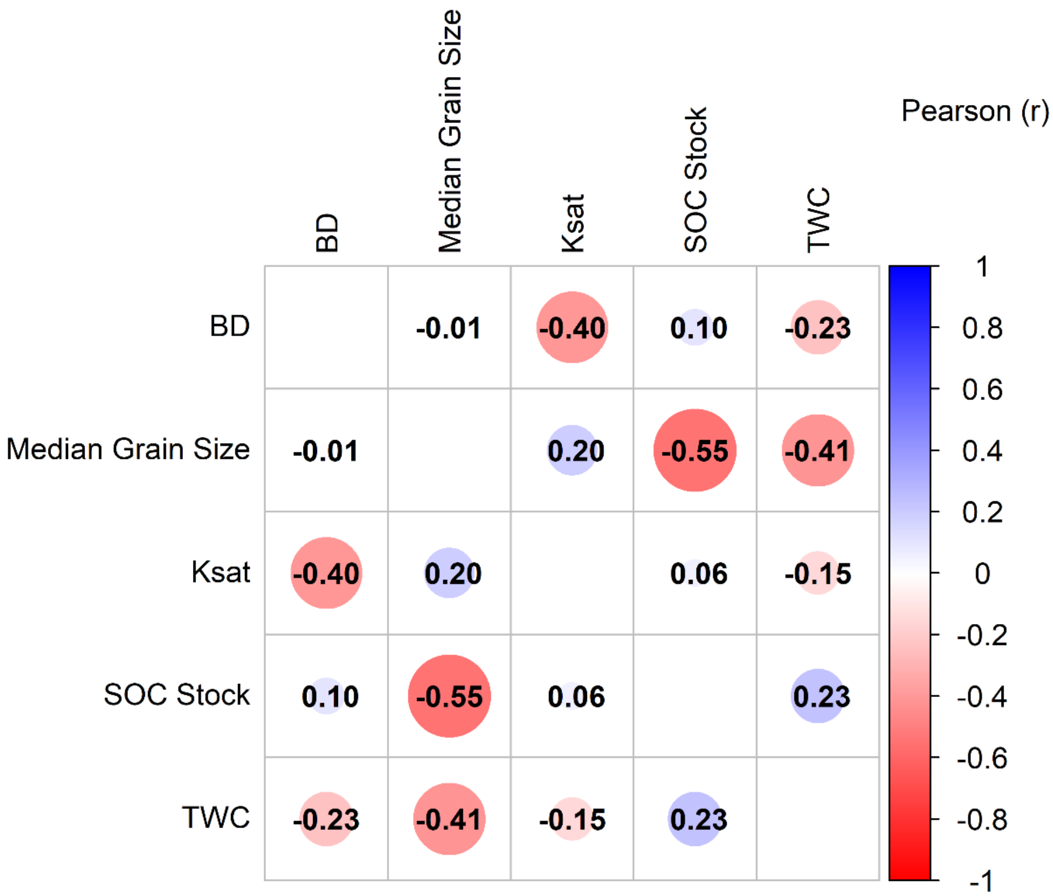

Figure 3.10: Correlation matrix showing relationships among different soil properties: BD (bulk density), Median Grain Size, Ksat (saturated hydraulic conductivity), SOC stock (soil organic carbon stock), TWC (total water content). Positive correlations are shown in blue, and negative correlations are shown in red, with circle size and color intensity proportional to the Pearson correlation value.

Soil properties vary with landslide age (Figure 3.11) at both stable and slide landslide locations, with differences generally most pronounced shortly after failure and decreasing over time. This is most strongly the case for the SOC stock, bulk density, and soil resistance. At younger landslide sites, slide soils contain lower SOC stock (18 Mg ha^{-1} ± 3 Mg ha^{-1}) compared to stable soils (35 Mg ha^{-1} ± 6 Mg ha^{-1}). However, SOC stock at slide location (L1) increases to 37 Mg ha^{-1} ± 2 Mg ha^{-1} after 10 years, converging towards values at stable site (36 Mg ha^{-1} ± 2 Mg ha^{-1}). Similarly bulk density and soil surface resistance are initially lower at slide locations (1.46 g cm^{-3}

± 0.04 g cm^{-3} and 2.4 MPa ± 0.2 MPa) than at stable sites (1.59 g cm^{-3} ± 0.05 g cm^{-3} and 2.8 MPa ± 0.2 MPa), with the difference progressively decreasing after 7 years.

In other cases, TWC, GSD and Ksat show a weaker relationship with landslide age. TWC at younger landslide slide locations is lower (8% ± 1%) compared to stable locations (14% ± 2%). As the landslide age increases, TWC at slide locations exceeds that at stable locations; however, the difference becomes negligible after approximately 7 years. Grain size distribution, expressed as median grain size, indicates that soils at both slide (45.6μm ± 12.1μm) and stable (20.8μm ± 2.4μm) landslide locations are initially poorly sorted. GSD decreases with landslide age, and the differences between slide and stable locations diminish within approximately 4 years. Ksat values exhibit large variation, particularly at slide locations. With landslide age, no specific trend can be highlighted except that 4 out of 5 landslides have higher Ksat at slide locations that the stable locations.

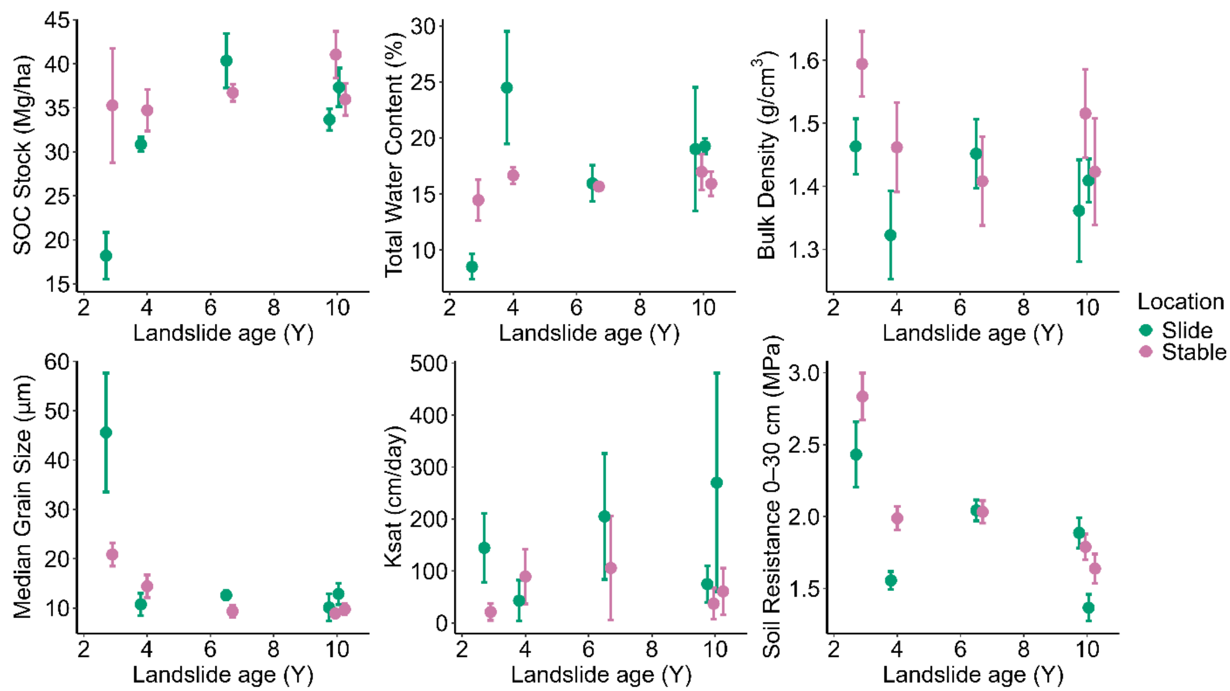

Figure 3.11: Variation in soil properties with landslide age for slide and stable locations.

3.5. Discussion

Among the soil properties we measured (Table 3.2), bulk density, SOC stock, and soil resistance showed the most consistent differences between slide and stable locations. Surprisingly, bulk density was significantly lower at slide locations than at stable locations, directly contradicting our initial expectation of higher bulk density in slide soils. The difference in bulk density between slide and stable locations is mostly in the sub-surface soils ($p<0.05$), whereas at the surface, the difference is negligible. One possible reason for higher bulk density in the sub-surface at the stable locations may be due to natural prolonged compaction by topsoil over time and the development of plow pans caused by prolonged tillage, as Adhikari et al. (2014) reported for Danish agricultural soils. At the slide locations, the lower bulk density in the subsurface layer may then be due to disturbance of this expected pattern during landsliding, by disrupting pre-existing compact layers and increasing pore space through fracturing, cracking, and mixing of soil layers.

A further reason for lower bulk density at the slide locations in the subsurface might be due to greater biodiversity than at stable locations. We found a variety of organisms, including beetles, spiders, mixed insects, and snails, at slide areas, which were more numerous than at stable locations. Zhang et al. (2021) reported that adding organisms such as bacterial manure decreases the soil bulk density. Microbes and insects breed in soil, penetrate it, increase soil porosity, reduce bulk density, and enhance hydraulic conductivity. An initial reduction in bulk density through mixing of soil layers might be stronger and persist longer in this way than without increased biological activity at depth.

Similarly, soil resistance was lower at slide locations than at stable locations, supporting our hypothesis for this property. We expected soil resistance to be lower because penetration resistance decreases with increasing water content (Lardy et al., 2022), and we expected slide locations to have higher water content. Indeed, slide locations had higher total water content than stable locations, but the difference was not significant.

Importantly, the contrasts in bulk density and soil resistance between slide and stable locations were strong in younger slides and diminished strongly with landslide age, becoming minimal after 7-10 years. This suggests that, compared to adjacent stable soil conditions, landslides do affect soil bulk density, soil resistance, and soil moisture content, but these changes are temporary. Soil properties tend to recover until the differences between slide and stable locations eventually disappear.

Table 3.2: Difference in soil properties between slide and stable locations averaged across all 5 landslides, along with corresponding statistical significance. The positive values (+) indicate values are higher at slide locations than stable locations, while negative (-) values indicate values are lower at slide locations compared to stable locations.

Soil Property	Difference between slide and stable locations	p-value
Saturated hydraulic conductivity	+84 cm day^{-1}	0.12
Total water content	+1.5%	0.41
Bulk density	-0.08 g cm^{-3}	0.02
Soil organic carbon stock	-5 Mg ha^{-1}	0.08
Median Grain Size	+5.8µm	0.18
Surface soil resistance	-0.2 MPa	<0.05

We found that total SOC stock was greater at stable locations than in the slide locations with marginal statistical support (p = 0.08); therefore, we provisionally accept our hypothesis, awaiting further data points. Landslides generally reduce SOC stock at the hillslope level by eroding carbon rich soil horizons and exporting it downslope (Błońska et al., 2018). Several researchers have reported lower SOC in soils of recent landslides as compared to undisturbed soils because lower surface soil has low SOC and other nutrients that get exposed and relocated (Goyal et al., 2022; Reddy & Singh, 1993; K. P. Singh et al., 2001; Sparling et al., 2003; Wilcke et al., 2003). This decline is due to geomorphic removal of the organic rich and biologically active soil layer during landsliding, which exposes immature subsoil horizon, and thereby resetting soil development process.

Older slide locations have higher SOC stocks, and the difference with stable locations becomes minimal after 10 years. This finding is consistent with that of Van Eynde et al. (2017), who reported that soil organic content is directly proportional to the age of the landslide. The possible reasons for increased SOC with landslide age are vegetation regrowth, re-accumulation of organic inputs (e.g., leaf litter, plan residues, and root biomass), soil structure stabilization (Schomakers et al., 2018). This indicates that the impact of landslides on SOC is transient and that soil organic carbon gradually recovers as the ecosystem stabilizes with time. The original decrease in SOC stock during or soon after a landslide occurs may be due to mixing with the deeper subsurface during sliding (although we still observe lower SOC stocks in slide locations than stable locations at 30 cm under the surface), or due to accelerated decomposition of organic matter after a slide happens - possibly due to the observed lower bulk density and corresponding better aeration of slide locations relative to stable locations.

Saturated hydraulic conductivity was higher at slide locations than at adjacent stable locations, although the difference was non-significant, so we fail to accept our hypothesis. This pattern is opposite to that shown in the study by Mirus et al. (2017) at a landslide location in Mukilteo (Washington, USA), who observed higher hydraulic conductivity at stable locations than slide area. The difference may be due to variations in geomorphic settings. Moreover, lower soil resistance and bulk density may have contributed to higher hydraulic conductivity in slide areas than in nearby stable landslide locations. Saturated hydraulic conductivity was lower at the landslide initiation area (top position) compared to the zone of accumulation (bottom position) for both slide and stable landslide locations. However, bulk density was higher at the top than at the bottom position for the slide as well as the stable locations. The elevated bulk density at the head scarp likely reduced soil porosity, resulting in lower hydraulic conductivity at the head scarp (Frene et al., 2024).

Median grain size, an indicator of soil texture, did not differ significantly between slide and stable locations. Therefore, for this type of landslides, soil texture appears to remain unchanged. Apparently, landsliding does change aggregate-level soil physical properties by redistributing soil materials, but fails to affect the textural mix involved in moving. In our case, there was no clear textural differentiation between soil horizons at stable locations, and thus no possibility that mixing during sliding would erase this difference. It is conceivable that in other settings, where soils are stable for long enough to develop textural differentiation, for instance with an A-E-Bt horizonation, landsliding would impact surface and subsurface median grain size by erasing this differentiation. Such impact would likely be transient only over timescales of thousands of years.

Overall, our results suggest that landslides in Collazzone substantially and transiently impact soil physical properties, while leaving soil texture largely unchanged. Slide soils differ from adjacent stable soils shortly after the landslide, but for some properties (SOC stock, surface soil resistance, and bulk density) this difference progressively diminishes with increasing landslide age, becoming minimal after 7-10 years after the landslide, indicating convergence of slide soil properties toward stable soil conditions (Figure 3.12**Figure *3.12***). This temporal evolution of soil properties provides a physical basis for understanding patterns of landslide recurrence in Collazzone. Earlier, Samia et al. (2017) reported that landslides in Collazzone increased susceptibility to subsequent landslides for about 10 years following the initial failure. Our results suggest that transient changes in soil physical properties caused by landslides can be the reason for elevated susceptibility during post-landslide window. Reduced bulk density, soil resistance, lower SOC, and more water content at slide locations collectively reduced soil strength, soil cohesion, shear stress, thereby increasing the landslide susceptibility. As soil properties gradually recover and the difference between soil properties at slide and stable locations becomes minimal, the landslide susceptibility might decline back to its previous levels, determined by semi-permanent location properties such as slope steepness, concavity, and the lithological properties of the region.

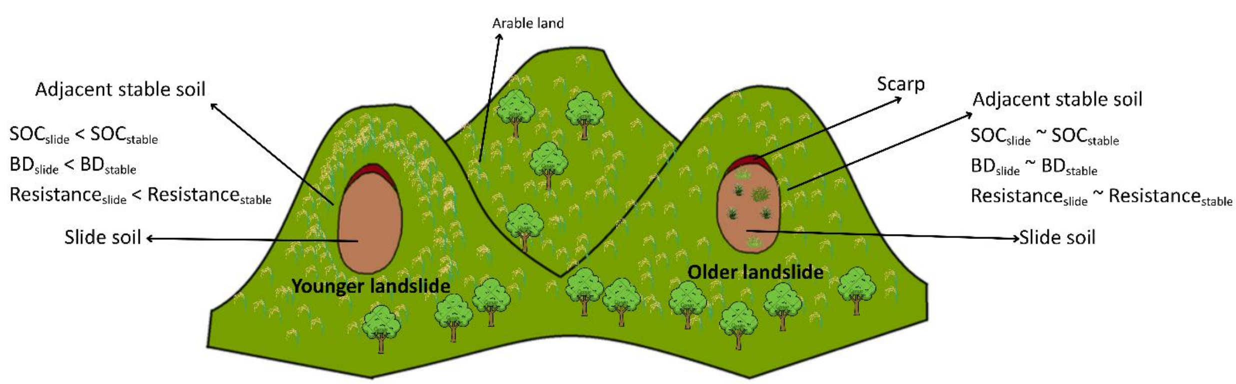

Figure 3.12: Conceptual diagram illustrating transient impact on soil organic carbon (SOC) stock, bulk density (BD), and surface soil resistance.

3.6. Conclusion

This study demonstrated that landslides in Collazzone significantly altered soil physical properties across slope positions, locations, and depths, over a timescale of up to 10 years. Shortly after landslides, soils within slide locations exhibit lower bulk density, soil resistance, and reduced soil organic carbon stocks compared to nearby stable soils, which may increase their susceptibility to follow-up landsliding. However, these differences gradually decrease with landslide age, and most soil properties at slide locations converge with those in stable locations within 7 to 10 years following the landslide. This transient recovery provides a process-based explanation for empirical observations of landslide path dependency in Collazzone, where landslide susceptibility remains elevated for a decade following initial failure.

CRediT authorship contribution statement

Harsimran Singh Sodhi: Writing – review & editing, Writing – original draft, Methodology, Visualization, Validation, Conceptualization, Formal analysis, Data curation, Investigation. **Arnaud Temme**: Writing – review & editing, Visualization, Conceptualization, Supervision, Methodology, Project administration. **Fabian Ellermann:** Writing – review and editing, Data curation. **Mauro Rossi:** Writing – review & editing, Resources, Validation. **Francesca Ardizzone:** Writing – review and editing, Resources, Validation.

Funding

This research forms part of H.S. Sodhi's Ph.D. dissertation at Kansas State University and was supported by internal funding from the Department of Geography and Geospatial Sciences, Kansas State University as well as internal funding from the University of Innsbruck, Austria.

Declaration of competing interest

Arnaud Temme serves as an Editor of Catena. This author had no involvement in the peer-review process of this article and had no access to information regarding its review. The remaining authors declare no competing interests.

Data availability

The data of this study are available from the corresponding author upon request.

Chapter 4 : Do large earthquakes impact landslide properties and their path dependency?

Harsimran Singh Sodhi[1], Sarah J. Boulton[2], Douglas Goodin[1], Mauro Rossi[3], Francesca Ardizzone[3], Arnaud Temme[4]

[1]Department of Geography and Geospatial Sciences, Kansas State University, Manhattan, Kansas, United States of America

[2] Centre for Research in Natural Hazards and Risk Reduction, School of Geography, Earth and Environmental Sciences, University of Plymouth, Plymouth, PL4 8AA, UK

[3]Consiglio Nazionale delle Ricerche, Istituto di Ricerca per la Protezione Idrogeologica, via della Madonna Alta 126, 06128 Perugia, Italy

[4]Institute for Geography, University of Innsbruck, Innrain 52f, 6020 Innsbruck, Austria

Abstract

Earthquakes have a significant impact on landslide occurrence, including immediate triggering and preconditioning for future landslides by altering slope stability conditions. There has been significant research investigating the impact of earthquakes and subsequent preconditioning on landslide susceptibility; however, the impact of earthquakes on landslide path dependency (LPD) across different geomorphic settings remains unexplored. This study compares the impact of earthquakes on landslides and their path dependency in Collazzone (Italy) and the central region of Nepal. We analyzed the impact of earthquakes on the geometry and topographic properties of landslides, as well as on the properties of landslides that cause follow-up failures and those that do not. In Collazzone, landslide occurrence did not increase significantly after recorded earthquakes, whereas in Nepal, there is a significant increase in monsoon-triggered landslides after the 2015 earthquakes, which then decreases to pre-earthquake level within 4 years. Moreover, the 2009 earthquake significantly affected key landslide properties and their path dependency, leading landslides in Collazzone to shift to lower elevations. However, in Nepal, post-2015 landslides were larger, steeper, and occurred at higher elevations than pre-2015 landslides, indicating that the Nepal earthquake tended to precondition slopes near ridges, where many monsoon-triggered landslides occurred, whereas in Collazzone, rainfall-triggered landslides tend to occur near valleys

following the earthquake. In both regions, landslides that followed path dependency were larger than those that did not. Moreover, in Collazzone, we found that path dependency strengthened after an earthquake, unlike Nepal. In Collazzone, lower shaking intensity (4-5 MMI) due to 1997 and 2009 earthquakes likely preconditioned slopes near earlier landslides, increasing overlaps and strengthened LPD, while in Nepal, earthquakes were strong (7-8.6 MMI) causing widespread hillslope damage, triggering landslides both near and even farther from earlier landslides, and did not overall increase LPD. Therefore, the impact of earthquakes on LPD depends upon their intensity and the area's geomorphology.

Keywords: earthquakes, landslide path dependency, preconditioning, landslide properties, shaking intensity

4.1. Introduction

Landslide mitigation generally depends upon landslide hazard assessment, which forecasts the statistical likelihood of future landslides occurring at particular locations (Guzzetti, Reichenbach, et al., 2006). Reliable hazard assessment requires a clear understanding of factors, both natural and anthropogenic, that control landslide occurrence. These factors can broadly be categorized into conditioning and triggering factors. Conditioning factors represent the topographic, hydrological, anthropogenic, and environmental factors, which include slope angle, elevation, aspect, distance to drainage, distance to roads, land cover, among many others (Meena et al., 2022); while triggering factors are events acting on the hillslope, including intensive rainfall or earthquakes, that directly initiate a landslide (Rodríguez et al. 1999; Wang and Sassa 2003; Malamud et al. 2004; Mugagga et al. 2012; Regmi et al. 2013; Prokešová et al. 2013; Jaafari 2024). The relationships between causes and triggers are complex because a single triggering factor can produce different responses in landslide occurrence due to interactions among conditioning factors and legacy effects from past events (He et al., 2022; Phillips, 2006).

Landslide susceptibility assessments have been commonly considered time-invariant, i.e. landslide susceptibility is assumed to remain constant over human and infrastructure relevant timescales . However, recent studies show that landslide susceptibility changes over time and may depend upon past landslide events as well as external triggers. Samia et al. (2017) demonstrated that the locations of earlier landslides and the time interval between landslides affect future landslide susceptibility. This effect, in which future landslide susceptibility increases due to nearby earlier landslides, was termed landslide path dependency (LPD) (Samia et al., 2017b). Building on this work, Samia et al. (2017b) quantified the path dependency effect using a follow-up landslide fraction index, showing that landslide susceptibility increases 15-fold immediately after a landslide. Moreover, Samia et al. (2020) found that the path dependency, initially higher, decreases exponentially by a factor of e every 17 years and every 60 m of horizontal distance from earlier landslides, ultimately reaching a background value where path dependency is negligible. This effect is also seen in the Nepal Himalayas, where Roberts et al. (2021) showed that landslide path dependency is not only due to the spatial-temporal association of earlier landslides but also depends on the total number of landslides, the size of the study area, and the size/type of the landslides. Therefore, it was shown that LPD exists in different geomorphic settings.

In addition to LPD, earthquakes as well as external triggers may significantly affect future landslide susceptibility and occurrence. Large earthquakes ($M_w \geq 6.6$) can trigger thousands of landslides, causing significant damage to life, destroying infrastructure, and blocking rivers (Bayram et al., 2023; M. Kobayashi, 2014; Xu et al., 2022). For example in China, the Haiyuan (1920), Wenchuan (2008), Lushan (2013), and Jiuzhaigou (2017) earthquakes cumulatively triggered more than 69500 landslides, causing damage to life and property (Lu et al., 2022). More importantly for this study, Marc et al. (2015) studied the post-trigger evolution of landslide rates after four significant earthquakes (1993 Finisterre, Papua New Guinea; 1999 ChiChi, Taiwan; 2004 Niigata, Japan; 2008 Iwate, Japan), all of which had moment magnitude (M_w) greater than 4. Their analysis found that landslide rates significantly increased immediately after an earthquake and gradually decreased to a background value within 1 to 4 years. Marc et al. (2015) tentatively attributed the observed trends to a reduction in ground strength followed by recovery. In contrast, in regions with low to moderate seismicity, direct relationships between earthquakes and landslides are difficult to identify. However, Vanmaercke et al. (2017) showed that weaker but more frequent earthquakes exhibit stronger correlations with sediment yield, suggesting a possible cumulative impact on landslide susceptibility also for such weaker triggers over a longer time scale.

Despite progress in understanding landslide path dependency and earthquake-induced landslides preconditioning, existing studies have largely focused on earthquakes as either triggering events, or, as conditioning processes that weaken soil and slope over time (e.g., Vanmaercke et al. 2017; Zhang et al. 2024). However, no research has been conducted that quantifies the impact of triggers such as earthquakes on LPD, resulting in a significant research gap in understanding the spatial and temporal evolution of landsliding.

Earthquakes may change path-dependency parameters, such as the characteristic decay time and the value of the characteristic spatial distance from earlier landslides. These effects may arise from earthquake magnitude-distance relationships, in which the impact on landsliding depends on magnitude and distance from the epicenter (Keefer, 1984). After an earthquake, slopes do not fail randomly or all at once; instead, landslides continue to occur over time as the ground weakens (Leshchinsky et al., 2021). This is also seen in the case of the 1998 Chi-Chi earthquake in Taiwan. Landslide rates remain elevated during subsequent rainfall, with rates being 59-66% higher than baseline levels, even when total seasonal rainfall was much lower than average (Chuang et al., 2009; Leshchinsky et al., 2021). These data suggests that earthquakes may weaken slopes, making them more susceptible to landslides during remarkable rainfall levels. Therefore, it is extremely important to study post-seismic landslides across different climatic and tectonic settings and to examine how earthquakes in these settings affect LPD.

This paper aims to quantify how large earthquakes ($M_w \geq 4$) modify LPD. We hypothesize that earthquakes increase existing levels of LPD, such that after an earthquake landslides will more often follow each other in the same location. We operationalize this as the hypothesis that earthquakes increase the landslide overlap fraction. To test this hypothesis across different geomorphic settings, our objectives are to: 1) Calculate landslide overlap index from multi-temporal landslide inventories in Italy and Nepal, and 2) compare this index and properties of landslides that cause follow-up and landslides that do not follow up immediately before and after large earthquakes.

4.2. Study areas

4.2.1. Collazzone, Italy

The Collazzone area (Figure 4.1) covers approximately 80 km^2 within the Perugia Province of the Umbria region, Italy, with elevations ranging from 145 m along the Tiber River floodplain to 634 m at Monte di Grutti (Guzzetti, Galli, et al., 2006). The geology consists of recent fluvial deposits, continental gravel, sand, and clay; travertine deposits; sandstone; and marl in varying proportions, and thinly bedded limestones (Volpe et al., 2022). The area has a Mediterranean climate, with precipitation mainly occurring between October and December, and from February to May (Lombardo et al., 2020). The natural triggers of landslides are intense rainfall events and rapid snowmelt (Ardizzone et al., 2013; Cardinali et al., 2000). Soils vary in thickness from a few decimeters to more than one meter, have fine to medium textures, and exhibit a xeric moisture regime. Landslides are widespread, encompassing a wide range of types and volumes, from old, deep-seated slides to shallow slides and flows (Guzzetti, Galli, et al., 2006).

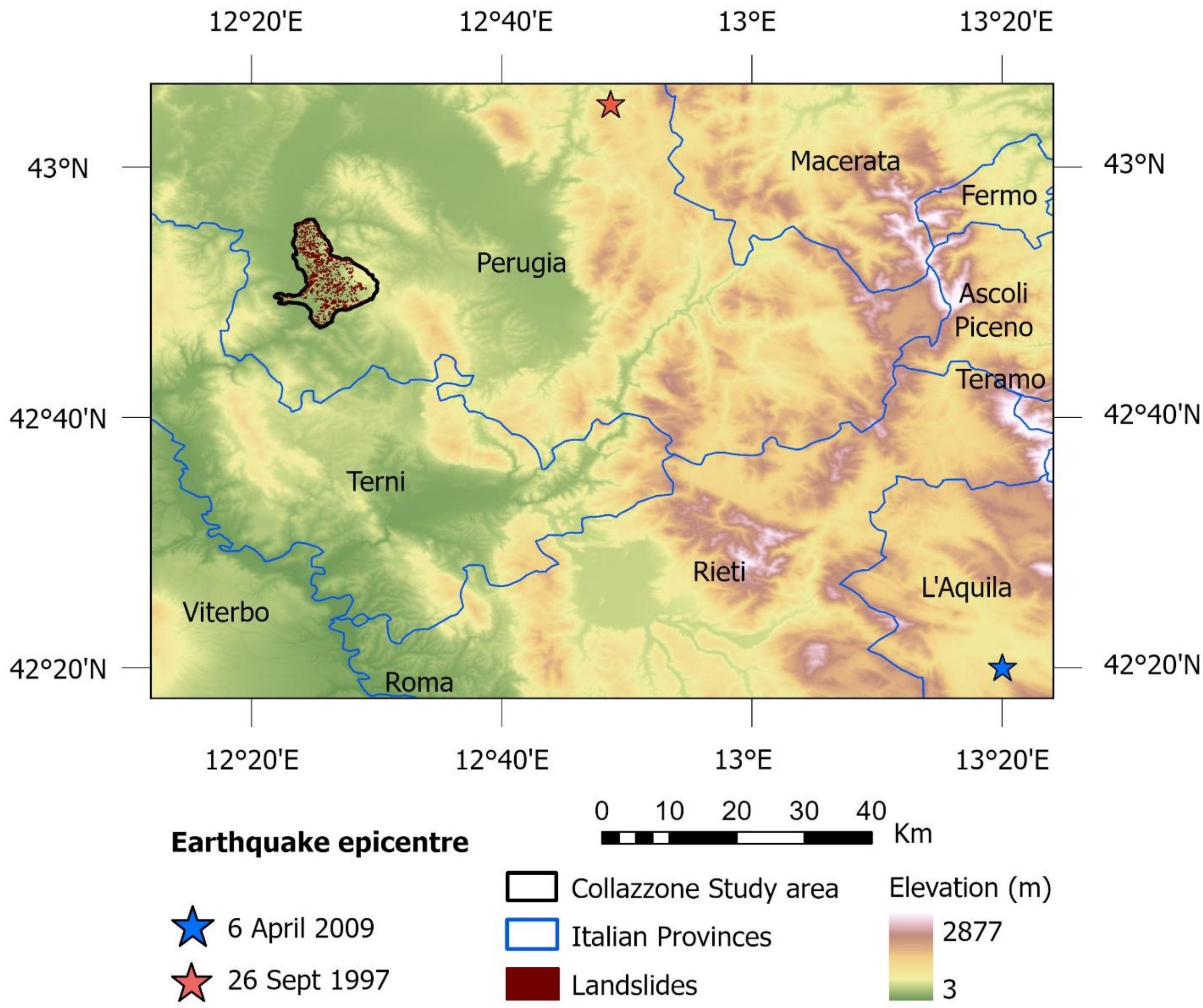

Figure 4.1: Landslides (Ardizzone et al., 2013) in the Collazzone study area overlaid on DEM downloaded from SRTM using Google Earth Engine. Locations of two significant earthquakes affecting Collazzone: the 1997 earthquake in Perugia ($M_w = 6.0$) and 2009 earthquake in L'Aquila ($M_w = 6.3$).

4.2.2. Nepal

The selected Nepal region (Figure 4.2) covers approximately 45000 km^2 within the central-eastern Nepal Himalaya (Jones et al., 2021). Most of the landslides in Nepal are triggered by monsoon rainfall. The selected central region covers catchments across all four major tectonic units of the Nepal Himalaya: Sub, Lesser, Greater, and Tethyan Himalaya (DeCelles et al., 2001). These tectonic units are characterized by different geomorphologies and geological settings (Roberts et al., 2021). For example, the Tethyan Himalaya Sequence consists of late Proterozoic to Eocene sedimentary rocks, separated from the high-grade metamorphic rocks of the Greater Himalayan Crystalline Complex by the South Tibetan Detachment System, which is characterized by top-to-north kinematics (Burchfiel et al., 1992). In contrast, the Greater and Lesser Himalaya are underlain by lower-grade metamorphic, metasedimentary, and sedimentary rocks (Robinson et al., 2001; Upreti, 1999). The Sub-Himalayan Sequence mainly consists of Cenozoic foreland sedimentary rocks (Yin, 2006).

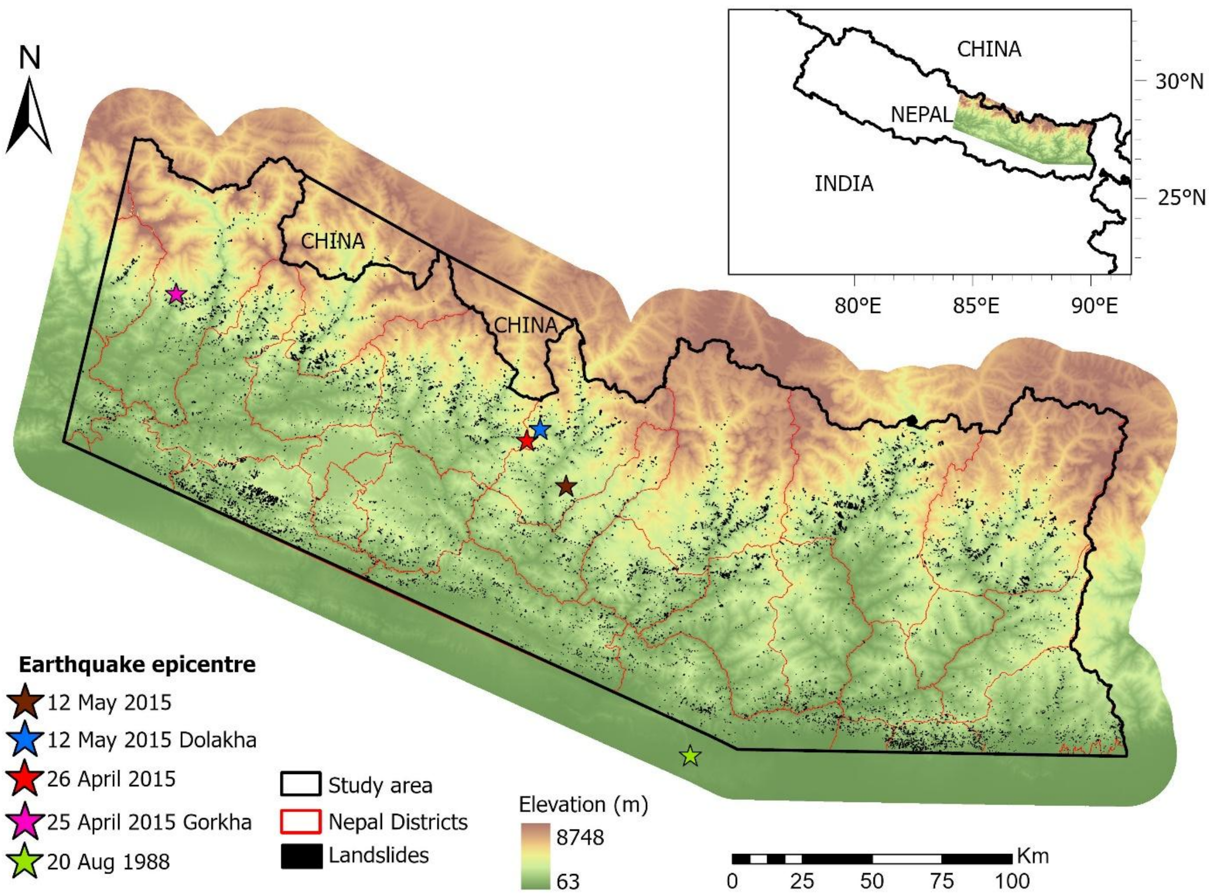

Figure 4.2: Nepal central region including all mapped landslides from 1988 to 2018 (Jones et al. 2021). Landslides and the central boundary of Nepal are overlaid on a DEM downloaded from SRTM using Google Earth Engine. Also shown are the epicenters of five major earthquakes (M_w = 6.3 – 7.8) relevant to landslide occurrence.

4.3. Methods

4.3.1. Data acquisition

For Collazzone (Italy), we used the multi-temporal landslide inventory from 1937 to April 2014, mapped using aerial photographs and stereo remote sensing from GEOEYE and Worldview images (Ardizzone et al., 2013). A detailed description of this inventory, including its preparation, time-slice mapping, age of landslides, spatial-temporal uncertainties, and frequency-area relationships, is given in (Guzzetti, Reichenbach, et al., 2006; Samia et al., 2017b). For Nepal, we used Jones et al.'s (2021) multi-temporal landslide inventory developed from 15-30 m Landsat 4/5/7/8 imagery. It consists of 29 time-slices, with each slice representing a single monsoon season between 1988 and 2018, excluding 2011 and 2012 due to Landsat-7 scanline errors (Alexandridis et al., 2013).

Earthquake data were obtained from the USGS earthquake catalog. Initially, we selected earthquakes with a $M_w \geq 4$, as they can possibly trigger landslides (Keefer, 1984). For Collazzone, earthquakes were extracted for the period 1937-2014, and for Nepal, 1988-2018, consistent with the temporal range of the respective landslide inventories. The centroid of each study area was used as the reference location for subsequent earthquake filtering. Filtering was based on the magnitude-distance relationship from Keefer (1984) which identifies the distance over which an earthquake of a certain magnitude is capable of causing landslides.

In the Collazzone region, most earthquakes (Figure 4.3) fall outside Keefer's (1984) threshold distance, i.e., they have limited influence on landslide occurrence between 1937 and 2014. However, two earthquakes lie within the threshold distance. These occurred in September 1997 (M_w = 6) and April 2009 (M_w=6.3). In the central region of Nepal, five landslide-relevant earthquakes occured between 1988 and 2018: one in August 1988 (M_w = 6.9), two in April 2015 (M_w= 7.8 & 6.7), and two in May 2015 (M_w= 7.3 & 6.3) fall within the magnitude-distance threshold proposed by Keefer (1984).

Therefore, for the Collazzone region, we selected landslide inventories from 1981 to 1997 (pre-1997 earthquake), from 1999 to 2009 (between the 1997 and 2009 earthquakes), and post-2009 inventories to evaluate LPD. For the Nepal central region, we considered time slices spanning 2009–2014 (pre-2015 earthquakes) and 2015–2018 (post-2015 earthquakes). The 1988 Nepal earthquake was excluded from this analysis because no landslide inventories were available prior to that event.

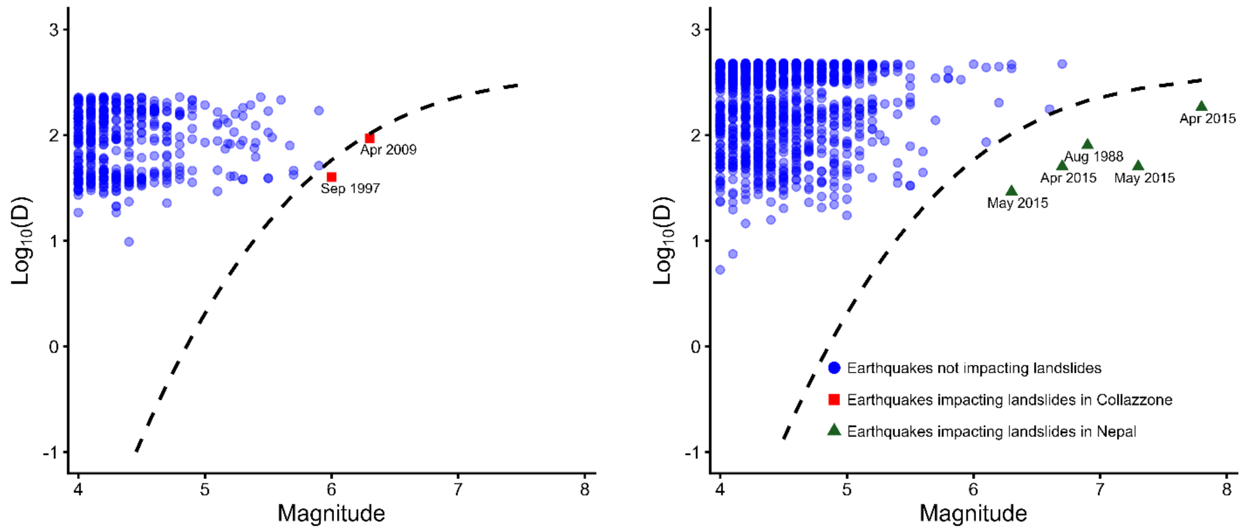

Figure 4.3: Identification of earthquakes impacting landslides based on Keefer (1984) distance-magnitude relationship in Collazzone (left plot) and Nepal central region (right plot). D is the distance between the epicenter and the study area's centroid. The dashed line is the threshold curve that separates earthquakes capable of triggering landslides from those unlikely to produce.

4.3.2. Quantifying earthquake impact on landslide properties

To answer this question, we first calculated the direct impact of earthquakes on landslide geometric and topographic properties using the Wilcoxon rank-sum test. Then we compared the impact of earthquakes between landslides, that have a follow up landslide and landslides that do not, using the Aligned Rank Transform (ART) Test, a non-parametric alternative to two-way analysis of variance (ANOVA) (Wobbrock et al., 2011).

Geometric properties included landslide size and shape, with the shape quantified using the roundness index, as calculated by Samia et al. (2017a) and Roberts et al. (2021). A roundness value approaching 1 indicates more circular landslides, whereas a value closer to 0 represents elongated forms. Topographic factors included elevation, slope, Northness, Eastness, topographic position index (TPI), topographic wetness index (TWI), plan and profile curvature, LS factor, and relative slope position (Guisan et al., 1999; Jiang et al., 2018; Panagos et al., 2015; Pucha-Cofrep & Fries, 2025; Samia et al., 2017a; A. J. Temme et al., 2022). Northness refers to how much slope faces north, which represents the cosine of the aspect angle, while eastness refers to how much slope faces east, which is calculated as the sine of the aspect angle.

4.3.3. Quantifying earthquake impact on landslide path dependency

To quantify LPD in the few years before and after earthquakes, we calculated the follow-up landslide fraction (eq (*4.1*)) as defined by Samia et al. (2017b). Follow-up landslides (Samia et al. 2017b) are those that shows spatial association, i.e., that are inside, overlap, or touch an earlier; if a landslide lies entirely outside the earlier time slice, showing no overlap or contact, it is not considered a follow-up landslide. If a landslide is spatially associated with landslides from multiple earlier time slices, it is considered a follow-up with respect to the most recent preceding landslide, not earlier time slices. With these definitions, we calculated the follow-up landslide overlap index (ρ) before and after earthquakes as (Samia et al., 2017a):

$$\rho = \frac{FL_{T2}}{TL_{T2}} \times \frac{AS}{AL_{T1}} \tag{4.1}$$

where FL_{T2} is the number of follow-up landslides in the younger time slice T_2, TL_{T2} is the total number of landslides in T_2, AS (m^2) is the study area, and AL_{T1} (m^2) is the area affected by landslides in the older time slice T_1. The first division in eq (4.1) captures the fraction of landslides that follow others, the second division normalizes that for the size of the target (i.e. how much area was available to overlap with)

We calculated the landslide overlap index (ρ) for four time-slices before and after the earthquake to evaluate the impact of the earthquake on ρ.

4.4. Results

4.4.1. Landslide occurrence in Collazzone and Nepal central region

In Collazzone, during the pre-1997 earthquake period (1981 to 1997), landslide occurrence ranged between 63 and 413 per inventory year (Figure 4.4). Between 1997 and 2009, landslide activity showed variability, and ranged between 17 and 224 per inventory year. Post-2009 earthquake period (2009 - 2014) landslide ranged from 118 to 217 per inventory year. On the contrary in central Nepal, ignoring co-seismic landslides, during the pre-2015 earthquake period (2009 - 2015), landslide occurrence was lower (175 – 507 landslides per inventory year) than during the post-2015 earthquake period (406-1328 landslides per inventory year). The 2015 earthquakes in Nepal led to a raised frequency of monsoon-triggered landslides in 2015, followed by a gradual decline in subsequent years. This effect was not apparent in Collazzone after the 1997 and 2009 earthquakes.

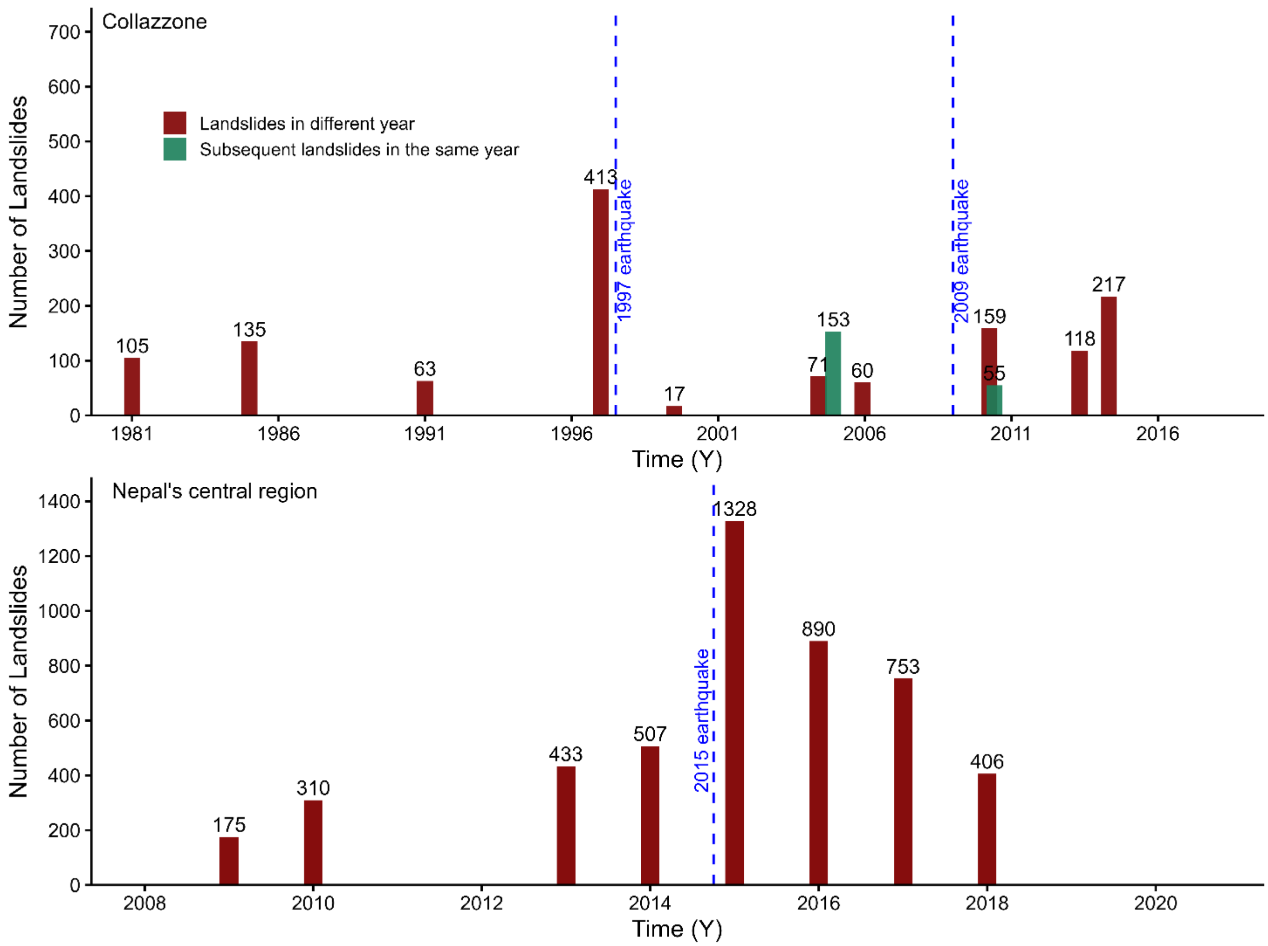

Figure 4.4: Number of landslides triggered in Collazzone, Italy (top) from 1981 to 2014, and in central Nepal (bottom) from 2009 to 2018. Red bars represent the non-co-seismic landslides at a specific time of the year, while green bars represent subsequent landslides occurring later within the same year. Dashed blue lines represent earthquakes that happened at a particular time.

4.4.2. Impact of earthquake on geometric and topographic properties of landslides

To evaluate the independent impact of earthquakes on landslides (assuming no path dependency), we selected time slices immediately before and after each earthquake. In Collazzone, for the 1997 earthquake, the pre-event includes landslides that occurred in 1991 and 1997, while the post-event includes landslides that happened in 1999 and May 2004. Similarly, for the 2009 earthquake, the pre-event comprises the December 2004 and December 2005 time slices, whereas the post-event includes landslides that occurred in March 2010 and May 2010.

In Collazzone, the 1997 earthquake significantly increased landslide size (0.22 ± 0.02 ha to 0.38 ± 0.06 ha; $p < 0.01$), while mean elevation significantly decreased (257 m to 246 m; $p = 0.03$). No other landslide properties showed statistically significant differences (Table 4.1).

For the 2009 earthquake, several properties exhibited significant changes. This time, landslide size decreased significantly after the earthquake (0.26 ± 0.04 ha to 0.18 ± 0.02 ha; $p = 0.03$). Elevation (279 m to 271 m) and roundness (0.85 to 0.76) decreased significantly, indicating that landslides after the 2009 earthquake were more elongated and occurred at lower elevations. Among topographic properties, TPI decreased, while TWI increased significantly. Moreover, LS factor increased significantly from 9.03 to 10.06. Other properties did not show statistically significant differences.

Table 4.1: Impact of earthquakes on geometric and topographic properties of landslides before and after earthquakes in Collazzone

Parameters	1997 Earthquake			2009 Earthquake		
	Before	After	p-value	Before	After	p-value
Size (ha)	0.22 ± 0.02	0.38 ± 0.06	<0.01	0.26 ± 0.04	0.18 ± 0.02	0.03
Roundness (-)	0.87 ± 0.04E-01	0.89 ± 0.01	0.55	0.85 ± 0.01	0.76 ± 0.01	<0.01
Elevation (m)	2.57E+02 ± 2.4	2.46E+02 ± 6.01	0.03	2.79E+02 ± 4.61	2.71E+02 ± 4.86	0.03
Slope (°)	11.1 ± 0.16	11.48 ± 0.32	0.29	11.09 ± 0.24	10.73 ± 0.21	0.29
Northness (-)	-0.16E-02 ± 0.03	0.14 ± 0.07	0.14	-0.25E-01 ± 0.05	0.01 ± 0.05	0.82
Eastness (-)	-0.36 ± 0.03	-0.44 ± 0.06	0.13	-0.35 ± 0.04	-0.33 ± 0.04	0.5
TPI (m)	-0.94 ± 0.1	-0.59 ± 0.23	0.15	-0.35 ± 0.15	-0.87 ± 0.14	0.01
TWI (radians^{-1})	7.11 ± 0.05	7.03 ± 0.12	0.7	6.82 ± 0.07	7.22 ± 0.07	<0.01
Profile Curvature (-)	0.35E-01 ± 0.01	0.04 ± 0.03	0.98	0.19E-01 ± 0.02	2.8E-02 ± 0.02	0.61
Planform Curvature (-)	-0.57E-01 ± 0.01	-0.065 ± 0.02	0.83	-0.33E-01 ± 0.02	-0.07 ± 0.01	0.08
LS factor (-)	10.05 ± 0.21	10.26 ± 0.41	0.31	9.03 ± 0.3	10.06 ± 0.33	0.03
Relative Slope Position (-)	0.37 ± 0.99E-02	0.33 ± 0.02	0.07	0.33 ± 0.01	0.36 ± 0.01	0.18

To evaluate the impact of earthquakes on landslides in Nepal's central region (assuming no path dependency), we selected two time slices immediately preceding (2013 and 2014) the 2015 earthquake and two time slices after it (2015 and 2016).

In Nepal, the size and mean elevation of landslides also increased significantly after the series of 2015 earthquakes (Table 4.2). Roundness decreased significantly, indicating that landslides were more elongated in the post-earthquake period. Moreover, slope values were significantly higher after the earthquake (31.68 ± 0.32° to 34.38 ± 0.21°; $p < 0.01$), suggesting a shift towards steeper terrain. Among topographic properties, TPI and LS factor significantly increased after earthquakes, while northness and relative slope position significantly decreased. All other properties did not show significant differences before and after 2015 earthquakes.

Table 4.2: Impact of earthquakes on geometric and topographic properties of landslides before and after 2015-earthquakes in Nepal's central region

Parameters	2015 Earthquakes		
	Before	After	p-value
Size (ha)	0.75 ± 0.08	1.11 ± 0.05	<0.01
Roundness (-)	0.79 ± 5.0E-03	0.76 ± 3.3E-03	<0.01
Elevation (m)	1.35E+03 ±24.09	1.75E+03 ± 3.6E-36	<0.01
Slope (°)	31.68 ± 0.32	34.38 ± 0.21	<0.01
Northness (-)	-0.59 ± 0.01	-0.62 ± 0.01	0.04
Eastness (-)	0.23 ± 0.02	0.24 ± 0.01	0.84
TPI (m)	4.41E+04 ± 9.59	4.43E+04 ± 6.61	<0.01
TWI (radians^{-1})	6.29 ± 0.05	6.24 ± 0.03	0.56
Profile Curvature (m^{-1})	4.2E-02 ± 0.02	5.8E-02 ± 0.01	0.39
Planform Curvature (m^{-1})	-2.1E-02 ± 0.02	-3.7E-02 ± 0.01	0.87
LS factor (-)	52.51 ± 2.07	54.74 ± 0.93	<0.01
Relative Slope Position (-)	0.50 ± 0.01	0.48 ± 4.7E-03	0.04

4.4.3. Impact of earthquakes on geometric and topographic properties of follow-up and non-follow-up landslides.

To evaluate how earthquakes modify the geometric and topographic properties of path-dependent landslides, the inventory was divided into pre- and post-earthquake periods around the 1997 and 2009 earthquakes that affected Collazzone. For the 1997 earthquake, the pre-event period includes landslides that occurred between 1985 and 1997, whereas the post-event period comprises landslides from 1999 to December 2004. Similarly, for the 2009 earthquake, the pre-event period covers landslides recorded between May 2004 and December 2005, and the post-event period covers landslides recorded between March 2010 and April 2013. These periods were intentionally selected because earthquake impacts on landslides are typically transient, as reported by Marc et al. (2015).

The 1997 earthquake did not have a significant impact on landslide size when comparing the pre- and post-earthquake periods (Table 4.3). However, the landslides that experienced follow-up landslides were larger than those that did not. Moreover, the interaction between the 1997 earthquake period and landslide roundness was statistically different between follow-up and non-follow-up landslides.

Compared with the 1997 earthquake, the 2009 earthquake produced more pronounced changes in the geometric and topographic properties of landslides. Landslides that experienced follow-up are larger than those that do not, both before and after the 2009 earthquake. Also, the interaction between earthquake period and the follow-up status was significant.

In the post-2009 earthquake period, landslides with follow-up status have a higher mean elevation than those without follow-up. In the pre- and post-2009 earthquake period, the mean slope of landslides that cause follow-up were significantly higher (11.20 ± 0.40; 11.87° ± 0.53°) than the landslides that do not cause follow-up landslides (10.92 ± 0.25; 10.43° ± 0.22°). This trend was absent in the pre-1997 and post-1997 periods.

Table 4.3: Impact of earthquakes on geometric and topographic properties of landslides that cause follow-up (Y) and those that do not cause follow-up (N) before (b) and after earthquakes (a) in Collazzone. Only significant properties are shown.

Parameters	Follow-up	1997 earthquake			2009 earthquake		
		before	after	p(b=a)	before	after	p(b=a)
Size (ha)	Y	0.48 ± 0.08	0.41 ± 0.13	0.66	0.51 ± 0.13	0.19 ± 0.03	0.03
	N	0.33 ± 0.04	0.37 ± 0.06		0.24 ± 0.02	0.17 ± 0.02	
	p (Y = N)	<0.01		0.29	<0.01		0.01
Roundness (-)	Y	0.79 ± 0.02	0.90 ± 0.01	<0.01	0.87 ± 0.02	0.77 ± 0.01	<0.01
	N	0.84 ± 0.01	0.88 ± 0.01		0.85 ± 0.01	0.76 ± 0.01	
	p (Y = N)	0.10		0.01	0.48		0.56
Elevation (m)	Y	2.53E+02 ± 5.46	2.62E+02 ± 15.02	0.19	2.69E+02 ± 10.36	3.01E+02 ± 12.84	0.65
	N	2.5E+02 ± 4.17	2.40E+02 ± 5.97		2.71E+02 ± 5.19	2.63E+02 ± 4.98	
	p (Y = N)	0.18		0.86	0.04		0.04
Slope (°)	Y	11.88 ± 0.46	10.82 ± 0.54	0.75	11.20 ± 0.40	11.87 ± 0.53	0.50
	N	11.14 ± 0.29	11.73 ± 0.39		10.92 ± 0.25	10.43 ± 0.22	
	p (Y = N)	0.66		0.11	0.02		0.19
Northness (-)	Y	-0.16 ± 0.96E-01	0.25 ± 0.12	<0.01	0.18 ± 0.10	-0.20 ± 0.11	0.68
	N	-0.17 ± 0.05	0.10 ± 0.08		-0.42E-01 ± 0.05	0.65E-01 ± 0.05	
	p (Y = N)	0.42		0.47	0.81		<0.01
TWI (m)	Y	7.19 ± 0.16	7.02 ± 0.18	0.21	6.75 ± 0.13	7.23 ± 0.12	0.01
	N	7.33 ± 0.12	7.04 ± 0.16		7.00 ± 0.08	7.22 ± 0.08	
	p (Y = N)	0.85		0.65	0.82		0.22
LS factor (-)	Y	11.46 ± 0.55	9.51 ± 0.83	0.32	9.21 ± 0.60	12.16 ± 0.87	0.37
	N	10.90 ± 0.42	10.54 ± 0.46		9.45 ± 0.34	9.52 ± 0.33	
	p (Y = N)	0.83		0.08	0.03		0.03
Relative Slope Position (-)	Y	0.38 ± 0.03	0.35 ± 0.04	<0.01	0.31 ± 0.03	0.33 ± 0.03	0.19
	N	0.42 ± 0.02	0.32 ± 0.03		0.33 ± 0.02	0.37 ± 0.02	
	p (Y = N)	0.74		0.25	0.40		0.74

In Nepal, the landslides that cause follow-up, size (1.34 ha to 1.96 ha) and elevation (132 m to 146m) significantly increased after the 2015 earthquakes, indicating that post-earthquake landslides that cause follow-up are larger and located at higher elevations. Also, landslides that exhibit path dependency are larger than those that lack this mechanism. Other properties of follow-up and non-follow-up landslides before and after 2015 remain non-significant (Table 4.4).

Table 4.4: Impact of earthquakes on geometric and topographic properties of landslides that cause follow-up (Y) and those that do not cause follow-up (N) before (b) and after earthquakes (a) in Nepal. Only significant properties are shown.

Parameters	Follow-up	2015 earthquakes		
		Before (b)	After (a)	p(b=a)
Size (ha)	Y	1.34 ± 0.23	1.96 ± 0.57	<0.01
	N	0.96 ± 0.05	0.96 ± 0.03	
	p (Y = N)	<0.01		0.59
Roundness (-)	Y	0.80 ± 0.02	0.76 ± 0.01	0.01
	N	0.80 ± 0.01	0.77 ± 0.03E-01	
	p (Y = N)	0.40		0.99
Elevation (m)	Y	1.32E+03 ± 1.5E+02	1.46E+03 ± 6.5E+01	<0.01
	N	1.39E+03 ± 0.26E+02	1.6E+03 ± 0.16E+02	
	p (Y = N)	0.11		1.00
TPI (m)	Y	4.41E+04 ± 49.94	4.42E+04 ± 24.05	<0.01
	N	4.41E+04 ± 10.26	4.42E+04 ± 5.84	
	p (Y = N)	0.12		0.95

4.4.4. Impact of earthquake on landslides overlap index.

In Collazzone, prior to the 1997 earthquake, the overlap index was generally lower (Figure 4.5). Following the 1997 earthquake, overlap index values increased and were associated with shorter time differences, indicating stronger landslide path dependency. Moreover, the mean overlap index was higher in the post-1997 earthquake period than in the pre-1997 period. Similarly, before the 2009 earthquake (the period between the post-1997 earthquake and the pre-2009 earthquake), the overlap index was lower compared to the post-2009 period, and the mean fractional overlap index was higher in the post-2009 period compared to pre-2009 period. This indicates that path dependency became stronger.

In Nepal, there is no clear difference in the overlap index (Figure 4.6) before and after the 2015 earthquakes.

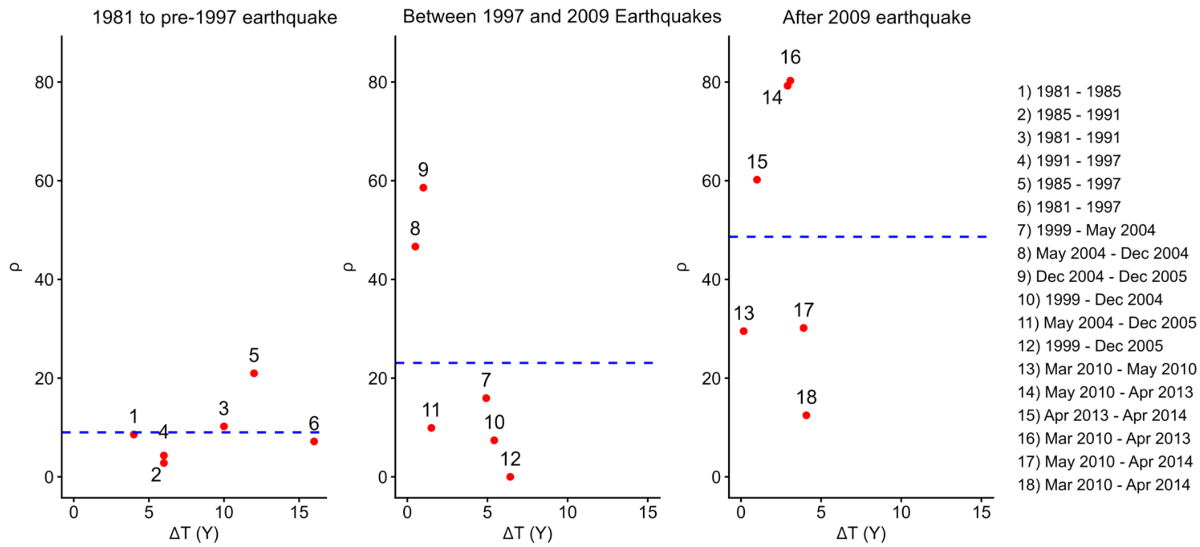

Figure 4.5: Relationship between the overlap index (ρ) and time difference (ΔT) for landslides in Collazzone. Plots show overlap trend before the 1997 earthquake (left), between the 1997 and 2009 earthquakes (middle), and after the 2009 earthquake (right). Blue line represents the mean overlap index for respective periods.

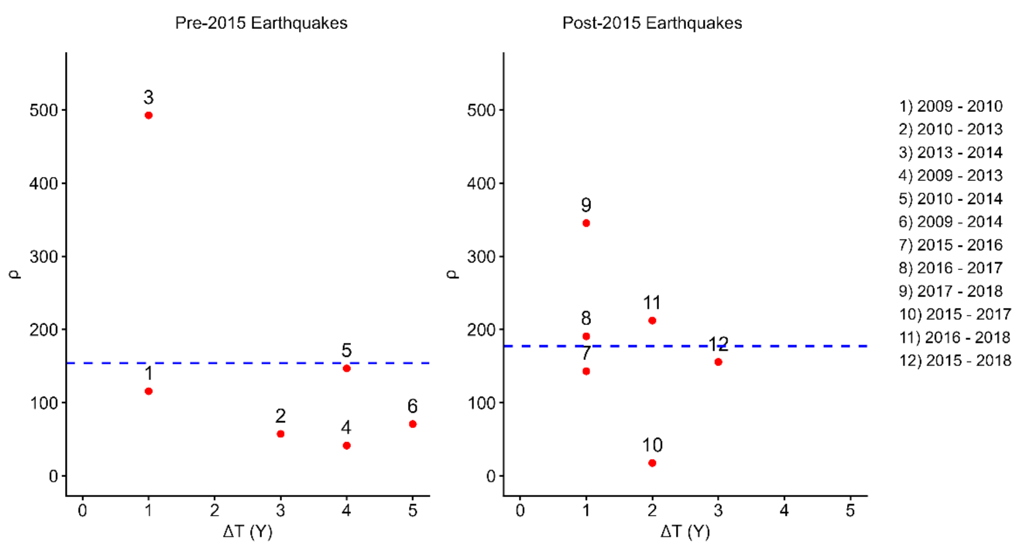

Figure 4.6: Relationship between the overlap index (ρ) and time difference (ΔT) for landslides in the central region of Nepal. Plots show overlap trend before the 2015 earthquakes (left) and after the 2015 earthquakes (right). Blue line represents the mean overlap index for respective periods.

4.5. Discussion

4.5.1. Impact of earthquakes on landslide properties and their occurrence under different geomorphic settings.

The different patterns of landslide occurrence in Italy and Nepal showed how earthquakes affect landslides across different tectonic, geomorphic, and climatic settings. In Collazzone, we did not observe a significant increase in landslide occurrence immediately after the 1997 or 2009 earthquakes compared to pre-earthquake periods. Apparently, in this setting with marly lithology, Mediterranean climate, and moderate steepness of landsliding hillslopes around 11°, earthquakes did not cause additional landsliding.

However, in Nepal's central region, the frequency of monsoon-triggered landslides increased significantly immediately after the 2015 earthquakes compared to the pre-earthquake period. Landslide frequency gradually returned to normal background levels by the end of 2018. This pattern closely resembles the transient post-seismic landslide pulse identified in Taiwan by Marc et al. (2015), who demonstrated that landslide rates are higher after large earthquakes and then decay over several years probably due to progressive recovery of ground strength following coseismic damage. Our observations for the Nepal dataset are likely related to this mechanism. Like in Taiwan, earthquakes in the central region of Nepal, probably reduce slope strength, and increase landslide susceptibility, which is likely why monsoon-triggered landslides were high immediately after the 2015 earthquakes, consistent with the findings reported by Jones et al. (2021). As fractured materials stabilize, landslide rates would decline with time. But apparently this mechanism is absent in Collazzone. One possible reason for the limited impact of earthquakes on rainfall-triggered landslides in Collazzone is that the epicenters of the 1997 and 2009 earthquakes are located away from the study area. As a result, the shaking intensity in Collazzone was relatively low, with Modified Mercalli Intensity (MMI) values of approximately V and IV for the 1997 and 2009 earthquakes, respectively, which likely limited hillslope damage, while in Nepal four of the five major earthquakes in 2015 were located in central Nepal and produced much stronger shaking intensity (MMI ~ 7 – 8.6). In addition, slopes are less steep on average in Italy than in Nepal, which minimizes the topographic amplification.

In Collazzone, the 2009 earthquake (M = 6.3, max PGA = 0.66g, and MMI = 4) in central Italy produced more significant changes in landslide properties than the 1997 earthquake (M = 6, max PGA = 0.6g, MMI = 5). Multiple parameters showed significant changes after the 2009 earthquake, including landslide size, elevation, roundness, TPI, TWI, and LS factor. After the 2009 earthquake, the roundness was low, indicating that landslides were more elongated than during the pre-2009 period. The 2009 earthquake reduced the mean elevation and TPI of landslides, while increasing TWI, suggesting that, after 2009, the spatial distribution of landslides changed, with landslides more likely to initiate in low-slope positions and at elevations with high water-saturation potential. This indicates that landslides tend to occur in valleys. Because the LS factor is high after the 2009 earthquake, landslides apparently occur at valley sidewalls.

In Nepal, we observed a contrasting pattern. The 2015 earthquakes increased landslide size, and the mean landslide elevation after 2015 was higher, indicating that larger landslides tend to occur at higher elevations with steeper slopes. A possible reason for the contrast is that there were stronger earthquakes in the Nepal central region than in Collazzone. In higher-magnitude earthquakes in elevated mountains, landslides tend to cluster near ridge crests, where susceptibility is highest (Meunier et al., 2008). However, in Collazzone, the slopes are lower than in the central region of Nepal, and earthquakes are of relatively lower magnitude, which explains the contrasting trend. However, more research is needed to explain how different earthquakes trigger landslides across different geomorphic settings and to identify the underlying factors that drive post-seismic landslide occurrence.

The post-seismic decrease in landslide roundness in both Nepal and Collazzone indicates that landslides are more elongated following earthquakes, suggesting a shift toward more flow-like behavior. We are unable to explain the underlying mechanisms driving this change, as further investigation is required. However, such elongation may be associated with increased mobility and longer runout distances, potentially impacting infrastructure.

4.5.2. Impact of earthquakes on landslide path dependency

In both Collazzone (specifically after 2009) and Nepal, the landslides that caused follow-up were larger than those that did not. This finding is consistent with that of Samia et al. (2017a) and Roberts et al. (2021) who reported that landslides that experience subsequent landslides have a larger mean size than those that do not. This effect is to be expected on geometric and mechanistic grounds. Geometrically, larger landslides are larger targets, so that even follow-up landslides that are not conditioned by the earlier landslide have a larger chance of overlapping with them.

Mechanistically, larger landslides are typically also deeper landslides, and the impact on topography, soils and vegetation increases with landslide size.

Moreover, in Collazzone, the mean elevation and slope of landslides that trigger follow-up landslides are higher than those of non-follow-up landslides after an earthquake. There can be several possible reasons for this trend. This remains a significant research gap that needs to be explored.

Moreover, we found that the overall fraction overlap index increased after an earthquake in Collazzone; however, in Nepal, the trend was unclear. We believe this trend in Collazzone is due to earthquake preconditioning, in which earthquakes make hillslopes more susceptible to future slides. According to Parker et al. (2015), landslide occurrence depends on both current earthquake shaking and accumulated damage from past events. Also, Samia et al. (2017a) stated that landslide susceptibility is a function of conditioning attributes and previous landslides. Therefore, landslide susceptibility increases where both past earthquakes and previous landslides have occurred, potentially leading to greater overlap under their combined effects. As a result, fractional overlaps were higher in the post-earthquake period in Collazzone. This is due to earthquakes having low shaking intensity; therefore, instead of causing widespread hillslope damage, they produced localized pre-conditioning and raised susceptibility near earlier landslides, rather than in other locations. That is why overlaps were higher and thus path dependency became stronger in Collazzone. However, in Nepal, earthquakes were intense and caused widespread damage. Due to increased damage to hillslopes, it preconditioned not only areas near earlier landslides but also other areas where landslides are normally absent. Therefore, during the next monsoon season, the total number of landslides was higher, including nonspatially associated landslides, which is why we were unable to detect a difference in the fractional overlap index between the pre-2015 and post-2015 earthquake periods.

4.6. Conclusion

In this study, we found that large earthquakes in Collazzone and the Nepal central region impacted the properties of landslides. In Collazzone, the earthquake did not affect post-earthquake non-coseismic landslide rates, whereas in Nepal, non-coseismic landslide rates increased after the 2015 earthquake and gradually decreased over the following four years. In Collazzone, LPD was high after the earthquake due to more localized earthquake preconditioning rather than widespread hillslope damage, whereas in Nepal, widespread hillslope damage after the 2015 earthquakes did not increase overall LPD.

Funding

This research forms part of H.S. Sodhi's Ph.D. dissertation at Kansas State University and was supported by internal funding from the Department of Geography and Geospatial Sciences, Kansas State University. Boulton is supported by NERC award NE/Y000080/1.

Chapter 5 : Synthesis

Landslides are widespread geohazards in hilly areas and pose a significant threat to humans and infrastructure (Kohler et al., 2023). Traditionally, landslide susceptibility has been treated as static; however, recent studies (Roberts et al., 2021; Samia et al., 2017b) challenged this assumption by demonstrating that landslides exhibit landslide path dependency (LPD). Therefore, landslide susceptibility changes with time, as past landslides modify hillslopes by altering their topography, soil, and vegetation. In the synthesis chapter, I want to discuss possible mechanisms underlying LPD and potential directions for future research to improve the understanding of LPD.

5.1. Why does the downslope direction play a more important role than the lateral direction in driving landslide path dependency in Collazzone?

In Chapter 2, I found that LPD in Collazzone is stronger in the downslope direction than lateral direction. Moreover, LPD is 47 times higher near recent landslides than at locations farther away. This indicates that locations close to earlier landslides, particularly within a short temporal window, are more likely to exhibit path dependency. One possible explanation for more LPD downslope than lateral is the geomorphological processes that occur after landslides in Collazzone. In Collazzone (Umbria, Italy), the landslides are generally shallow and do not completely evacuate from the hillslopes (Guzzetti, Galli, et al., 2006; Samia et al., 2017b; A. J. A. M. Temme, 2021a). Therefore, landslide deposits remain on the hillslopes. These deposits constitute the positive soil-landslide feedback loop, as explained by Temme (2021), in which shallow landslides create weakly permeable soil layers that further increase water saturation and increase susceptibility to future landslides (Duzgoren-Aydin & Aydin, 2006; Parry et al., 2000). Therefore, in such settings, there may be a higher probability of follow-up landslides in the downslope direction than the lateral direction, specifically shortly after an earlier landslide. According to Samia et al. (2017b), small ponds formed after rainfall events within landslide deposits (Figure 5.1), leading to water saturation and higher pore pressure. Moreover, they found smeared shear surfaces (Figure 5.2) along the sliding planes, which might reduce infiltration and increase water accumulation within the landslide deposit. Downslope, due to gravity, landslide deposits accumulate at the toe of the landslide. As these deposits are poorly structured and have greater potential for water accumulation, the landslide toe accumulates more water, increasing pore pressure downslope and further triggering the landslide.

Figure 5.1: Small ponds at the landslide deposit after rainfall in Collazzone (Samia et al. 2017b)

Figure 5.2: Smeared soil surface at the scarp of the landslides in Collazzone (Samia et al. 2017b)

In my Chapter 4, I found that landslides in Collazzone are mostly triggered where the profile and plan curvature are concave, indicating topographic convergence in the downslope direction. Such topography promotes water accumulation downslope, particularly within the landslide deposit, thereby increasing the water pore pressure. Therefore, when there is a landslide, the deposit tends to accumulate downslope, where water becomes saturated after rainfall. Therefore, there is increased susceptibility to subsequent landslides, which promotes path dependency in such geomorphic settings.

In other cases, if shallow landslide deposits are completely removed from the hillslope, then weakly permeable soil deposits are absent at the hillslope, which might not reduce hydraulic conductivity or have no impact on pore pressure, which is oppositely stated above. Therefore, in such cases, we might expect less downslope LPD effect, or the LPD effect might be isotropic. Further research should be conducted to investigate the LPD effect in such scenarios where the landslide deposit is absent on the hillslope and to determine how LPD varies. Additionally, the LPD effect should also be examined in geomorphic settings with more deep-seated landslides, and how LPD varies with slope direction.

5.2. If a landslide affects soil properties, can an altered soil property explain landslide path dependency?

In chapter 3 (research objective 2), I investigated the role of landslides in modifying soil physical properties, including bulk density, saturated soil hydraulic conductivity, total water content, soil organic carbon (SOC) stock, soil resistance, and soil texture (grain size distribution). I compared landslide-affected soils with adjacent stable soils across the landslide of different ages. My results show that SOC stock, bulk density, and surface soil resistance exhibit the greatest differences between landslide-affected soils and adjacent stable areas shortly after a landslide, and this difference decrease with increasing landslide age and become minimal within 7-10 years of the landslide; in contrast, for some properties such as hydraulic conductivity, soil texture, and total water content, the differences between landslide affected soils and adjacent stable areas were not statistically significant, indicating that not all soil properties are equally influenced by landslides. Some inconsistencies were observed, specifically in ~10-year-old landslides (Figure 5.3), where soil property differences within and outside the landslides were not identical. This variation can be due to differences in lithology, which greatly influence soil physical properties (Gray et al., 2016). Therefore, future research should focus on how different soil properties evolve with landslide age under different lithological conditions.

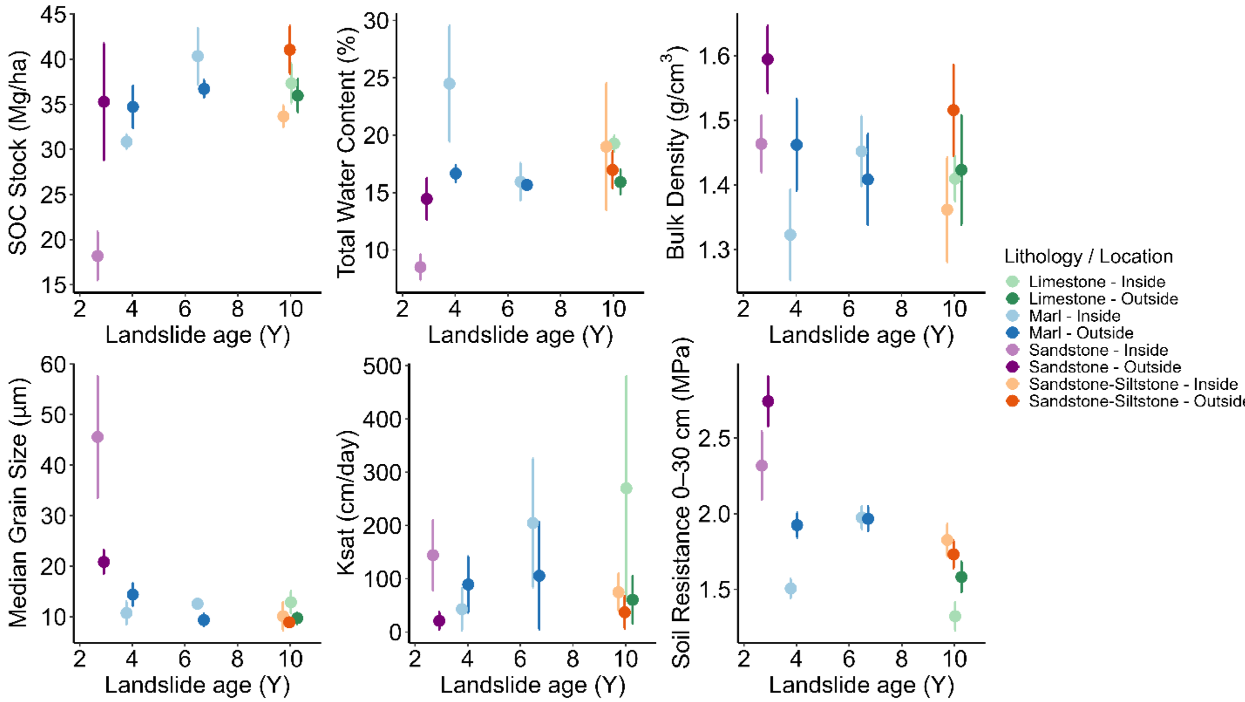

Figure 5.3: Variation in soil properties with landslide age under different lithological conditions

Importantly, the relationship between SOC stock and landslide age in Collazzone is easily noticeable in Chapter 3, where with landslide age, SOC stock (in the 0-30 cm soil layer) inside the landslide tends to increase, and the difference in SOC stock between slide soils and stable soils decreases. This finding is consistent with the findings of Van Eynde et al. (2017), who investigated landslides on Mt. Elgon in the Bududa district. In their study, they found that landslides significantly lower SOC compared to adjacent undisturbed soils, and SOC increases with landslide age and reaches levels comparable to those of surrounding stable soils approximately 60 years after the landslide. In Collazzone, SOC stock in slide soils tends to reach levels comparable to those in stable soils within 7-10 years. The lower SOC in slide soils immediately after slope failure is likely due to mixing of the low-SOC subsurface soil layers with the surface soil layer during landsliding. Moreover, Samia et al. (2017a) stated that LPD is strong within a decade of the earlier landslide. Also, Samia et al. (2017a) stated that LPD decreases over time, and one of the reasons they gave is that, over time, soil structure repairs and stabilizes due to cohesion. In my study, I found that SOC is higher in older landslides. According to Karami et al. (2012), SOC increases the soil aggregate stability because SOC acts as a nucleus and a binding agent in the formation of soil aggregates (Bronick & Lal, 2005). Therefore, over time, increased SOC enhances soil structural stability, potentially reducing landslide susceptibility. As the SOC recovery timescale is 7-10 years in Collazzone, closely during which LPD remains strongest, as reported by Samia et al., (2017a), I suspect that due to SOC recovery, along with improvement of surface soil resistance of landslide soils with respect to stable soil conditions, might be one of the reasons that LPD is strongest within a decade, and gradually weakens thereafter.

5.3. Do earthquakes impact LPD in Collazzone, and do they also influence LPD in central Nepal?

In Collazzone, I did not observe a clear increase in non-coseismic landslide rates immediately after earthquakes (1997 and 2009) compared to pre-earthquake periods. This is in contrast with findings by Marc et al. (2015), and my own findings in Nepal. It is worthwhile to consider why earthquakes in Collazzone did not produce a noticeable increase in non-coseismic landslides during the post-earthquake periods. The 1997 earthquake had a moment magnitude (M_w) of 6.0 and a maximum Peak Ground Acceleration (PGA) of 0.6g, while the 2009 earthquake had a magnitude (M_w) of 6.3 and a maximum PGA of 0.66g; however, their epicenters were far from Collazzone. Therefore, local ground shaking at Collazzone was relatively low, with an intensity of about MMI 4 during the 2009 earthquake and MMI 5 during the 1997 earthquake. Due to low intensity, these earthquakes did not induce widespread slope damage capable of increasing rainfall-induced rates after the post-earthquake period. However, I did see that spatial association, i.e., the overlap between earlier landslides and subsequent landslides, was higher during the post-earthquake period. Therefore, I observed an increase in LPD after the earthquake, although the overall non-coseismic landslide rate did not increase. One possible explanation is that earthquakes did not increase rainfall-triggered landslide rates but instead enhanced localized preconditioning for future slides near previously failed areas through micro-fracturing, reduction in soil shear strength, or changes in soil properties. These already disturbed areas may be more susceptible to future slides rather than the entire slope. Such localized preconditioning led to greater overlap between subsequent landslides and earlier ones, thereby increasing LPD after an earthquake in Collazzone. Imagine a situation in which earthquakes in Collazzone were strong; I would expect higher post-seismic rainfall-triggered landslide rates immediately after an earthquake than we just saw. In such a scenario, I would also expect less overlaps or no impact on LPD.

To analyze the situation in areas with high earthquake impact, I examined the effects of earthquakes on LPD across different geomorphic setting, specifically in the central region of Nepal. In Nepal, I compared monsoon-triggered landslides before and after the 2015 earthquakes and analyzed the impact of earthquakes on LPD. The Nepal 2015 earthquakes were a series of strong earthquakes that included 4 earthquakes of magnitudes (M_w = 6.3 to 7.8). Moreover, 3 of 4 earthquakes occurred inside the Nepal study area. I saw that during the post-earthquake period, rainfall-triggered landslide rates were higher than in the pre-earthquake period. Therefore, in the central region of Nepal, as the Gorkha earthquake had an impact of 7-8.6 MMI, which is significantly higher than in Collazzone that is why these earthquakes caused widespread hillslope damage across large areas, causing landslides not only near to earlier landslides but also triggering landslides in other locations which did not show trend of increase in overlap as seen for Collazzone.

In addition to the impact on LPD, earthquakes also affected some landslide properties. I noticed that rainfall-triggered landslides in the post-earthquake period are more elongated than in the pre-earthquake period. One possible reason for this may be due to more fracture developments in rocks and the generation of highly fragmented material due to earthquakes (Fan et al., 2019), which may have led to greater mobility of fractured material downslope under gravitational pull, and the landslides appeared more elongated. However, further research is needed on how earthquakes develop crack patterns, whether they are more downslope or lateral.

Moreover, I found that the impact of earthquakes on the topographic properties of landslides in the post-earthquake period differs across geomorphic settings, as seen in Collazzone and Nepal. For Collazzone, I observed that after the 2009 earthquake, rainfall-triggered landslides were more downslope in lower elevations, specifically near valley sidewalls; however, in Nepal, they tend to trigger during monsoon rainfall in higher elevations than in the pre-earthquake period. Previously, Meunier et al. (2008) found that earthquake-triggered landslides on steep slopes were more near ridge crests. The reason for this trend, they mentioned, is the amplification of seismic shaking by topography. As a result, ground shaking was stronger at ridge crests and convex slope points. This explains that stronger earthquakes preconditioning near ridge crests increase the susceptibility of higher-elevation slopes in Nepal, which is why rainfall-triggered landslides after the 2015 earthquakes tended to occur at higher mean elevations than during the pre-earthquake period. However, the mechanism by which non-co-seismic landslides in Collazzone were located at lower elevations after the earthquake than in the pre-period remains unclear. Therefore, future research should focus on how topography interacts with earthquakes to trigger landslides under different geomorphic and climatic conditions.

5.4. Need for incorporating climate data to improve understanding of the mechanism behind LPD

Although the overall results in Chapter 4 indicated that LPD was more prevalent after the earthquake in Collazzone, some data points deviate from this pattern (Figure 5.4). For example, points 7, 10 and 12 (marked with a black circle in Figure 5.4), which represent landslide pairs that occur soon after the earthquake, exhibit lower overlap than other pairs within the same period. One possible explanation is that these data points have a larger time difference between the landslide events. Samia et al. (2017a) reported that LPD decreases over time since the earlier landslide due to soil stabilization, vegetation regrowth, and soil structure repair. Therefore, a large time difference between landslide pairs represented by points 7, 10, and 12 may have reduced the fractional overlap index, even though it occurred in the post-earthquake period. However, point 13 shows relatively low overlap even though the time difference between landslides is small. This indicates that factors beyond time may also control LPD variability. One possible way to explain this variability in the overlap index is to integrate climate variables, such as cumulative rainfall during the overlap period between landslide events, to account for the climate's influence on LPD. I hypothesize that lower rainfall, even after an earthquake, between landslides within a given time slice and those in subsequent time slices results in lower overlap.

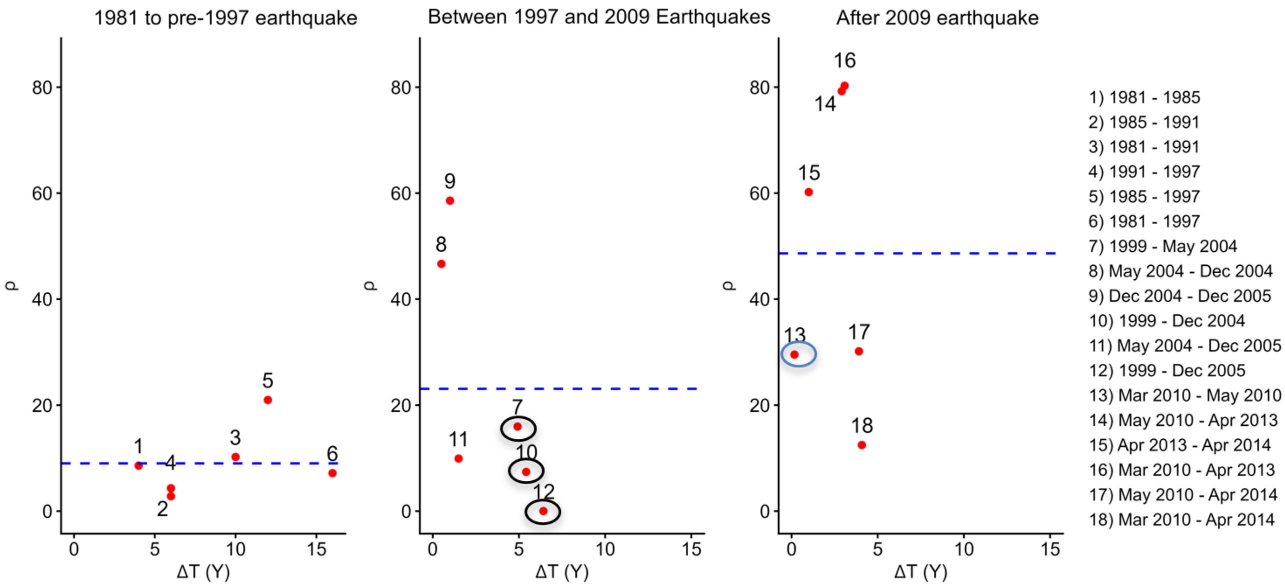

Figure 5.4: Relationship between overlap index (ρ) and time difference (ΔT) for landslides in Collazzone before the 1997 earthquake (left), between the 1997 and 2009 earthquakes (middle), and after the 2009 earthquake (right). The blue dashed line is mean overlap index for each period. The black and blue circle represents points where overlap is low even after earthquake.

References

Adhikari, K., Kheir, R., Greve, M., Malone, B., Minasny, B., Mcbratney, A., & Greve, M. (2014). Mapping soil pH and bulk density at multiple soil depths in Denmark. In *GlobalSoilMap: Basis of the Global Spatial Soil Information System—Proceedings of the 1st GlobalSoilMap Conference* (pp. 155–160). https://doi.org/10.1201/b16500-31

Alessio, P. (2019). Spatial variability of saturated hydraulic conductivity and measurement-based intensity-duration thresholds for slope stability, Santa Ynez Valley, CA. *Geomorphology*, *342*, 103–116. https://doi.org/10.1016/j.geomorph.2019.06.004

Alexandridis, T. K., Cherif, I., Kalogeropoulos, C., Monachou, S., Eskridge, K., & Silleos, N. (2013). Rapid error assessment for quantitative estimations from Landsat 7 gap-filled images. *Remote Sensing Letters*, *4*(9), 920–928. https://doi.org/10.1080/2150704X.2013.815380

Alvioli, M., Marchesini, I., Reichenbach, P., Rossi, M., Ardizzone, F., Fiorucci, F., & Guzzetti, F. (2016). Automatic delineation of geomorphological slope units with \texttt{r.slopeunits v1.0} and their optimization for landslide susceptibility modeling. *Geoscientific Model Development*, *9*(11), 3975–3991. https://doi.org/10.5194/gmd-9-3975-2016

Ardizzone, F., Bucci, F., Cardinali, M., Fiorucci, F., Pisano, L., Santangelo, M., & Zumpano, V. (2023). Geomorphological landslide inventory map of the Daunia Apennines, southern Italy. *Earth System Science Data*, *15*(2), 753–767. https://doi.org/10.5194/essd-15-753-2023

Ardizzone, F., Cardinali, M., Galli, M., Guzzetti, F., & Reichenbach, P. (2007). Identification and mapping of recent rainfall-induced landslides using elevation data collected by airborne Lidar. *Natural Hazards and Earth System Sciences*, *7*(6), 637–650. https://doi.org/10.5194/nhess-7-637-2007

Ardizzone, F., Fiorucci, F., Santangelo, M., Cardinali, M., Mondini, A. C., Rossi, M., Reichenbach, P., & Guzzetti, F. (2013). *Very-High Resolution Stereoscopic Satellite Images for Landslide Mapping BT - Landslide Science and Practice: Volume 1: Landslide Inventory and Susceptibility and Hazard Zoning* (C. Margottini, P. Canuti, & K. Sassa, Eds.; pp. 95–101). Springer Berlin Heidelberg. https://doi.org/10.1007/978-3-642-31325-7_12

B. Fang, G. Chen, L. Pan, R. Kou, & L. Wang. (2021). GAN-Based Siamese Framework for Landslide Inventory Mapping Using Bi-Temporal Optical Remote Sensing Images. *IEEE Geoscience and Remote Sensing Letters*, *18*(3), 391–395. https://doi.org/10.1109/LGRS.2020.2979693

B. Kalantar, N. Ueda, U. S. Lay, H. A. H. Al-Najjar, & A. A. Halin. (2019). Conditioning Factors Determination for Landslide Susceptibility Mapping Using Support Vector Machine Learning. *IGARSS 2019 - 2019 IEEE International Geoscience and Remote Sensing Symposium*, 9626–9629. https://doi.org/10.1109/IGARSS.2019.8898340

Bayram, H., Rastgeldi Dogan, T., Şahin, Ü. A., & Akdis, C. A. (2023). Environmental and health hazards by massive earthquakes. *Allergy*, *78*(8), 2081–2084. https://doi.org/10.1111/all.15736

Bernat Gazibara, S., Krkač, M., & Mihalić Arbanas, S. (2019). Landslide inventory mapping using LiDAR data in the City of Zagreb (Croatia). *Journal of Maps*, *15*(2), 773–779. https://doi.org/10.1080/17445647.2019.1671906

Biçer, Ç. T., & Ercanoglu, M. (2020). A semi-quantitative landslide risk assessment of central Kahramanmaraş City in the Eastern Mediterranean region of Turkey. *Arabian Journal of Geosciences*, *13*(15), 732. https://doi.org/10.1007/s12517-020-05697-w

Biswakarma, P., Joshi, V., Abdo, H. G., Almohamad, H., Abdullah Al Dughairi, A., & Al-Mutiry, M. (2023). An integrated quantitative and qualitative approach for landslide susceptibility mapping in West Sikkim district, Indian Himalaya. *Geomatics, Natural Hazards and Risk*, *14*(1), 2273781. https://doi.org/10.1080/19475705.2023.2273781

Błońska, E., Lasota, J., Piaszczyk, W., Wiecheć, M., & Klamerus-Iwan, A. (2018). The effect of landslide on soil organic carbon stock and biochemical properties of soil. *Journal of Soils and Sediments*, *18*(8), 2727–2737. https://doi.org/10.1007/s11368-017-1775-4

Blume, H.-P., Stahr, K., & Leinweber, P. (2011). *Bodenkundliches Praktikum: Eine Einführung in pedologisches Arbeiten für Ökologen, Land-und Forstwirte, Geo-und Umweltwissenschaftler*. Springer-Verlag.

Brabb, E. E. (1984). *Innovative approaches to landslide hazard and risk mapping.*

Bronick, C. J., & Lal, R. (2005). Soil structure and management: A review. *Geoderma*, *124*(1), 3–22. https://doi.org/10.1016/j.geoderma.2004.03.005

Brunsden, D. (1985). *Landslide types, mechanisms, recognition, identification*. 1–3.

Burchfiel, B. C., Zhiliang, C., Hodges, K. V., Yuping, L., Royden, L. H., Changrong, D., & Jiene, X. (1992). *The South Tibetan detachment system, Himalayan orogen: Extension contemporaneous with and parallel to shortening in a collisional mountain belt*.

Cardinali, M., Ardizzone, F., Galli, M., Guzzetti, F., & Reichenbach, P. (2000). *Landslides triggered by rapid snow melting: The December 1996–January 1997 event in Central Italy*. 439–448.

Chandra, N., & Vaidya, H. (2024). Automated detection of landslide events from multi-source remote sensing imagery: Performance evaluation and analysis of YOLO algorithms. *Journal of Earth System Science*, *133*(3), 127. https://doi.org/10.1007/s12040-024-02327-x

Chang, Z., Catani, F., Huang, F., Liu, G., Meena, S. R., Huang, J., & Zhou, C. (2023). Landslide susceptibility prediction using slope unit-based machine learning models considering the heterogeneity of conditioning factors. *Journal of Rock Mechanics and Geotechnical Engineering*, *15*(5), 1127–1143. https://doi.org/10.1016/j.jrmge.2022.07.009

Chen, C.-Y. (2009). Sedimentary impacts from landslides in the Tachia River Basin, Taiwan. *Geomorphology*, *105*(3), 355–365. https://doi.org/10.1016/j.geomorph.2008.10.009

Cheng, S., Yang, G., Yu, H., Li, J., & Zhang, L. (2012). Impacts of Wenchuan Earthquake-induced landslides on soil physical properties and tree growth. *Ecological Indicators*, *15*(1), 263–270. https://doi.org/10.1016/j.ecolind.2011.09.028

Chuang, S.-C., Chen, H., Lin, G.-W., Lin, C.-W., & Chang, C.-P. (2009). Increase in basin sediment yield from landslides in storms following major seismic disturbance. *Engineering Geology*, *103*(1), 59–65. https://doi.org/10.1016/j.enggeo.2008.08.001

Clague, J. J., & Stead, D. (2012). *Landslides: Types, mechanisms and modeling*. Cambridge University Press.

Climate-Data.org. (2025). *Collazzone Climate* [Dataset]. https://en.climate-data.org/europe/italy/umbria/collazzone-115144/

Cruden, D. M. (1991). A simple definition of a landslide. *Bulletin of the International Association of Engineering Geology - Bulletin de l'Association Internationale de Géologie de l'Ingénieur*, *43*(1), 27–29. https://doi.org/10.1007/BF02590167

Cruden, D. M., & Varnes, D. J. (1996). Landslides: Investigation and mitigation. Chapter 3-Landslide types and processes. *Transportation Research Board Special Report*, (247).

DeCelles, P. G., Robinson, D. M., Quade, J., Ojha, T. P., Garzione, C. N., Copeland, P., & Upreti, B. N. (2001). Stratigraphy, structure, and tectonic evolution of the Himalayan fold-thrust belt in western Nepal. *Tectonics*, *20*(4), 487–509. https://doi.org/10.1029/2000TC001226

Diggle, P. J., Chetwynd, A. G., Häggkvist, R., & Morris, S. E. (1995). Second-order analysis of space-time clustering. *Statistical Methods in Medical Research*. https://doi.org/10.1177/096228029500400203

Dixon, P. M. (2014). Ripley's K Function. In *Wiley StatsRef: Statistics Reference Online*. https://doi.org/10.1002/9781118445112.stat07751

Duzgoren-Aydin, N. S., & Aydin, A. (2006). Chemical and mineralogical heterogeneities of weathered igneous profiles: Implications for landslide investigations. *Natural Hazards and Earth System Sciences*, *6*(2), 315–322. https://doi.org/10.5194/nhess-6-315-2006

Fan, X., Scaringi, G., Korup, O., West, A. J., van Westen, C. J., Tanyas, H., Hovius, N., Hales, T. C., Jibson, R. W., Allstadt, K. E., Zhang, L., Evans, S. G., Xu, C., Li, G., Pei, X., Xu, Q., & Huang, R. (2019). Earthquake-Induced Chains of Geologic Hazards: Patterns, Mechanisms, and Impacts. *Reviews of Geophysics*, *57*(2), 421–503. https://doi.org/10.1029/2018RG000626

Frene, J. P., Pandey, B. K., & Castrillo, G. (2024). Under pressure: Elucidating soil compaction and its effect on soil functions. *Plant and Soil*, *502*(1), 267–278. https://doi.org/10.1007/s11104-024-06573-2

Galli, M., Ardizzone, F., Cardinali, M., Guzzetti, F., & Reichenbach, P. (2008). Comparing landslide inventory maps. *GIS Technology and Models for Assessing Landslide Hazard and Risk*, *94*(3), 268–289. https://doi.org/10.1016/j.geomorph.2006.09.023

Gariano, S. L., & Guzzetti, F. (2016). Landslides in a changing climate. *Earth-Science Reviews*, *162*, 227–252. https://doi.org/10.1016/j.earscirev.2016.08.011

Geertsema, M., Highland, L., & Vaugeouis, L. (2009). *Environmental Impact of Landslides BT - Landslides – Disaster Risk Reduction* (K. Sassa & P. Canuti, Eds.; pp. 589–607). Springer Berlin Heidelberg. https://doi.org/10.1007/978-3-540-69970-5_31

Goyal, D., Joshi, V., Gupta, N., & Cabral-Pinto, M. M. S. (2022). Soil Quality Assessment in a Landslide Chronosequence of Indian Himalayan Region. *Land*, *11*(10). https://doi.org/10.3390/land11101819

Gray, J. M., Bishop, T. F. A., & Wilford, J. R. (2016). Lithology and soil relationships for soil modelling and mapping. *CATENA*, *147*, 429–440. https://doi.org/10.1016/j.catena.2016.07.045

Guisan, A., Weiss, S. B., & Weiss, A. D. (1999). GLM versus CCA spatial modeling of plant species distribution. *Plant Ecology*, *143*(1), 107–122. https://doi.org/10.1023/A:1009841519580

Guzzetti, F. (2006). *Landslide hazard and risk assessment*.

Guzzetti, F., Ardizzone, F., Cardinali, M., Rossi, M., & Valigi, D. (2009). Landslide volumes and landslide mobilization rates in Umbria, central Italy. *Earth and Planetary Science Letters*, *279*(3), 222–229. https://doi.org/10.1016/j.epsl.2009.01.005

Guzzetti, F., Galli, M., Reichenbach, P., Ardizzone, F., & Cardinali, M. (2006). Landslide hazard assessment in the Collazzone area, Umbria, Central Italy. *Natural Hazards and Earth System Sciences*, *6*(1), 115–131. https://doi.org/10.5194/nhess-6-115-2006

Guzzetti, F., Mondini, A. C., Cardinali, M., Fiorucci, F., Santangelo, M., & Chang, K.-T. (2012). Landslide inventory maps: New tools for an old problem. *Earth-Science Reviews*, *112*(1), 42–66. https://doi.org/10.1016/j.earscirev.2012.02.001

Guzzetti, F., Reichenbach, P., Ardizzone, F., Cardinali, M., & Galli, M. (2006). Estimating the quality of landslide susceptibility models. *Geomorphology*, *81*(1), 166–184. https://doi.org/10.1016/j.geomorph.2006.04.007

Guzzetti, F., Reichenbach, P., Cardinali, M., Galli, M., & Ardizzone, F. (2005). Probabilistic landslide hazard assessment at the basin scale. *Geomorphology*, *72*(1), 272–299. https://doi.org/10.1016/j.geomorph.2005.06.002

Hampton, M. A., Lee, H. J., & Locat, J. (1996). Submarine landslides. *Reviews of Geophysics*, *34*(1), 33–59. https://doi.org/10.1029/95RG03287

Hastie, T., & Tibshirani, R. (2014). Generalized Additive Models. In *Wiley StatsRef: Statistics Reference Online*. John Wiley & Sons, Ltd. https://doi.org/10.1002/9781118445112.stat03141

He, K., Lombardo, L., Chang, L., Sadhasivam, N., Hu, X., Fang, Z., Dahal, A., Fadel, I., Luo, G., & Tanyas, H. (2022). *Hillslope recovery after a major earthquake: InSAR-derived time series analyses to capture earthquake-legacy effect*.

Hungr, O., Leroueil, S., & Picarelli, L. (2014). The Varnes classification of landslide types, an update. *Landslides*, *11*(2), 167–194. https://doi.org/10.1007/s10346-013-0436-y

Jaafari, A. (2024). An Overview of Triggering and Causing Factors of Landslides. In U. Chatterjee, K. C. Lalmalsawmzauva, B. Biswas, & S. C. Pal (Eds.), *Landslides in the Himalayan Region: Risk Assessment and Mitigation Strategy for Sustainable Management* (pp. 25–45). Springer Nature Singapore. https://doi.org/10.1007/978-981-97-4680-4_2

Jackson, L. E. (2013). Slide and Slump. In P. T. Bobrowsky (Ed.), *Encyclopedia of Natural Hazards* (pp. 913–919). Springer Netherlands. https://doi.org/10.1007/978-1-4020-4399-4_323

Jemec Auflič, M., Bezak, N., Šegina, E., Frantar, P., Gariano, S. L., Medved, A., & Peternel, T. (2023). Climate change increases the number of landslides at the juncture of the Alpine, Pannonian and Mediterranean regions. *Scientific Reports*, *13*(1), 23085. https://doi.org/10.1038/s41598-023-50314-x

Jiang, L., Ling, D., Zhao, M., Wang, C., Liang, Q., & Liu, K. (2018). Effective Identification of Terrain Positions from Gridded DEM Data Using Multimodal Classification Integration. *ISPRS International Journal of Geo-Information*, *7*(11), 443. https://doi.org/10.3390/ijgi7110443

Jones, J. N., Boulton, S. J., Bennett, G. L., Stokes, M., & Whitworth, M. R. Z. (2021). Temporal Variations in Landslide Distributions Following Extreme Events: Implications for Landslide Susceptibility Modeling. *Journal of Geophysical Research: Earth Surface*, *126*(7), e2021JF006067. https://doi.org/10.1029/2021JF006067

Karakas, G., Unal, E. O., Cetinkaya, S., Ozcan, N. T., Karakas, V. E., Can, R., Gokceoglu, C., & Kocaman, S. (2024). Analysis of landslide susceptibility prediction accuracy with an event-based inventory: The 6 February 2023 Turkiye earthquakes. *Soil Dynamics and Earthquake Engineering*, *178*, 108491. https://doi.org/10.1016/j.soildyn.2024.108491

Karami, A., Homaee, M., Afzalinia, S., Ruhipour, H., & Basirat, S. (2012). Organic resource management: Impacts on soil aggregate stability and other soil physico-chemical properties. *Agriculture, Ecosystems & Environment*, *148*, 22–28. https://doi.org/10.1016/j.agee.2011.10.021

Kayastha, P., Dhital, M. R., & De Smedt, F. (2013). Application of the analytical hierarchy process (AHP) for landslide susceptibility mapping: A case study from the Tinau watershed, west Nepal. *Computers & Geosciences*, *52*, 398–408. https://doi.org/10.1016/j.cageo.2012.11.003

Keefer, D. K. (1984). Landslides caused by earthquakes. *Geological Society of America Bulletin*, *95*(4), 406–421.

Kincey, M. E., Rosser, N. J., Robinson, T. R., Densmore, A. L., Shrestha, R., Pujara, D. S., Oven, K. J., Williams, J. G., & Swirad, Z. M. (2021). Evolution of Coseismic and Post-seismic Landsliding After the 2015 Mw 7.8 Gorkha Earthquake, Nepal. *Journal of Geophysical Research: Earth Surface*, *126*(3), e2020JF005803. https://doi.org/10.1029/2020JF005803

Kiskowski, M. A., Hancock, J. F., & Kenworthy, A. K. (2009). On the Use of Ripley's K-Function and Its Derivatives to Analyze Domain Size. *Biophysical Journal*, *97*(4), 1095–1103. https://doi.org/10.1016/j.bpj.2009.05.039

Kohler, M., Hodel, D., Keller, L., Molinari, A., & Puzrin, A. M. (2023). Case study of an active landslide at the flank of a water reservoir and its response during earthquakes. *Engineering Geology*, *323*, 107243. https://doi.org/10.1016/j.enggeo.2023.107243

Kovács, I. P., Czigány, Sz., Dobre, B., Fábián, Sz. Á., Sobucki, M., Varga, G., & Bugya, T. (2019). A field survey–based method to characterise landslide development: A case study at the high bluff of the Danube, south-central Hungary. *Landslides*, *16*(8), 1567–1581. https://doi.org/10.1007/s10346-019-01205-8

Lardy, J. M., DeSutter, T. M., Daigh, A. L. M., Meehan, M. A., & Staricka, J. A. (2022). Effects of soil bulk density and water content on penetration resistance. *Agricultural & Environmental Letters*, *7*(2), e20096. https://doi.org/10.1002/ael2.20096

Leshchinsky, B., Lehmann, P., & Or, D. (2021). Enhanced Rainfall-Induced Shallow Landslide Activity Following Seismic Disturbance—From Triggering to Healing. *Journal of Geophysical Research: Earth Surface*, *126*(1), e2020JF005669. https://doi.org/10.1029/2020JF005669

Liao, M., Wen, H., & Yang, L. (2022). Identifying the essential conditioning factors of landslide susceptibility models under different grid resolutions using hybrid machine learning: A case of Wushan and Wuxi counties, China. *CATENA*, *217*, 106428. https://doi.org/10.1016/j.catena.2022.106428

Liu, J. G., Mason, P. J., Clerici, N., Chen, S., Davis, A., Miao, F., Deng, H., & Liang, L. (2004). Landslide hazard assessment in the Three Gorges area of the Yangtze river using ASTER imagery: Zigui–Badong. *Hazards of Mass Movements*, *61*(1), 171–187. https://doi.org/10.1016/j.geomorph.2003.12.004

Liu, L., Li, S., Li, X., Jiang, Y., Wei, W., Wang, Z., & Bai, Y. (2019). An integrated approach for landslide susceptibility mapping by considering spatial correlation and fractal distribution of clustered landslide data. *Landslides*, *16*(4), 715–728. https://doi.org/10.1007/s10346-018-01122-2

Liu, X., Zhao, C., Zhang, Q., Peng, J., Zhu, W., & Lu, Z. (2018). Multi-Temporal Loess Landslide Inventory Mapping with C-, X- and L-Band SAR Datasets—A Case Study of Heifangtai Loess Landslides, China. *Remote Sensing*, *10*(11), 1756. https://doi.org/10.3390/rs10111756

Lombardo, L., Opitz, T., Ardizzone, F., Guzzetti, F., & Huser, R. (2020). Space-time landslide predictive modelling. *Earth-Science Reviews*, *209*, 103318. https://doi.org/10.1016/j.earscirev.2020.103318

Lu, J., Li, W., Zhan, W., & Tie, Y. (2022). Distribution and Mobility of Coseismic Landslides Triggered by the 2018 Hokkaido Earthquake in Japan. *Remote Sensing*, *14*(16). https://doi.org/10.3390/rs14163957

M. Kobayashi. (2014). Experience of infrastructure damage caused by the Great East Japan Earthquake and countermeasures against future disasters. *IEEE Communications Magazine*, *52*(3), 23–29. https://doi.org/10.1109/MCOM.2014.6766080

Malamud, B. D., Turcotte, D. L., Guzzetti, F., & Reichenbach, P. (2004). Landslides, earthquakes, and erosion. *Earth and Planetary Science Letters*, *229*(1), 45–59. https://doi.org/10.1016/j.epsl.2004.10.018

Marc, O., Hovius, N., Meunier, P., Uchida, T., & Hayashi, S. (2015). Transient changes of landslide rates after earthquakes. *Geology*, *43*(10), 883–886. https://doi.org/10.1130/G36961.1

Matsushi, Y., Hattanji, T., & Matsukura, Y. (2006). Mechanisms of shallow landslides on soil-mantled hillslopes with permeable and impermeable bedrocks in the Boso Peninsula, Japan. *Geomorphology*, *76*(1), 92–108. https://doi.org/10.1016/j.geomorph.2005.10.003

Meena, S. R., Puliero, S., Bhuyan, K., Floris, M., & Catani, F. (2022). Assessing the importance of conditioning factor selection in landslide susceptibility for the province of Belluno (region of Veneto, northeastern Italy). *Natural Hazards and Earth System Sciences*, *22*(4), 1395–1417. https://doi.org/10.5194/nhess-22-1395-2022

Meter Group, 2025. KSAT – Saturated Hydraulic Conductivity in the Lab. Meter Group, Munich, Germany. Available at: https://metergroup.com/products/ksat/ (accessed 19 February 2026).

Metropolis, N., Rosenbluth, A. W., Rosenbluth, M. N., Teller, A. H., & Teller, E. (1953). Equation of State Calculations by Fast Computing Machines. *The Journal of Chemical Physics*, *21*(6), 1087–1092. https://doi.org/10.1063/1.1699114

Meunier, P., Hovius, N., & Haines, J. A. (2008). Topographic site effects and the location of earthquake induced landslides. *Earth and Planetary Science Letters*, *275*(3), 221–232. https://doi.org/10.1016/j.epsl.2008.07.020

Meusburger, K., & Alewell, C. (2008). Impacts of anthropogenic and environmental factors on the occurrence of shallow landslides in an alpine catchment (Urseren Valley, Switzerland). *Natural Hazards and Earth System Sciences*, *8*(3), 509–520. https://doi.org/10.5194/nhess-8-509-2008

Mirus, B. B., Smith, J. B., & Baum, R. L. (2017). Hydrologic Impacts of Landslide Disturbances: Implications for Remobilization and Hazard Persistence. *Water Resources Research*, *53*(10), 8250–8265. https://doi.org/10.1002/2017WR020842

Montgomery, D. R., Schmidt, K. M., Dietrich, W. E., & McKean, J. (2009). Instrumental record of debris flow initiation during natural rainfall: Implications for modeling slope stability. *Journal of Geophysical Research: Earth Surface*, *114*(F1). https://doi.org/10.1029/2008JF001078

Mugagga, F., Kakembo, V., & Buyinza, M. (2012). Land use changes on the slopes of Mount Elgon and the implications for the occurrence of landslides. *CATENA*, *90*, 39–46. https://doi.org/10.1016/j.catena.2011.11.004

Murray, A. B., Goldstein, E. B., & Coco, G. (2014). The shape of patterns to come: From initial formation to long-term evolution. *Earth Surface Processes and Landforms*, *39*(1), 62–70. https://doi.org/10.1002/esp.3487

Nhu, V.-H., Mohammadi, A., Shahabi, H., Ahmad, B. B., Al-Ansari, N., Shirzadi, A., Clague, J. J., Jaafari, A., Chen, W., & Nguyen, H. (2020). Landslide Susceptibility Mapping Using Machine Learning Algorithms and Remote Sensing Data in a Tropical Environment. *International Journal of Environmental Research and Public Health*, *17*(14). https://doi.org/10.3390/ijerph17144933

Nikolic, T. (2014). Direct and indirect impact of landslide on environment. In *Engineering Geology for Society and Territory-Volume 5: Urban Geology, Sustainable Planning and Landscape Exploitation* (pp. 1237–1241). Springer.

Noviyanto, A., Sartohadi, J., & Purwanto, B. H. (2020). The distribution of soil morphological characteristics for landslide-impacted Sumbing Volcano, Central Java—Indonesia. *Geoenvironmental Disasters*, *7*(1), 25. https://doi.org/10.1186/s40677-020-00158-8

Panagos, P., Borrelli, P., & Meusburger, K. (2015). A New European Slope Length and Steepness Factor (LS-Factor) for Modeling Soil Erosion by Water. *Geosciences*, *5*(2), 117–126. https://doi.org/10.3390/geosciences5020117

Parker, R. N., Hancox, G. T., Petley, D. N., Massey, C. I., Densmore, A. L., & Rosser, N. J. (2015). Spatial distributions of earthquake-induced landslides and hillslope preconditioning in the northwest South Island, New Zealand. *Earth Surface Dynamics*, *3*(4), 501–525. https://doi.org/10.5194/esurf-3-501-2015

Parry, S., Campbell, S. D. G., & Churchman, G. J. (2000). *Kaolin-Rich Zones In Hong Kong Saprolites Their Interpretation And Engineering Significance: All Days*.

Pašek, J. (1975). Landslides inventory. *Bulletin of the International Association of Engineering Geology - Bulletin de l'Association Internationale de Géologie de l'Ingénieur*, *12*(1), 73–74. Scopus. https://doi.org/10.1007/BF02635432

Phillips, J. D. (2006). Evolutionary geomorphology: Thresholds and nonlinearity in landform response to environmental change. *Hydrology and Earth System Sciences*, *10*(5), 731–742. https://doi.org/10.5194/hess-10-731-2006

Phillips, J. D. (2014). Thresholds, mode switching, and emergent equilibrium in geomorphic systems. *Earth Surface Processes and Landforms*, *39*(1), 71–79. https://doi.org/10.1002/esp.3492

Poeplau, C., Vos, C., & Don, A. (2017). Soil organic carbon stocks are systematically overestimated by misuse of the parameters bulk density and rock fragment content. *Soil*, *3*(1), 61–66.

Pollock, W., & Wartman, J. (2020). Human Vulnerability to Landslides. *GeoHealth*, *4*(10), e2020GH000287. https://doi.org/10.1029/2020GH000287

Prancevic, J. P., Lamb, M. P., McArdell, B. W., Rickli, C., & Kirchner, J. W. (2020). Decreasing Landslide Erosion on Steeper Slopes in Soil-Mantled Landscapes. *Geophysical Research Letters*, *47*(10), e2020GL087505. https://doi.org/10.1029/2020GL087505

Prokešová, R., Medveďová, A., Tábořík, P., & Snopková, Z. (2013). Towards hydrological triggering mechanisms of large deep-seated landslides. *Landslides*, *10*(3), 239–254. https://doi.org/10.1007/s10346-012-0330-z

Pu, R., & Bell, S. (2017). Mapping seagrass coverage and spatial patterns with high spatial resolution IKONOS imagery. *International Journal of Applied Earth Observation and Geoinformation*, *54*, 145–158. https://doi.org/10.1016/j.jag.2016.09.011

Pucha-Cofrep, F., & Fries, A. (2025). *ArcGIS Pro Manual*. Franz Pucha Cofrep.

Pyakurel, A., K.C., D., & Dahal, B. K. (2024). Enhancing co-seismic landslide susceptibility, building exposure, and risk analysis through machine learning. *Scientific Reports*, *14*(1), 5902. https://doi.org/10.1038/s41598-024-54898-w

Reddy, V. S., & Singh, J. S. (1993). Changes in Vegetation and Soil During Succession Following Landslide Disturbance in the Central Himalaya. *Journal of Environmental Management*, *39*(4), 235–250. https://doi.org/10.1006/jema.1993.1068

Regmi, A. D., Yoshida, K., Dhital, M. R., & Devkota, K. (2013). Effect of rock weathering, clay mineralogy, and geological structures in the formation of large landslide, a case study from Dumre Besei landslide, Lesser Himalaya Nepal. *Landslides*, *10*(1), 1–13. https://doi.org/10.1007/s10346-011-0311-7

Reichenbach, P., Rossi, M., Malamud, B. D., Mihir, M., & Guzzetti, F. (2018). A review of statistically-based landslide susceptibility models. *Earth-Science Reviews*, *180*, 60–91. https://doi.org/10.1016/j.earscirev.2018.03.001

Ripley, B. D. (1979). Tests of “Randomness” for Spatial Point Patterns. *Journal of the Royal Statistical Society: Series B (Methodological)*, *41*(3), 368–374. https://doi.org/10.1111/j.2517-6161.1979.tb01091.x

Roberts, S., Jones, J. N., & Boulton, S. J. (2021). Characteristics of landslide path dependency revealed through multiple resolution landslide inventories in the Nepal Himalaya. *Geomorphology*, *390*, 107868. https://doi.org/10.1016/j.geomorph.2021.107868

Robinson, D. M., DeCelles, P. G., Patchett, P. J., & Garzione, C. N. (2001). The kinematic evolution of the Nepalese Himalaya interpreted from Nd isotopes. *Earth and Planetary Science Letters*, *192*(4), 507–521. https://doi.org/10.1016/S0012-821X(01)00451-4

Rodríguez, C. E., Bommer, J. J., & Chandler, R. J. (1999). Earthquake-induced landslides: 1980–1997. *Soil Dynamics and Earthquake Engineering*, *18*(5), 325–346. https://doi.org/10.1016/S0267-7261(99)00012-3

Rossi, L. M. W., Rapidel, B., Roupsard, O., Villatoro-sánchez, M., Mao, Z., Nespoulous, J., Perez, J., Prieto, I., Roumet, C., Metselaar, K., Schoorl, J. M., Claessens, L., & Stokes, A. (2017). Sensitivity of the landslide model LAPSUS_LS to vegetation and soil parameters. *Soil Bio- and Eco-Engineering: The Use of Vegetation to Improve Slope Stability - Proceedings of the Fourth International Conference*, *109*, 249–255. https://doi.org/10.1016/j.ecoleng.2017.08.010

Samia, J. (2018). Landslide Path Dependency and Its Impact on Space-Time Modelling of Landslide Susceptibility [Ph.D., Wageningen University and Research]. In *PQDT - Global*. ProQuest One Academic (2564133855). https://er.lib.k-state.edu/login?url=https://www.proquest.com/dissertations-theses/landslide-path-dependency-impact-on-space-time/docview/2564133855/se-2?accountid=11789

Samia, J., Temme, A., Bregt, A. K., Wallinga, J., Stuiver, J., Guzzetti, F., Ardizzone, F., & Rossi, M. (2018). Implementing landslide path dependency in landslide susceptibility modelling. *Landslides*, *15*(11), 2129–2144. https://doi.org/10.1007/s10346-018-1024-y

Samia, J., Temme, A., Bregt, A., Wallinga, J., Guzzetti, F., & Ardizzone, F. (2020). Dynamic path-dependent landslide susceptibility modelling. *Natural Hazards and Earth System Sciences*, *20*(1), 271–285. https://doi.org/10.5194/nhess-20-271-2020

Samia, J., Temme, A., Bregt, A., Wallinga, J., Guzzetti, F., Ardizzone, F., & Rossi, M. (2017a). Characterization and quantification of path dependency in landslide susceptibility. *Geomorphology*, *292*, 16–24. https://doi.org/10.1016/j.geomorph.2017.04.039

Samia, J., Temme, A., Bregt, A., Wallinga, J., Guzzetti, F., Ardizzone, F., & Rossi, M. (2017b). Do landslides follow landslides? Insights in path dependency from a multi-temporal landslide inventory. *Landslides*, *14*(2), 547–558. https://doi.org/10.1007/s10346-016-0739-x

Samuel-Rosa, A. (2019). *Optimization of Spatial Samples via Simulated Annealing* (Version 2.2.0) [R]. Laboratorio-de-Pedometria. https://github.com/Laboratorio-de-Pedometria/spsann-package

Santangelo, M., Marchesini, I., Cardinali, M., Fiorucci, F., Rossi, M., Bucci, F., & Guzzetti, F. (2015). A method for the assessment of the influence of bedding on landslide abundance and types. *Landslides*, *12*(2), 295–309. https://doi.org/10.1007/s10346-014-0485-x

Schomakers, J., Mayer, H., Lee, J. Y., Lee, T. Y., Jien, S. H., Mentler, A., Hein, T., Huang, J. C., Hseu, Z. Y., Cheng, L. W., Yu, C. K., & Zehetner, F. (2018). Soil aggregate breakdown and carbon release along a chronosequence of recovering landslide scars in a subtropical watershed. *CATENA*, *165*, 530–536. https://doi.org/10.1016/j.catena.2018.03.004

Schuster, R. L., & Highland, L. M. (2003). *Impact of landslides and innovative landslide-mitigation measures on the natural environment*. *8*(10), 46.

Shen, Z., Wang, D., Arabameri, A., Santosh, M., Egbueri, J. C., & Arora, A. (2024). Landslide susceptibility assessment and mapping using new ensemble model. *Advances in Space Research*, *74*(7), 2859–2882. https://doi.org/10.1016/j.asr.2024.06.018

Sim, K., Lee, M., Remenyte-Prescott, R., & Wong, S. Y. (2022). *An Overview of Causes of Landslides and Their Impact on Transport Networks*.

Simonett, D. S. (1997). Landslides. In *Geomorphology* (pp. 639–641). Springer Berlin Heidelberg. https://doi.org/10.1007/3-540-31060-6_219

Singh, A., Dhiman, N., Niraj, K. C., & Shukla, D. P. (2024). "Ensembled transfer learning approach for error reduction in landslide susceptibility mapping of the data scare region." *Scientific Reports*, *14*(1), 29060. https://doi.org/10.1038/s41598-024-76541-4

Singh, K., Mehrotra, A., & Pal, K. (2014). Landslide detection from satellite images using spectral indices and digital elevation model. *Disaster Adv*, *7*(6), 25–32.

Singh, K. P., Mandal, T. N., & Tripathi, S. K. (2001). Patterns of restoration of soil physciochemical properties and microbial biomass in different landslide sites in the sal forest ecosystem of Nepal Himalaya. *Ecological Engineering*, *17*(4), 385–401. https://doi.org/10.1016/S0925-8574(00)00162-2

Singh, R. G., Botha, G. A., Richards, N. P., & McCarthy, T. S. (2008). Holocene landslides in KwaZulu-Natal, South Africa. *South African Journal of Geology*, *111*(1), 39–52. https://doi.org/10.2113/gssajg.111.1.39

Sparling, G., Ross, D., Trustrum, N., Arnold, G., West, A., Speir, T., & Schipper, L. (2003). Recovery of topsoil characteristics after landslip erosion in dry hill country of New Zealand, and a test of the space-for-time hypothesis. *Soil Biology and Biochemistry*, *35*(12), 1575–1586. https://doi.org/10.1016/j.soilbio.2003.08.002

Sun, Q., Ding, Y., Hou, J., Zhu, Q., Wu, Y., Wu, T., Wang, X., Zhao, X., & Shao, S. (2025). LHAKG: a knowledge graph construction framework for landslide hazard assessment by using XLNet-BiLSTM-CRF from geoscience literature. *International Journal of Digital Earth*, *18*(2), 2577292. https://doi.org/10.1080/17538947.2025.2577292

Tao, Z., Shu, Y., Yang, X., Peng, Y., Chen, Q., & Zhang, H. (2020). Physical model test study on shear strength characteristics of slope sliding surface in Nanfen open-pit mine.

International Journal of Mining Science and Technology, *30*(3), 421–429. https://doi.org/10.1016/j.ijmst.2020.05.006
Tehrani, F. S., Calvello, M., Liu, Z., Zhang, L., & Lacasse, S. (2022). Machine learning and landslide studies: Recent advances and applications. *Natural Hazards*, *114*(2), 1197–1245. https://doi.org/10.1007/s11069-022-05423-7
Temme, A., Guzzetti, F., Samia, J., & Mirus, B. B. (2020). The future of landslides' past—A framework for assessing consecutive landsliding systems. *Landslides*, *17*(7), 1519–1528. https://doi.org/10.1007/s10346-020-01405-7
Temme, A. J. A. M. (2021a). *Relations Between Soil Development and Landslides* (pp. 177–185). https://doi.org/10.1002/9781119563952.ch9
Temme, A. J. A. M. (2021b). Relations Between Soil Development and Landslides. In *Hydrogeology, Chemical Weathering, and Soil Formation* (pp. 177–185). American Geophysical Union (AGU). https://doi.org/10.1002/9781119563952.ch9
Temme, A. J. A. M., Keiler, M., Karssenberg, D., & Lang, A. (2015). Complexity and non-linearity in earth surface processes – concepts, methods and applications. *Earth Surface Processes and Landforms*, *40*(9), 1270–1274. https://doi.org/10.1002/esp.3712
Temme, A. J., Schoorl, J. M., & van der Meij, W. M. (2022). New geomorphometric variables for non-continuous hillslopes – Assessing the value for digital soil mapping. *Geoderma*, *418*, 115848. https://doi.org/10.1016/j.geoderma.2022.115848
Upreti, B. N. (1999). An overview of the stratigraphy and tectonics of the Nepal Himalaya. *Journal of Asian Earth Sciences*, *17*(5), 577–606. https://doi.org/10.1016/S1367-9120(99)00047-4
USGS. (2012). USGS CoreCast: Landslide Hazards. *USGS CoreCast: Landslide Hazards*. https://www.usgs.gov/media/videos/usgs-corecast-landslide-hazards?
Van Eynde, E., Dondeyne, S., Isabirye, M., Deckers, J., & Poesen, J. (2017). Impact of landslides on soil characteristics: Implications for estimating their age. *CATENA*, *157*, 173–179. https://doi.org/10.1016/j.catena.2017.05.003
van Westen, C. J., van Asch, T. W. J., & Soeters, R. (2006). Landslide hazard and risk zonation—Why is it still so difficult? *Bulletin of Engineering Geology and the Environment*, *65*(2), 167–184. https://doi.org/10.1007/s10064-005-0023-0
Vanmaercke, M., Ardizzone, F., Rossi, M., & Guzzetti, F. (2017). Exploring the effects of seismicity on landslides and catchment sediment yield: An Italian case study. *Geomorphology*, *278*, 171–183. https://doi.org/10.1016/j.geomorph.2016.11.010
Varnes, D. J. (1978). Slope movement types and processes. *Special Report*, *176*, 11–33.
Volpe, E., Gariano, S. L., Ardizzone, F., Fiorucci, F., & Salciarini, D. (2022). A Heuristic Method to Evaluate the Effect of Soil Tillage on Slope Stability: A Pilot Case in Central Italy. *Land*, *11*(6). https://doi.org/10.3390/land11060912
Wang, G., & Sassa, K. (2003). Pore-pressure generation and movement of rainfall-induced landslides: Effects of grain size and fine-particle content. *Engineering Geology*, *69*(1), 109–125. https://doi.org/10.1016/S0013-7952(02)00268-5
Wang, Y., Wen, H., Sun, D., & Li, Y. (2021). Quantitative Assessment of Landslide Risk Based on Susceptibility Mapping Using Random Forest and GeoDetector. *Remote Sensing*, *13*(13), 2625. https://doi.org/10.3390/rs13132625
WIECZOREK, G. F. (1984). Preparing a Detailed Landslide-Inventory Map for Hazard Evaluation and Reduction. *Environmental & Engineering Geoscience*, *xxi*(3), 337–342. https://doi.org/10.2113/gseegeosci.xxi.3.337

Wilcke, W., Valladarez, H., Stoyan, R., Yasin, S., Valarezo, C., & Zech, W. (2003). Soil properties on a chronosequence of landslides in montane rain forest, Ecuador. *CATENA*, *53*(1), 79–95. https://doi.org/10.1016/S0341-8162(02)00196-0

Wobbrock, J. O., Findlater, L., Gergle, D., & Higgins, J. J. (2011). *The aligned rank transform for nonparametric factorial analyses using only anova procedures*. 143–146.

Xu, W.-J., Wang, L., & Cheng, K. (2022). The Failure and River Blocking Mechanism of Large-Scale Anti-dip Rock Landslide Induced by Earthquake. *Rock Mechanics and Rock Engineering*, *55*(8), 4941–4961. https://doi.org/10.1007/s00603-022-02903-x

Yeon, Y.-K., Han, J.-G., & Ryu, K. H. (2010). Landslide susceptibility mapping in Injae, Korea, using a decision tree. *Engineering Geology*, *116*(3), 274–283. https://doi.org/10.1016/j.enggeo.2010.09.009

Yin, A. (2006). Cenozoic tectonic evolution of the Himalayan orogen as constrained by along-strike variation of structural geometry, exhumation history, and foreland sedimentation. *Earth-Science Reviews*, *76*(1), 1–131. https://doi.org/10.1016/j.earscirev.2005.05.004

Youssef, A. M., & Pourghasemi, H. R. (2021). Landslide susceptibility mapping using machine learning algorithms and comparison of their performance at Abha Basin, Asir Region, Saudi Arabia. *Geoscience Frontiers*, *12*(2), 639–655. https://doi.org/10.1016/j.gsf.2020.05.010

Zhang, A., Wang, X., Pedrycz, W., Yang, Q., Wang, X., & Guo, H. (2024). Near real-time spatial prediction of earthquake-triggered landslides based on global inventories from 2008 to 2022. *Soil Dynamics and Earthquake Engineering*, *185*, 108890. https://doi.org/10.1016/j.soildyn.2024.108890

Zhang, N., Yan, J., & Liu, P. (2021). Effect of Bacterial Manure on the Properties of Complex Soil and Growth of Ryegrass. *Agronomy*, *11*(3). https://doi.org/10.3390/agronomy11030568

Zhang, Q., Yu, H., Li, Z., Zhang, G., & Ma, D. T. (2020). Assessing potential likelihood and impacts of landslides on transportation network vulnerability. *Transportation Research Part D: Transport and Environment*, *82*, 102304. https://doi.org/10.1016/j.trd.2020.102304